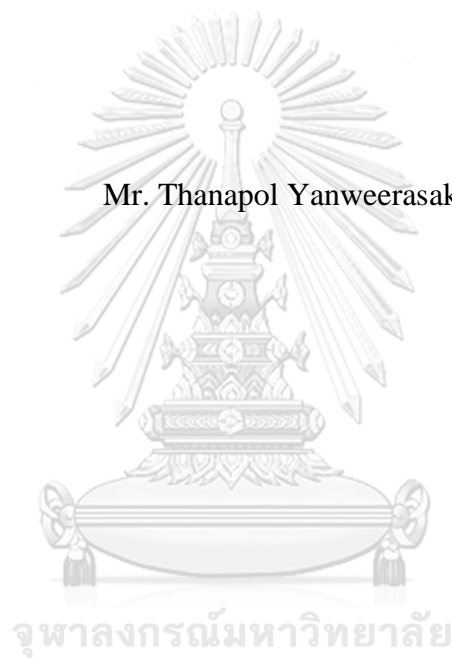


Life-Cycle Reliability Assessment of Existing RC Bridge Structures under Multiple Hazards Using Inspection Data

Mr. Thanapol Yanweerasak



บทคัดย่อและแฟ้มข้อมูลฉบับเต็มของวิทยานิพนธ์ตั้งแต่ปีการศึกษา 2554 ที่ให้บริการในคลังปัญญาจุฬาฯ (CUIR)
เป็นแฟ้มข้อมูลของนิสิตเจ้าของวิทยานิพนธ์ ที่ส่งผ่านทางบัณฑิตวิทยาลัย

The abstract and full text of theses from the academic year 2011 in Chulalongkorn University Intellectual Repository (CUIR) are the thesis authors' files submitted through the University Graduate School.

A Dissertation Submitted in Partial Fulfillment of the Requirements
for the Degree of Doctor of Philosophy Program in Civil Engineering
Department of Civil Engineering
Faculty of Engineering
Chulalongkorn University
Academic Year 2017
Copyright of Chulalongkorn University

การวิเคราะห์ความน่าเชื่อถือของวัฏจักรชีวิต โครงสร้างสะพานคอนกรีตเสริมเหล็กที่มีอยู่ภายใต้
ภาวะภัยที่หลากหลายด้วยข้อมูลจากการตรวจสอบ



วิทยานิพนธ์นี้เป็นส่วนหนึ่งของการศึกษาตามหลักสูตรปริญญาวิศวกรรมศาสตรดุษฎีบัณฑิต
สาขาวิชาวิศวกรรมโยธา ภาควิชาวิศวกรรมโยธา
คณะวิศวกรรมศาสตร์ จุฬาลงกรณ์มหาวิทยาลัย
ปีการศึกษา 2560
ลิขสิทธิ์ของจุฬาลงกรณ์มหาวิทยาลัย

| | |
|-------------------|---|
| Thesis Title | Life-Cycle Reliability Assessment of Existing RC Bridge Structures under Multiple Hazards Using Inspection Data |
| By | Mr. Thanapol Yanweerasak |
| Field of Study | Civil Engineering |
| Thesis Advisor | Associate Professor Withit Pansuk, Ph.D. |
| Thesis Co-Advisor | Professor Mitsuyoshi Akiyama, Ph.D. |

Accepted by the Faculty of Engineering, Chulalongkorn University in
Partial Fulfillment of the Requirements for the Doctoral Degree

..... Dean of the Faculty of Engineering
(Associate Professor Supot Teachavorasinskun, Ph.D.)

THESIS COMMITTEE

..... Chairman
(Professor Thanyawat Pothisiri, Ph.D.)

..... Thesis Advisor
(Associate Professor Withit Pansuk, Ph.D.)

..... Thesis Co-Advisor
(Professor Mitsuyoshi Akiyama, Ph.D.)

..... Examiner
(Sawekchai Tangaramvong, Ph.D.)

..... Examiner
(Associate Professor Jaroon Rungamornrat, Ph.D.)

..... External Examiner
(Ali Awaluddin, Ph.D.)

ชนพล ญาณวีรศักดิ์ : การวิเคราะห์ความน่าเชื่อถือของวัฏจักรชีวิตโครงสร้างสะพานคอนกรีตเสริมเหล็กที่มีอยู่ภายใต้ภาวะภัยที่หลากหลายด้วยข้อมูลจากการตรวจสอบ (Life-Cycle Reliability Assessment of Existing RC Bridge Structures under Multiple Hazards Using Inspection Data) อ.ที่ปริกษาวิทยานิพนธ์หลัก: รศ. ดร. วิจิต ปานสุข, อ.ที่ปริกษาวิทยานิพนธ์ร่วม: ศ. ดร. มิตชีโยชิ อะกิยาม่า, 132 หน้า.

การศึกษานี้แนะนำเสนอวิธีการประเมินความน่าเชื่อถือของวัฏจักรชีวิตโครงสร้างสะพานคอนกรีตเสริมเหล็กที่มีอยู่ภายใต้ภาวะภัยที่หลากหลาย ความน่าเชื่อถือของวัฏจักรชีวิตโครงสร้างคานสะพานภายใต้น้ำหนักบรรทุกจากการจราจรและการกักร่อนของเหล็กเสริมเนื่องจากคลอไรด์ในอากาศจะถูกนำไปเปรียบเทียบกับความน่าเชื่อถือของวัฏจักรชีวิตของตอม่อสะพานภายใต้แรงกระทำจากแผ่นดินไหวและการกักร่อนของเหล็กเสริมเนื่องจากคลอไรด์ในอากาศ เมื่อต้องการที่จะประเมินความน่าเชื่อถือของวัฏจักรชีวิตโครงสร้างสะพานคอนกรีตเสริมเหล็กที่มีอยู่ ข้อมูลที่ได้จากการตรวจสอบโครงสร้างเพื่อที่จะทราบปริมาณการกักร่อนของเหล็กเสริมในปัจจุบันจะถูกนำมาพิจารณา ตัวแปรสุ่มต่างๆที่ใช้ในการประมาณปริมาณการกักร่อนของเหล็กเสริมจะถูกปรับปรุงด้วยวิธีการจำลองแบบซีเคเวนเซียล มอนติคาร์โล เพื่อให้ผลการประมาณปริมาณการกักร่อนสอดคล้องกับปริมาณการกักร่อนที่ได้จากการตรวจสอบ การปรับปรุงนี้ส่งผลให้การวิเคราะห์ความน่าเชื่อถือของวัฏจักรชีวิตโครงสร้างสะพานมีความถูกต้องและแม่นยำมากขึ้น การเปรียบเทียบผลของความน่าเชื่อถือของคานสะพานและตอม่อสะพานสามารถช่วยให้วิศวกรหรือผู้ที่เกี่ยวข้องสามารถตัดสินใจและจัดลำดับความสำคัญในการดำเนินการบำรุงรักษาส่วนของโครงสร้างที่จำเป็นต้องดำเนินการก่อนได้ โดยผลของการวิเคราะห์ความน่าเชื่อถือของวัฏจักรชีวิตขององค์ประกอบทั้งสองของโครงสร้างสะพานภายใต้ภาวะภัยที่หลากหลายและการใช้ผลจากการตรวจสอบโครงสร้างได้ถูกนำเสนอและอภิปรายผลในการศึกษานี้

ภาควิชา วิศวกรรมโยธา

สาขาวิชา วิศวกรรมโยธา

ปีการศึกษา 2560

ลายมือชื่อนิติศ

ลายมือชื่อ อ.ที่ปริกษาหลัก

ลายมือชื่อ อ.ที่ปริกษาร่วม

5871450521 : MAJOR CIVIL ENGINEERING

KEYWORDS: LIFE-CYCLE RELIABILITY, STEEL CORROSION, INSPECTION DATA, MULTIPLE HAZARDS, UPDATING

THANAPOL YANWEERASAK: Life-Cycle Reliability Assessment of Existing RC Bridge Structures under Multiple Hazards Using Inspection Data.
 ADVISOR: ASSOC. PROF. WITHIT PANSUK, Ph.D., CO-ADVISOR:
 PROF. MITSUYOSHI AKIYAMA, Ph.D., 132 pp.

This study presented a novel methodology to estimate the life-cycle reliability of existing reinforced concrete (RC) corroded bridges under multiple hazards. The life-cycle reliability of a bridge girder under traffic load and airborne chloride hazards was compared with that of a bridge pier under seismic ground motion and airborne chloride hazards. When predicting the life-cycle reliability of existing RC corroded bridges, inspection results could be used to estimate the current material corrosion level. Random variables associated with the estimation of time-variant steel weight loss will be updated to be consistent with the given inspection results by using Sequential Monte Carlo Simulation (SMCS). This updating process can help to conduct reliability assessment more precisely. Comparing life-cycle reliabilities among the bridge components under multiple hazards can help decision maker to determine the priority of intervention and/or maintenance actions possible. The life-cycle reliabilities of two bridge components under multiple hazards using inspection results were presented and discussed.

Department: Civil Engineering

Field of Study: Civil Engineering

Academic Year: 2017

Student's Signature

Advisor's Signature

Co-Advisor's Signature

ACKNOWLEDGEMENTS

I would like to express my gratitude to all of those who helped me during the conducting research and writing my thesis. A special acknowledgement should be mentioned to Associate Professor Withit Pansuk who is my supervisor for his constant encouragement and guidance. He has guided me through all the stages of my research and thesis. Without his consistent and illuminating instruction, this thesis could not be achieved. And I also would like to say thank you very much to Professor Mitsuyoshi Akiyama, who is my co-supervisor, he always give me several good ideas and suggestions to conduct the research and he is a big supporter to help my journal until it can be finally published. Second, I am obliged to my lab mates who helped me to overcome cross-culture life and very tough work. I could not imagine how I could conduct my research without their full cooperation. My big thank would go to my beloved family for their loving care and great confidence in me for years. I also owe my sincere gratitude to my friends who share their time to discuss and help me work out the problems and difficulty during my research. Lastly, my research and journal was supported by the 100th Anniversary Chulalongkorn University Fund for Doctoral Scholarship and the 90th Anniversary of Chulalongkorn University Fund (Ratchadaphiseksomphot Endowment Fund).

CONTENTS

| | Page |
|--|------|
| THAI ABSTRACT | iv |
| ENGLISH ABSTRACT..... | v |
| ACKNOWLEDGEMENTS | vi |
| CONTENTS..... | vii |
| LIST OF FIGURES | ix |
| LIST OF TABLES..... | xiv |
| CHAPTER 1 INTRODUCTION | 1 |
| CHAPTER 2 LITERATURE REVIEWS | 6 |
| 2.1 Corrosion Process of Steel Rebar in Concrete..... | 6 |
| 2.2 Parameter affecting Steel Corrosion in Reinforced Concrete (RC) Structure | 7 |
| 2.3 Relationship between Steel Corrosion on Concrete Structure and Properties of Concrete | 9 |
| 2.4 Properties of Concrete Cover and Thickness..... | 9 |
| 2.5 Modelling of Steel Corrosion Process | 12 |
| 2.6 Spatial Distribution of Steel Corrosion..... | 14 |
| 2.7 Effect of Steel Corrosion on Structural Capacity of RC structures | 19 |
| 2.8 Reliability Assessment of RC Bridge Structures Subjected to Steel Corrosion | 24 |
| 2.9 Role of Inspection Information provided by Existing RC Structures..... | 26 |
| 2.10 Threshold Reliability for Assessing the Safety Level of Existing RC Structures | 28 |
| CHAPTER 3 RESEARCH OBJECTIVES | 30 |
| CHAPTER 4 LIFE CYCLE RELIABILITY ASSESSMENT OF EXISTING CORRODED REINFORCED CONCRETE (RC) BRIDGES UNDER MULTIPLE HAZARDS USING INSPECTION DATA | 31 |
| 4.1 Procedures for Estimating the Life-Cycle Reliability of Corroded RC Bridges..... | 31 |
| 4.1.1 Flowchart for Estimating Life-Cycle Reliability of Existing RC Bridges | 31 |
| 4.2 Loading and Environmental Hazards Assessment (Part B in Figure 12) | 35 |

| | Page |
|---|------|
| 4.3 Prediction of Structural Capacity using Section Analysis (Part A in Figure 12)..... | 40 |
| 4.4 Hazard Assessment Associated with Airborne Chloride and Estimation of Time-Variant Steel Weight Loss (Part C in Figure 12)..... | 41 |
| 4.5 Estimation of Average and Variance of Steel Weight Loss by Incorporating a Spatial Variability of Steel Corrosion..... | 44 |
| 4.6 Updating Based on Inspection Result by using SMCS | 57 |
| CHAPTER 5 ILLUSTRATIVE EXAMPLE | 59 |
| 5.1 Analyzing the Configuration of an RC Pier and a PC Girder..... | 59 |
| 5.2 Structural Fragility and Degradation of Structural Performance..... | 61 |
| 5.3 Results of Hazard Assessment..... | 62 |
| 5.4 Assumed Inspection Results | 64 |
| 5.5 Results and Discussion | 71 |
| CHAPTER 6 CONCLUSIONS | 116 |
| CHAPTER 7 FUTURE RESEARCH WORK..... | 117 |
| REFERENCES | 122 |
| VITA..... | 132 |

LIST OF FIGURES

| | |
|---|----|
| Figure 1 Existing corroded RC bridge located in an aggressive environment (Photograph was taken by Mitsuyoshi Akiyama)..... | 2 |
| Figure 2 Corrosion process of steel rebar in concrete..... | 6 |
| Figure 3 Effect of water-cement ratio on time to initiation of steel corrosion | 8 |
| Figure 4 Description of steel corrosion process in two identical RC structures with different crack width (Berke 1993)..... | 12 |
| Figure 5 Steel corrosion processes of RC structures (Melchers 2008)..... | 13 |
| Figure 6 Occurrence of steel corrosion crack | 14 |
| Figure 7 X-ray configuration | 16 |
| Figure 8 Configuration of RC specimen for capturing the X-ray picture..... | 17 |
| Figure 9 Spatial distributions of steel weight losses of RC specimens (Lim et al., 2016, 2017) | 18 |
| Figure 10 Effects of steel corrosion on RC members | 19 |
| Figure 11 Effect of steel corrosion on bond strength..... | 21 |
| Figure 12 Flowchart for estimating life-cycle reliability of existing RC bridges.. | 32 |
| Figure 13 Relationship between cumulative failure probability (P_f) and reliability index (β)..... | 35 |
| Figure 14 Data collection locations to observe amount of airborne chloride in Japan | 38 |
| Figure 15 Relationship between amount of airborne chlorides (mdd) and distance from coastal line (km) (Akiyama 2012)..... | 38 |
| Figure 16 Estimation of the average steel weight loss and variance using discrete inspection results (adapted and extended from Yanweerasak et al. (Yanweerasak 2016))..... | 44 |
| Figure 17 X-ray configuration | 45 |
| Figure 18 Configuration of the RC beam specimen for capturing the X-ray picture | 46 |
| Figure 19 Process of taking X-ray from different viewing angles (Lim 2017) | 46 |
| Figure 20 X-ray image of the corroded steel bar at $\theta_1 = 0^\circ$ (a) before and (b) after enhancement | 48 |

| | |
|--|----|
| Figure 21 X-ray image of a 5-mm (a) non-corroded bar and (b) corroded bar | 48 |
| Figure 22 Steel weight losses along the length of specimen A..... | 50 |
| Figure 23 Steel weight losses along the length of specimen B..... | 50 |
| Figure 24 Steel weight losses along the length of specimen C..... | 51 |
| Figure 25 Steel weight losses along the length of specimen D..... | 51 |
| Figure 26 Steel weight losses along the length of specimen E..... | 52 |
| Figure 27 Inspection locations of steel weight loss along a plastic hinge of an RC pier and the region of a PC girder with the maximum bending moment..... | 52 |
| Figure 28 Relationship between the semi-variance and lag distance | 54 |
| Figure 29 Relationship between the steel weight loss (%) and inspected length .. | 55 |
| Figure 30 Flowchart of reliability estimation using SMCS | 58 |
| Figure 31 Structural details of the RC pier analyzed in this study | 60 |
| Figure 32 Structural details of the PC girder analyzed in this study | 60 |
| Figure 33 Seismic fragility curves of the RC pier with the various amount..... | 61 |
| Figure 34 Flexural degradation of the PC girder due to steel weight losses..... | 62 |
| Figure 35 Seismic hazard curves of Niigata City, Sendai City, and Uwajima City..... | 62 |
| Figure 36 CDF of an annual maximum bending moment due to traffic loading simulation..... | 63 |
| Figure 37 Amount of steel weight loss in each inspection location for the RC pier | 65 |
| Figure 38 Amount of steel weight loss in each inspection location for the PC pier in Niigata City..... | 66 |
| Figure 39 Amount of steel weight loss in each inspection location for the RC pier | 67 |
| Figure 40 Amount of steel weight loss in each inspection location for the PC girder | 68 |
| Figure 41 Amount of steel weight loss in each inspection location for the RC pier | 69 |
| Figure 42 Amount of steel weight loss in each inspection location for the PC girder | 70 |

| | |
|--|----|
| Figure 43 Relationship between the steel weight loss (%) and the time after construction (years) for RC pier at $d=0.1$ km | 71 |
| Figure 44 Relationship between the steel weight loss (%) and the time after construction (years) for RC pier at $d=0.5$ km | 71 |
| Figure 45 Effect of distance from the coastal line on seismic reliability of the RC pier | 73 |
| Figure 46 Comparison of seismic reliabilities of the RC piers among Niigata City, Sendai City, and Uwajima City | 74 |
| Figure 47 Relationship between the steel weight loss (%) and the time after construction (years) for the PC girder at $d=0.1$ km | 75 |
| Figure 48 Relationship between the steel weight loss (%) and the time after construction (years) for the PC girder at $d=0.5$ km | 75 |
| Figure 49 Relationship between life-cycle reliability and time after construction (years) for the PC girder in Niigata City | 76 |
| Figure 50 Relationship between life-cycle reliability and time after construction (years) for the PC girder in Sendai City | 76 |
| Figure 51 Relationship between life-cycle reliability and time after construction (years) for the PC girder in Uwajima City | 77 |
| Figure 52 Comparison of life-cycle reliabilities for the PC bridge girder among Niigata City, Sendai City, and Uwajima City | 78 |
| Figure 53 Semi-variogram relation for Case NG4 | 79 |
| Figure 54 Semi-variogram relation for Case SP5b | 79 |
| Figure 55 Semi-variogram relation for Case NG7b | 80 |
| Figure 56 Kriging steel corrosion trend for Case NG4 | 81 |
| Figure 57 Kriging steel corrosion trend for Case SP5b | 81 |
| Figure 58 Kriging steel corrosion trend for Case NG7b | 82 |
| Figure 59 Relationship between updated steel weight loss (%) and time after construction (years) for the RC pier in Niigata City | 86 |
| Figure 60 Relationship between updated steel weight loss (%) and time after construction (years) for the RC pier in Sendai City | 87 |
| Figure 61 Relationship between updated steel weight loss (%) and time after construction (years) for the RC pier in Uwajima City | 88 |

| | |
|---|-----|
| Figure 62 Relationship between updated seismic reliability and time after construction (years) for the RC pier in Niigata City | 90 |
| Figure 63 Relationship between updated seismic reliability and time after construction (years) for the RC pier in Sendai City..... | 91 |
| Figure 64 Relationship between updated seismic reliability and time after construction (years) for the RC pier in Uwajima City | 92 |
| Figure 65 Relationship between updated steel weight loss (%) and time after construction (years) for PC girder in Niigata City..... | 94 |
| Figure 66 Relationship between updated steel weight loss (%) and time after construction (years) for PC girder in Sendai City..... | 95 |
| Figure 67 Relationship between updated steel weight loss (%) and the time after construction (years) for PC girder in Uwajima City..... | 96 |
| Figure 68 Relationship between updated life-cycle reliability and time after construction (years) for the PC girder in Niigata City | 98 |
| Figure 69 Relationship between updated life-cycle reliability and time after construction (years) for the PC girder in Sendai City..... | 99 |
| Figure 70 Relationship between updated life-cycle reliability and time after construction (years) for the PC girder in Uwajima City | 100 |
| Figure 71 Correlation between random variables x_3 and x_5 | 102 |
| Figure 72 Comparison between reliabilities of the RC pier and the PC girder at Niigata City..... | 105 |
| Figure 73 Comparison between reliabilities of the RC pier and the PC girder at Niigata City..... | 105 |
| Figure 74 Comparison between reliabilities of the RC pier and the PC girder at Sendai City..... | 106 |
| Figure 75 Comparison between reliabilities of the RC pier and the PC girder ... | 106 |
| Figure 76 Comparison between life-cycle reliabilities of the RC pier and the PC girder | 107 |
| Figure 77 Comparison between life-cycle reliabilities of the RC pier and the PC girder..... | 107 |
| Figure 78 Comparison between updated reliabilities of the RC pier and the PC girder | 108 |

| | |
|--|-----|
| Figure 79 Comparison between updated reliabilities of the RC pier and the PC girder | 108 |
| Figure 80 Comparison between updated reliabilities of the RC pier and the PC girder | 109 |
| Figure 81 Comparison between updated reliabilities of the RC pier and the PC girder | 110 |
| Figure 82 Comparison between updated reliabilities of the RC pier and the PC girder | 110 |
| Figure 83 Comparison between updated reliabilities of the RC pier and the PC girder | 111 |
| Figure 84 Comparison between updated reliabilities of the RC pier and the PC girder | 112 |
| Figure 85 Comparison between updated reliabilities of the RC pier and the PC girder | 112 |
| Figure 86 Comparison between updated reliabilities of the RC pier and the PC girder | 113 |
| Figure 87 Flowchart for estimating life-cycle reliability of existing RC bridges structure including the improvement of inspection process | 119 |
| Figure 88 Flowchart explaining the experimental plan for improving the inspection process | 120 |

LIST OF TABLES

| | |
|--|-----|
| Table 1 Reliability Classification for Different Reference Periods according to EN1990 2002 | 28 |
| Table 2 Threshold reliability index in accordance with ISO/DIN 2394 (1998) | 29 |
| Table 3 List of random variables | 43 |
| Table 4 Lists of parameters for predicting amount of airborne chloride | 63 |
| Table 5 Details of the inspection process of the RC pier in Niigata City | 65 |
| Table 6 Details of the inspection process of the PC girder in Niigata City | 66 |
| Table 7 Details of the inspection process of the RC pier in Sendai City | 67 |
| Table 8 Details of the inspection process of the PC girder in Sendai City | 68 |
| Table 9 Details of the inspection process of the RC pier in Uwajima City | 69 |
| Table 10 Details of the inspection process of the PC girder in Uwajima City | 70 |
| Table 11 Semi-variogram parameters | 80 |
| Table 12 Average and variance of steel weight loss for the RC pier in Niigata City | 83 |
| Table 13 Average and variance of steel weight loss for the PC girder in Niigata City | 83 |
| Table 14 Average and variance of steel weight loss for RC pier in Sendai City ... | 83 |
| Table 15 Average and variance of steel weight loss for PC girder in Sendai City | 84 |
| Table 16 Average and variance of steel weight loss for RC pier in Uwajima City | 84 |
| Table 17 Average and variance of steel weight loss for PC girder in Uwajima City | 84 |
| Table 18 Times at which maintenance action is required at Niigata City | 105 |
| Table 19 Times at which maintenance action is required at Sendai City | 106 |
| Table 20 Times at which maintenance action is required at Uwajima City | 107 |
| Table 21 Times at which maintenance action is required at Niigata City (with inspection results) | 109 |
| Table 22 Times at which maintenance action is required at Sendai City | 111 |
| Table 23 Times at which maintenance action is required at Uwajima City | 113 |

CHAPTER 1

INTRODUCTION

The structural performance of reinforced concrete (RC) bridges deteriorates over their service life due to various mechanical stressors and/or multiple hazards (Frangopol 2011, Akiyama 2014). Structural deterioration strongly depends on the specific environmental hazards which vary in time and space. Therefore, it is difficult to accurately predict the deterioration of structural performance of RC structures under uncertainties. Considering the uncertainties in a systematic way requires the application of reliability concepts and methods to estimate long-term structural performance (Ellingwood 2005, Frangopol 2011, Frangopol 2016).

Life-cycle reliability concepts have become an important research topic in the structural engineering community over the past few decades (Frangopol 1997, Frangopol 2008). They provide significant information for estimating the life-cycle performance of bridges over their service life. The reliability approach is one of the most important components of life-cycle engineering. The main objective of life-cycle engineering is to help decision makers determine when, where, and how to spend bridge funds to preserve public safety and maintain existing infrastructure (Estes 2003). Bridge structures normally deteriorate due to aging, mechanical stressors, and aggressive environments. The combined effects of these factors necessitate the use of life-cycle assessment, including performance prediction models, deterioration model, inspection and/or monitoring process, maintenance plan, and cost and integrating uncertainty.

Steel corrosion is considered as the most important problem on deterioration of RC bridges. Many studies have studied to predict the effects of the propagation of steel corrosion on structural performance. For example, Akiyama et al. (Akiyama 2012) presented a methodology for probabilistic hazard assessment associated with airborne chloride for estimating the time-variant steel weight loss for RC structures located in a marine environment. They found that the reliability of RC bridge significantly decreased as an increasing of amount of steel weight loss. Within the last few decades, several models used for evaluating the reliability of corroded RC structures have been proposed. Mori and Ellingwood (Mori 1993) and Frangopol et al. (Frangopol 1997) proposed reliability-based service life assessments for corroded RC girders and investigated the effects of steel corrosion on the flexural reliability of RC girders. Stewart and Rosowsky (Stewart 1998) assessed the time-dependent reliability of deteriorating RC bridge superstructures, examining the effect of de-icing salts and atmospheric exposure in marine environments on the long-term deterioration of RC bridge superstructures. Enright and Frangopol (Enright 1999) proposed a reliability-based condition assessment for deteriorating concrete bridges that considered the load distribution. They investigated the influence of resistance degradation and post-failure load distribution, and compared the performance of several system models in determining existing T-beam bridge reliability. Choe et al. (Choe 2009) developed probabilistic models for the seismic demands of reinforced concrete bridges subject to corrosion, and conducted a seismic fragility assessment considering model uncertainties associated with the predictions of seismic demand, seismic capacity and material corrosion. Akiyama et al. (Akiyama 2011) examined the life-cycle reliability

of RC piers under seismic and airborne chloride hazards. Ghosh et al. (Ghosh 2014) discussed the influence of traffic loading on the seismic reliability assessment of bridges; however, they did not account for the effect of steel corrosion on bridge performance.



Figure 1 Existing corroded RC bridge located in an aggressive environment (Photograph was taken by Mitsuyoshi Akiyama)

Few previous studies have incorporated inspection results into evaluations of the life-cycle reliability of corroded RC structures exposed to multiple hazards. Figure 1 shows a corroded RC bridge located in a seismic-prone region with an aggressive environment associated with chloride attack and high traffic demands. It is difficult to determine how long such a corroded RC structure will maintain its structural reliability beyond threshold levels even if inspection results are available. Inspection results depend on the location of a structure because of the spatial features associated with the material deterioration. Although structural capacity estimation must integrate modeling of the spatial variability in steel corrosion based on inspection results from various locations, it is difficult to determine the likely spatial distribution of steel corrosion in an existing RC structure. In turn, this makes it difficult to estimate the reliability of an existing structure. Inspection results from existing corroded RC bridge structures exposed to multiple hazards can be used to evaluate the life-cycle reliability of bridge superstructures and piers; the results can help identify the components with the lowest reliability and determine whether maintenance actions are necessary.

Inspection information from existing structures has been widely used in life-cycle assessment. This information can provide an indication of the material deterioration of structures (Okasha 2012, Zhu 2013, Soliman 2014). Inspection and maintenance actions are used to reduce the uncertainties associated with prediction models (Zheng 1998). Inspection results are generally used for intervention planning (e.g., maintenance, repair, rehabilitation, or replacement) for existing structures (Frangopol

2008). Estes et al. (Estes 2003) applied visual inspection results to provide an updated reliability of highway-bridge based on bridge management systems. Frangopol et al. (Frangopol 2008) examined the utility of monitoring data for the development of a prediction model and presented a bridge reliability assessment based on monitoring data. Akiyama et al. (Akiyama 2010) established a procedure for updating multiple random variables based on inspection results using Sequential Monte Carlo Simulation (SMCS) and applied it to existing RC slabs in a marine environment. Although the difficulty of finding a solution using Bayesian updating depends on the relationships between observed physical quantities and the probability density functions (PDFs) of related random variables, SMCS can be applied even if nonlinear relations or non-Gaussian variables are involved. Yanweerasak et al. (Yanweerasak 2016) used inspection results indicating the spatial variability of steel corrosion to update a seismic reliability of existing RC bridge piers.

If maintenance is not performed, structural reliability will decrease until the safety threshold is reached (Frangopol 2016). Reliability assessments using inspection results help a determination when and where maintenance actions should be performed. Bridge components (e.g., piers, girders, decks, and abutments) are affected by multiple hazards. Therefore, the various maintenance actions and types (essential or preventive maintenance) for each bridge component must be prioritized (Barone 2013, Barone 2014, Barone 2014).

For existing RC structures located in severe chloride attack environments, the effect of the distribution of spatial steel corrosion on structural performance must be considered. Shafei and Alipour (Shafei 2015) presented a stochastic field approach for estimating the variability of initiation corrosion time by incorporating spatial and temporal uncertainties. Darmawan and Stewart (Darmawan 2007), Stewart ((Stewart 2004), and Stewart and Suo (Stewart 2009) investigated the effect of spatial variability of pitting corrosion on the reliability of RC structures. They suggested that the spatial variability of pitting corrosion can lead to a significant decrease in structural reliability. Neglecting localized steel corrosion can lead to overestimation of structural reliability (Stewart 2004) (Marsh 2007) (Marsh 2008). Kashani et al. (Kashani 2013) investigated the buckling behavior of corroded bars; their results indicated that a 10% mass loss will result in an approximately 20% reduction in the buckling capacity of corroded bars; non-uniform distribution of pitted sections can also change the buckling mechanism of the corroded bars. Based on these results, they developed a probabilistic distribution model for the geometrical properties of corroded rebars. Statistical analysis of steel corrosion patterns data showed that a lognormal distribution model could represent the non-uniform distribution of pitted cross-sections along the corroded bars. Ghosh and Sood (Ghosh 2016) proposed a seismic fragility assessment model for deteriorating bridges by considering realistic pitting steel corrosion and time-dependent capacity distributions under chloride attack conditions. Comparison between the proposed methodology and the simple uniform corrosion model indicated that the simple model significantly underestimated system level fragility; additionally, pitting corrosion had a greater impact on the seismic response of bridge components in both the transverse and longitudinal directions. It is important to include modeling of spatial variability in steel corrosion in structural capacity estimation. If parameters reflecting the spatial distribution of steel corrosion are available, the spatial distribution in steel corrosion of existing RC bridges can be estimated using the statistical estimation error evaluation

theory proposed by Honjo and Otake (Honjo 2013) Lim et al. (Lim 2016) (Lim 2017) presented experimental results in which they used X-ray technology to visualize steel corrosion in RC beams. The non-uniform steel corrosion distribution over an RC beam was determined using X-rays, from which parameters that reflect the spatial distribution of steel corrosion distribution were inferred.

This study presents a methodology for estimating the life-cycle reliability of existing corroded RC bridges under multiple hazards using inspection results. This study proposed a procedure for updating seismic reliability of a RC pier and updating reliability of a girder using inspection results associated with steel weight loss. The RC bridge consists of two main components (piers and girders) and both are subject to different hazards. This study present the novel methodology using a reliability framework for (1) conducting life-cycle reliability assessment of existing bridge pier and girder under multiple hazards using inspection data, the spatial variability of steel corrosion are incorporated to estimate the amount of steel weight loss provided by inspection data (2) identifying the component with the lowest reliability between the bridge components; (3) determining hazard that most threaten the structural safety; and (4) determining a time at which the maintenance actions are needed for bridge component. The proposed framework provides decision makers relevant information regarding priorities for upgrade and/or repair. To compare the reliability of bridge piers exposed to seismic and airborne chloride hazards with that of bridge girders exposed to traffic and airborne chloride hazards, the performance functions of bridge piers and girders are defined considering the recovery time from the event. The reliability of the piers and girders is determined by incorporating the distribution of spatial corrosion estimated from inspection results into SMCS. Previous experimental results that used X-rays to visualize corroded RC beams (Lim 2016) (Lim 2017) are used to reproduce the parameters in the stochastic field. The hypothetical RC bridge structure in the illustrative example is used to estimate life-cycle reliability. The reduced uncertainties after updating using SMCS are discussed. The effects of hazard intensities, and frequency and interval of inspection results, on life-cycle reliability are discussed.

Based on the inspection process used in the current reliability framework in this study, inspection location, interval of inspection location and time of conducting inspection process are assumed. In the final part of this paper, the flowchart presenting how to improve the inspection process for RC structures is presented. It is important to regularly assess the condition of the RC structures to know when they must proceed to some maintenance or reparations. The inspection process must be correctly conducted while keeping the cost/benefit ratio within reasonable limits. This flowchart consists of two main further experiments. One of the experiments is presented in this paper. The experimental investigation associated with a concrete cover quality is conducted. This experimental program is designed to determine the relationship between a spatial variability of concrete cover quality and that of amount of steel weight loss. The spatial variability of concrete cover quality is measured by non-destructive test (NDT) methods consisting of Ultra-Sonic Pulse Velocity (UPV), air permeability test, and water permeability test. The investigation is performed on 5 RC beams (single reinforcement) with have a difference in concrete strength and compaction state on the concrete cover. The RC beams are corroded by electrical accelerating steel corrosion process. The estimation of steel weight loss in longitudinal rebar within RC beams is conducted by X-rays technology and image processing. The spatial variability of concrete cover

quality measured by the three NDT tests, correlation between the NDT tests and its effectiveness, and relationship between NDT tests results and amount of steel weight losses are discussed in this study.



CHAPTER 2

LITERATURE REVIEWS

2.1 Corrosion Process of Steel Rebar in Concrete

Concrete is an alkaline material under exposure condition. The high alkalinity in concrete (pH is approximately 12.0-13.0) form a passive film around a surface of the reinforcing steel bar embedded in concrete content (John P 2006), this film help to protects the steel corrosion process. When the passive film layer around the reinforcing steel bar is destroyed by lowering in pH due to ingress of carbonation and chloride, steel corrosion will start. Steel corrosion is an electrochemical process. The electrochemical corrosion cells consist of anode, cathode. Electrolyte must be formed for steel corrosion. A moist reinforced concrete environment fulfills the requirements to form the electrochemical cell by providing an electrolyte in the form of aqueous medium and the anode/cathode in the form of the steel reinforcement. During the steel corrosion process, anodic and cathodic reactions occur. At the anode, the iron is oxidized releasing two electrons, which are transferred to the cathode where these electrons along with water reduced the oxygen (Weters 1998).

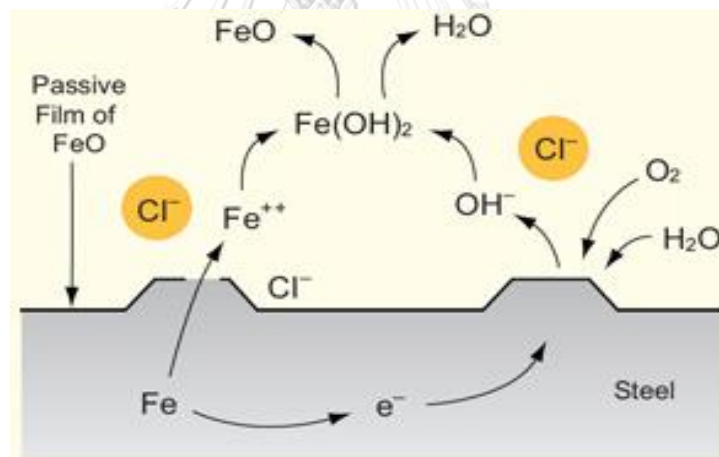


Figure 2 Corrosion process of steel rebar in concrete

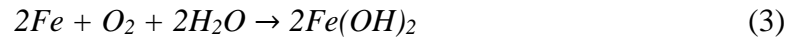
Steel corrosion in concrete is an electrochemical process. Figure 2 shows a mechanism of steel corrosion in concrete. For reinforcing steel rebar in concrete, as the passive film is damaged, the metallic, Fe at the anode is oxidized to form “ferrous ions (Fe^{2+})”



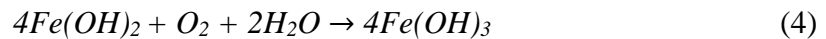
The above reaction is balanced by cathodic reaction of dissolved oxygen (O_2) and then “hydroxyl ions (OH^-)” are formed.



Two equal speed of reaction, $Fe(OH)_2$ can be generated from the following reaction formula;



Due to dissolved oxygen, it will be oxidized to $Fe(OH)_3$;



The presence of dissolved oxygen and water is mainly factors causing the steel corrosion. Therefore, concrete permeability will be significant factor affecting the steel corrosion. If oxygen and water are not available at cathodic side, the steel corrosion process will be stopped (Weters 1998). As shown in Figure 2, the steel corrosion process is occurred by current flow within closed loop. The electrical current within steel rebar is the electrons flowing from anode to cathode area. An external current will flow through the solution and concrete pore around the steel rebar. This external current consist of hydroxide ion (negative charged) moving from anode to cathode, and also ferrous ions (positive charged) moving from cathode to anode. It is essential to know that water inside the concrete pores is a dilute solution of alkali and calcium hydroxides. If the concrete is dense, it means the pores are not well inter-connected, the ions flow in the pores will be difficult.

2.2 Parameter affecting Steel Corrosion in Reinforced Concrete (RC) Structure

The steel corrosion will not begin until the passivation film which protects the steel rebar from the corrosion process is destroyed. It is related to the pH of the concrete pore solution, which is adversely affected by the presence of chloride ions. Therefore, steel corrosion will not initiate until a chloride concentration is reached the critical threshold value. Properties of concrete will affect steel corrosion through their influences the pore solution, and environmental factors cannot directly affect the steel corrosion processes, but they cause the deterioration of the concrete cover and accelerate the ingress of aggressive species, making the pore solution in contact with the steel more corrosive.

2.2.1 Chloride

Chloride ions from external environment are the main factor of initiation of steel corrosion (Akiyama 2012). Chloride ions firstly accumulate at the concrete surface and then ingress through concrete cover until reach to surface of steel rebar. When it is absorbed on the local passive film, it can cause a significantly decreasing in the PH value. Therefore the process that passive film is destroyed start, then the steel rebar is gradually corroded and finally, the steel rebar will losses their weight.

2.2.2 Water to Cement Ratio (W/C) of Concrete

Dense concrete can prevent the ingress of water and chloride to slow the steel corrosion process. Low W/C cause to have a stronger, denser, and high permeability in concrete. Figure 3 shows the example of steel corrosion initiation time (in days) for steel rebar embedded in concrete specimens made with different W/C ratios of 0.40,

0.45, 0.50, and 0.65 and exposed to the chloride environment (5% NaCl solution, the concrete cover is 25mm) (Rasheeduzzafar 1992).

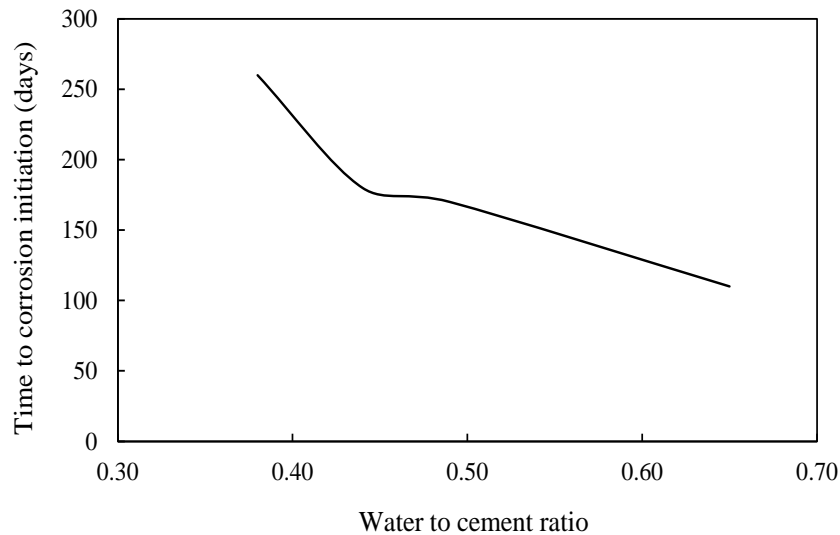


Figure 3 Effect of water-cement ratio on time to initiation of steel corrosion (Rasheeduzzafar 1992)

2.2.3 Environmental Conditions

Environmental conditions have great effect on the steel corrosion. Airborne chloride particles from seawater wound up into the air by the force of the wind and transport to the concrete structures at the coastal area causing severe damage to the embedded rebar in the concrete. Japan is an island country and most of the infrastructures are concentrated in the marine environment (Akiyama 2012). There is a large open by season chloride that is stored in the concrete surface under the influence of winter sea states, the volume of salt spray is much larger in winter compared with that of in summer. In addition, chloride by splashing differs depending on the distance from the coastal line. Chloride in the concrete surface rapidly decreases when the distance from the coastal line is farther away.

2.2.4 Crack

When the total amount of steel corrosion products reaches the critical value, the internal expansion stress will exceed the tensile strength of concrete and cause the cracking in the concrete cover. When corrosion crack is occurred, the chloride ions can penetrate easier into the surface of steel rebar and steel corrosion starts more quickly. The diffusion coefficient of the chloride ion is also increased rapidly (Nakagawa 2004) (Qi 2001).

2.3 Relationship between Steel Corrosion on Concrete Structure and Properties of Concrete

2.3.1 Mechanical Structure of Concrete

The corrosion of RC structure is totally different with the corrosion in exposed metal because the effect of concrete cover, protecting the steel rebar. Concrete cover is both physical and chemical barrier from external environment. The important function of concrete cover is used as a protective coating, the effectiveness depend on chemical composition and physical properties of the concrete. Main physical properties are total porosities, pores size distribution, and inter-connected pores that depend on the degree of hydration (Mindess 1981, Mehta 1993). The structure in concrete matrix is much denser and much permeable than the paste made by higher W/C . The concrete with high W/C , not only the total porosity is higher, but also there are higher numbers of inter-connected pores. However, it does not mean that concrete with low W/C can prevent the steel corrosion process, an enough compaction and workability in order to prevent a defects at the surface or inside the concrete content are needed. Proper field practice is very important to have a good concrete cover quality (Powers 1958).

2.3.2 Chemistry of Concrete related to Steel Corrosion Process

The hydration products of cement mainly consist of two components; 1) calcium hydroxide, $Ca(OH)_2$ (relatively large size) and 2) calcium silicate hydrate, $C-S-H$ (very small size). When concrete sets, the residual mix water is enclosed in the pores. When the curing process starts, some of this water is used up to form hydration products. Depending on the external exposure and the concrete permeability, it may be added by additional water from outside. Pores water is not the pure water, it always contains dissolved ions provided by cement. Therefore, it calls pore solution.

After several days of the hydration reaction, the pore solutions of concrete usually contain alkali and hydroxide ions in the high concentration, along with much smaller concentration of calcium and sulphate ions, and others. The OH^- ion concentration is ordinarily quite high, usually between 0.5 and 1.0 molar. If the concrete partially dry, concentration can be higher. PH related to these high concentrations of OH^- are approximately 13. The exact PH in concrete pores solution is affected by many factors that are the alkali content of the cement and the richness in cement. Other factors such as W/C ratio, the extent which alkalis have leached out of the concrete immersed in water, and the extent which alkalis have reached with aggregate components to form stable insoluble reaction products may also influence the PH value.

The ion of greatest concern is the chloride ion, Cl^- . Chloride has the property of destabilizing the passivating film surrounding the steel rebar, if chloride content has a sufficient high concentration. This effect causes the problem of steel corrosion in concrete (Browne 1980) (Hausman 1967).

2.4 Properties of Concrete Cover and Thickness

The time required to depassivate (passive film was destroyed) the steel rebar then the corrosion reactions starts, and the rate of corrosion reactions will happen, both depend on the properties of the concrete cover. The chloride ions penetrating through the concrete cover into the vicinity of steel rebar is controlled by the concrete cover

quality. Especially, they depend on the cover depth and the properties of the cover, i.e. moisture content, cracking, pores structure, the nature of the cement, and degree of hydration. The time required to initiation of steel corrosion by chloride penetration should be higher than the expected life of the structure (Browne 1980).

After steel corrosion process has been started, its rate will depend on the properties of the concrete cover. The rate is controlled by the availability of dissolved oxygen at the cathodic areas. Steel corrosion process is the rate of diffusion of oxygen through the concrete cover from external environment. The concrete in the vicinity of the steel rebar provide paths for the ionic current between the anodic and cathodic areas of the steel surface if corrosion is to be continued. The rate that a current can transport is expressed in term of the electrical resistivity of concrete, which is a function of physical and chemical property. To understand the effects of the concrete cover, three different condition of concrete cover need to be taken into consideration. These consist of a) uncracked concrete cover, b) cracked concrete cover, and c) defect in concrete cover other than cracks.

2.4.1 Uncracked Concrete Cover

Uncracked concrete cover is a barrier to the diffusion of Cl^- ions. The diffusion process is much related to the pore structure in concrete. Cl^- ions diffuse as ions in the solution. Hence, the chloride penetration occurs only through the aqueous solution within concrete pores. Cl^- diffusion into concrete happens when the activity of the dissolved ions in the external environment is greater than the same activity in the concrete pore. It is difference in activity providing the driving force for diffusing of chloride. Activity in physical-chemical terms is in term of concentration. Therefore, the driving force induced the chloride diffusion is the difference in concentration of the species outside of concrete and that of within the concrete pores. The chloride diffusion is always explained by Fick's law (Diamond 1986).

For chloride-induced corrosion, the depassivation process will start and steel corrosion will start when the concentration in concrete pore adjacent to steel surface reaches the critical value. After the steel corrosion has started, its rate is controlled by the flux of oxygen diffusing to the steel surface. The consumption rate of oxygen in the cathodic area is equal to the diffusing rate of oxygen. The diffusion coefficient is not a constant, it depends on temperature, diffusing substance, and the nature of material. Chloride diffusion process occurs primarily through the concrete pores component, sometimes it also occurs in the interfacial region between cement paste and aggregate. For the dense concrete with low W/C ratio, the pores are generally discontinuous and the diffusion path is very tortuous. Therefore, the diffusion coefficient is low. For concrete with high W/C ratio, the cement paste will have more porosity and the pores size is larger and have much interconnected pore. Therefore, the diffusion coefficient is larger.

The concrete cover quality is assessed by the water permeability under pressure. Such permeability tests measure the steady-state flow rate of water under a constant pressure head through a concrete specimen. The coefficient of permeability, K , is calculated from D'Arcy's Law (Anon 1982).

$$\frac{dq}{dt} = KAH / h \quad (5)$$

where dq/dt is the rate of water flow. A is the cross-sectional area. K is the coefficient of permeability in unit of m/s. H is the water pressure head in meters. h is the thickness of the concrete in meters.

Actually, the situation which the water permeability of the concrete is directly related to steel corrosion process occurs when chloride-containing-water penetrates into a dry concrete under pressure. Another mechanism which chloride can penetrate into concrete is by capillary absorption.

After depassivation process has started and the steel corrosion process commence, an ionic current is induced to pores in concrete cover surrounding the steel rebar. The resistance to the current flow, called the electrical resistivity, is normally influenced by three factors; the concrete pore structure, the degree of saturation, and the composition of pores solution. Concrete with low W/C ratio affect to have a low pore volume which have a few available way for transporting of ion and will have higher electrical resistivity than concretes with higher W/C ratio. Concretes with low W/C generally have smaller pores and pores which are more easily isolated by growth of hydration product. Therefore, the electrical resistivity is much higher over what are expected from the effect of reduced porosity alone. If the electrical resistance of the concrete is high, the extent of current flow per unit time is low. The steel corrosion rate can be limited by electrical resistivity (Martin 1969, 224 1994)

2.4.2 Cracked Concrete Cover

Load-induced cracking is an important characteristic of RC structures, since the maximum tensile strain that the concrete can resist without cracking must be expected to efficiently perform by steel rebar. Concrete cover must be expected to be cracked to a greater or lesser extent and in considering the practical effect of the concrete cover on steel corrosion. One must consider the effects of crack in the concrete cover. The steel corrosion itself causes the cracking on the concrete cover. The extent and effects of corrosion-induced cracks will be considered separately in the subsequent section on the steel corrosion damage.

Cracks in concrete cover generally provide three effects: a) they tend to generate the initiation of steel corrosion by easy way for chloride ions penetration, b) they accelerate the steel corrosion rate by reducing the barrier for diffusion of oxygen, c) they produces non-uniformity in the physical and chemical environment around the steel rebar. The effects of cracks are proportional to their widths. The wider cracks provide easier way for penetrating of aggressive substances. The overall effects of cracks with different widths are explained in Figure 4, for two identical RC structures with different crack width. The time to initiation of steel corrosion is significantly shorter for the wider cracks (concrete A) but the steel corrosion rate after depassivation process are not much affected by crack width. At time t_2 , steel corrosion has started for the structure with wider cracks, but still not occurs in the structure with narrow cracks. At time t_3 , there is steel corrosion in both structures and the extent of steel corrosion is not very different (Martin 1969). One another important factor is crack width ordinarily measured at only the outer surface of the concrete cover. This is not mentioned to the width on the inner surface of concrete cover in contact with the steel rebar (Berke 1993).

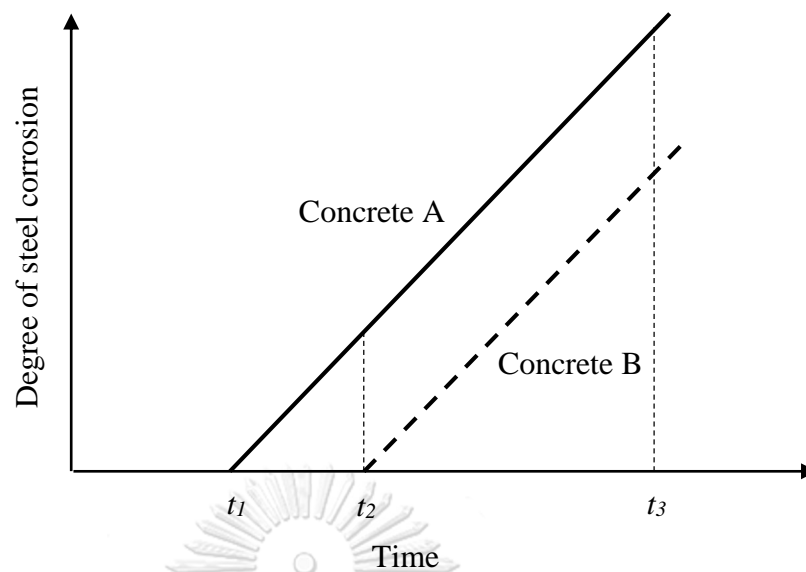


Figure 4 Description of steel corrosion process in two identical RC structures with different crack width (Berke 1993)

2.4.3 Defect in Concrete Cover other than Cracks

Defects in concrete cover other than cracks related to steel corrosion are classified within the concrete cover itself or separation between steel and concrete. Ideally, the mix design of the concrete should be able to form a dense layer. However, other defects in the concrete cover result from several aspects. Insufficient compaction resulting from inadequate vibration is not uncommon. Concrete mixes with too large a maximum aggregate size or insufficient content of fine aggregate cause a honeycombing. Bleeding in concrete normally provides water pockets which will be trapped under coarse aggregate and even under the steel rebar itself.

The presence of gaps in the concrete cover significantly reduces its effectiveness as a barrier to chloride diffusion and causes the de-passivation process to occur earlier. Separations between the steel rebar and the surrounding concrete have greater harmful effects. Areas of steel rebar not in contact with the concrete, where passivating films will not be formed since the pH of the local solution is not high enough, the steel corrosion process can start immediately. Insufficient cover depth is also a very important factor causing a faster steel corrosion process, since chloride ions can penetrate through the concrete cover in a shorter time, the time to initiation of steel corrosion will be shorter (Browne 1979).

2.5 Modelling of Steel Corrosion Process

2.5.1 Initiation of Steel Corrosion

The chloride concentration must reach a critical threshold value to cause the dissolution of the protective passive film around the steel rebar. The deterioration of RC structures in a salt-damage environment can be considered as the destruction of the passive film of steel rebar by chloride penetration. According to Fick's second law, the chloride concentration C from different concrete cover depths x from the surface at time t can be presented as (Tsutsumi 1996, Sasani 1997).

$$C(x,t) = C_0 + (C_s - C_0) \left\{ 1 - \operatorname{erf} \left[\frac{x}{2\sqrt{D_c t}} \right] \right\} \quad (6)$$

where $C(x,t)$ is the chloride concentration of concrete at x depth at time t . C_0 is the initial chloride concentration (%) of concrete. C_s is the surface chloride concentration of concrete. D_c is the coefficient of diffusion of chloride. $\operatorname{erf} (*)$ is the error function.

When chloride ions accumulate until it exceeds the critical value, the passive film on the steel rebar surface begins to destroy and steel corrosion occurs on the local surface of steel rebar. Due to the accumulation of steel corrosion products, localized cracking is induced in concrete. At this state, a large area of concrete cracks due to expansion of steel corrosion products; the steel corrosion accelerates and steel weight decreases, resulting in decreasing a structural safety performance.

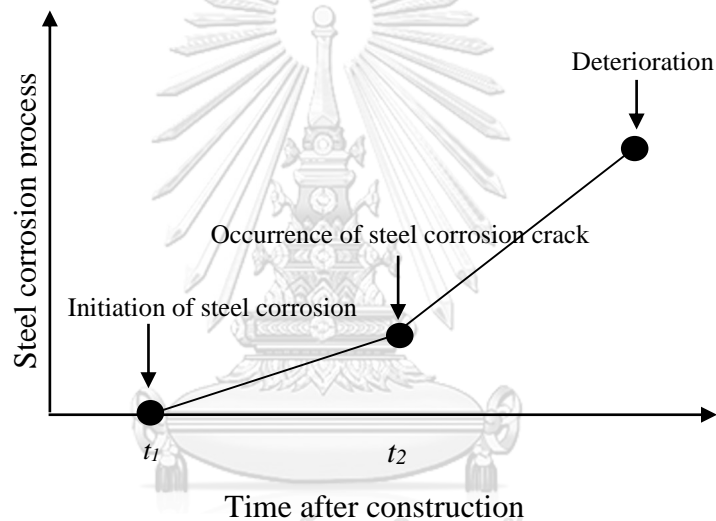


Figure 5 Steel corrosion processes of RC structures (Melchers 2008)

2.5.2 Occurrence of Steel Corrosion Cracking

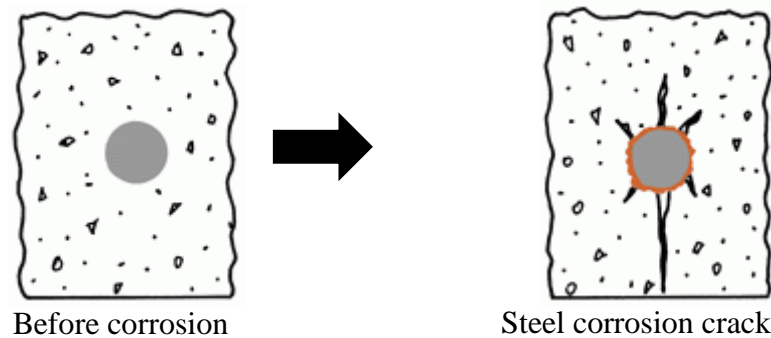


Figure 6 Occurrence of steel corrosion crack

Steel corrosion products are gradually accumulated. The expansion of steel rebar diameter due to the corrosion product will cause tensile stress in surrounding concrete cracks on the concrete cover (Weters 1998), since the tensile stress exceeds the maximum tensile strength of concrete. Figure 6 shows the formation process of crack induced-steel corrosion. The deterioration of RC structures due to salt-damage is rapidly accelerated after the occurrence of cracks.

To estimate the critical threshold of chloride concentration at the occurrence of steel corrosion cracking, cylinder model proposed by Qi and Seki (Qi 2001) are widely used indicate the relationship between critical threshold of corrosion (Q_{cr}) associated with crack initiation. By considering concrete cover, diameter of steel rebar, compressive strength of concrete etc., a modified formulation can be expressed as follow;

$$Q_{cr} = \frac{\rho}{\pi(\gamma - 1)} \left\{ \alpha_0 \beta_0 \frac{0.22[(2c + d)^2 + d^2]}{E(c + d)} f_c^{2/3} + \alpha_1 \beta_1 \frac{(c + d)}{(5c + 3d)} w_c \right\} \quad (7)$$

where Q_{cr} is the critical threshold of steel corrosion associated with crack initiation. ρ is the steel density. γ is the expansion rate of the volume of corrosion. c is the concrete cover depth. f_c is the concrete strength. w_c is the crack width due to the corrosion of the steel rebar. E is the modulus of elasticity of concrete. d is the diameter of the steel rebar. α_0 , α_1 , β_0 and β_1 are the coefficients related to the effects of the concrete cover, steel bar diameter and concrete strength respectively.

2.6 Spatial Distribution of Steel Corrosion

Steel corrosion process is strongly related to both chloride and carbonation diffusion. The iron-oxide compounds are formed during steel corrosion process usually known as brown rust. These compounds have much bigger volume than the metal itself and cause an expansive pressure into the surrounding concrete. This cause a cracking and concrete spalling at concrete cover before excessive loss of cross-sectional area. Structural performances associated with general steel corrosion are reduced due to decreasing in bond strength between the steel rebar and surrounding concrete.

Pitting steel corrosion is a localized corrosion. Pitting steel corrosion is occurred only from diffusion of chloride ion and not from diffusion of carbonation. The compounds formed during pitting steel corrosion are different with those formed in general steel corrosion. These compounds provide a lower volumetric expansion than the compounds formed for general steel corrosion. Therefore, there is less tendency of concrete cover spalling due to pitting steel corrosion. On the other hand, excessive loss of cross-section of the steel bar will occur without any obviously visible deterioration. RC structures with pitting steel corrosion shows a reduced strength and ductility due to the reduction in the tensile strength of steel rebar.

In actual material deterioration is spatial and temporal behavior especially steel corrosion process. General steel corrosion process causes the expansive rust products, loss of cross-sectional area, and reduction of bond strength. Spatial variability of steel corrosion is common in steel rebar subjected to chloride-induced corrosion. This can affect highly localized loss of cross section which can be very harmful to structural safety since loss of cross-sectional area are higher in the localized area than general steel corrosion process.

Recently, spatial variability of steel corrosion damage has been studied (Li 2004) (Malioka 2004) (Vu 2005). This work has focused on corrosion-induced concrete cover cracking, and not on spatial variability of pitting steel corrosion. However, Stewart (Stewart 2004) modelled the spatial effect of pitting steel corrosion on the structural reliability of RC beams in flexure capacity, and Val (Val 2005) extended this work to include a shear failure behavior. They proposed a stochastic model of pitting steel corrosion for a simply supported RC beam. The model used extreme value theory to predict the maximum pit depth as a function of rebar diameter and rebar length. It was found that when the spatial variability of pitting steel corrosion was considered in the analysis, it cause an increased the failure probability by approximately 70%. Shafei and Alipour (Shafei 2015) presented a stochastic field approach for estimating the variability of initiation corrosion time by incorporating spatial and temporal uncertainties. For corroded RC structures located in an aggressive environment, the effect of the spatial steel corrosion distribution over their steel rebar on the structural performance must be taken into consideration. The capacity of structural ductility and energy dissipation strongly depends on the steel corrosion level in the localized zone. Val (Val 2007) presented a reliability analysis to investigate the effects of general and pitting steel corrosion on the flexural and shear behavior of RC beams. Difference in steel corrosion rates were considered in the reliability analysis. The results showed that higher steel corrosion rates had a significant effect on the behavior of corroded beams and at these corrosion rates, pitting steel corrosion had a more effect on the behavior of the beams as compared to those with general steel corrosion. The results also showed that in case of pitting steel corrosion at higher steel corrosion rates, the shear failure becomes the dominant type of failure. Kashani et al. (Kashani 2013) investigated the buckling behavior of corroded bars; their results indicated that a 10% mass loss will result in an approximately 20% reduction in the buckling capacity of corroded bars; non-uniform distribution of pitted sections can also change the buckling mechanism of the corroded bars. Based on these results, they developed a probabilistic distribution model for the geometrical properties of corroded rebars. The modelling of the spatial variability of steel corrosion must be integrated into the estimation of the structural

capacity and structural reliability analysis (Marsh 2007) (Marsh 2008) (Akiyama 2011) (Lim 2017).

2.6.1 Visualization of Corroded Steel Rebar in RC Member using X-ray Technology and Digital Image Processing

For existing RC structures located in an aggressive environment, the effect of spatial steel corrosion distribution on the structural performance must be considered. The spatial variability in the steel corrosion must be integrated into the estimation of amount of steel weight loss and a structural capacity. Recently, X-ray techniques have been applied to visualize concrete cracking in order to investigate the behavior of the fracture process zone in the concrete (Akiyama 2011). Lim et al. (Lim 2016) (Lim 2017) presented the experimental results of the visualization of steel corrosion in RC members using X-ray technologies to understand the non-uniform steel corrosion distribution over the RC component. Figures 6 and 7 show the X-ray apparatus and RC specimens tested, respectively. An RC beam was corroded by electrical process using power supply. As indicated in Figure 8, the locations for taking X-ray images photographs start from distances of 250 to 1090 mm with 14 times of 60 mm interval from the left side of the specimen.

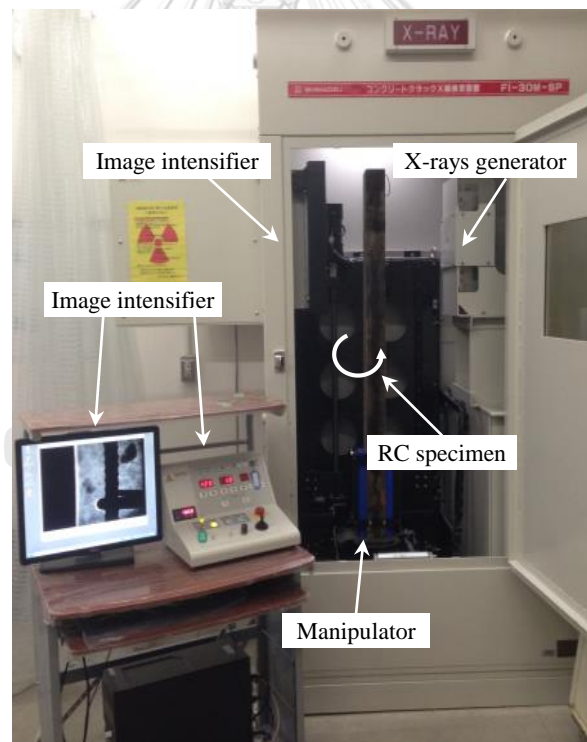


Figure 7 X-ray configuration

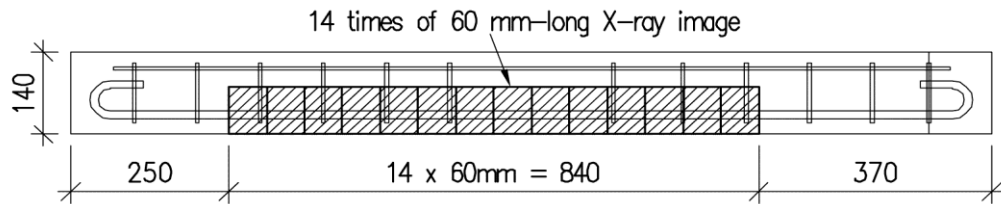
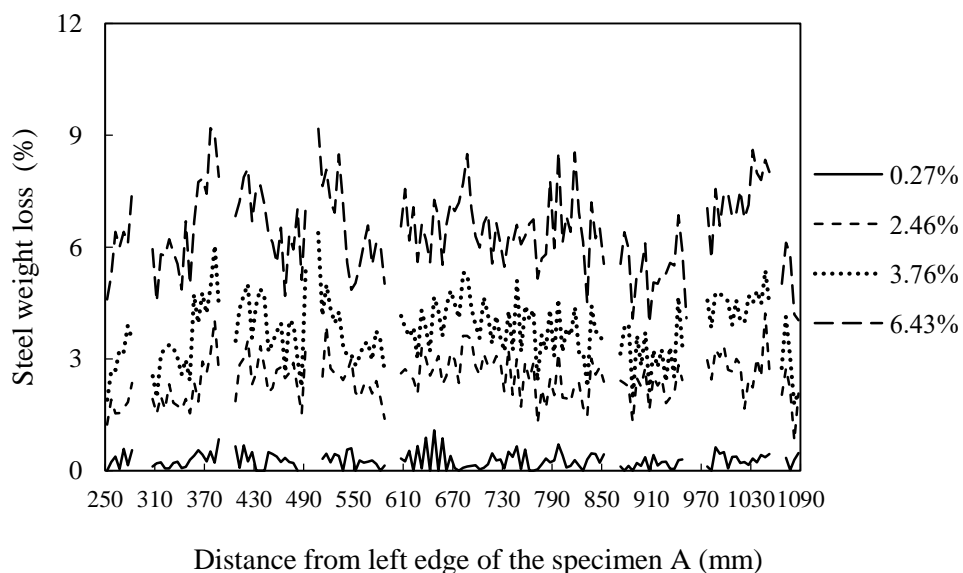


Figure 8 Configuration of RC specimen for capturing the X-ray picture
(all dimensions are in mm)

The example of steel corrosion distributions taken by X-ray photograph, as shown in Figure 9 could be used to reproduce a spatial variability of steel corrosion to estimate the average and variance of steel weight loss. Figure 9 demonstrates the relationship between the distance from the left edge of the RC specimen and the local steel weight loss of the longitudinal rebar. The local steel weight loss was calculated by the volume of the sound steel rebar estimated by X-ray. The difference between the maximum and minimum steel weight loss ranges from 10 to 15%, independent of the steel corrosion level. Based on the experimental result shown in Figure 9 by using statistical tools (semi-variogram and kriging interpolation), the parameters to reproduce spatially distributed steel corrosion can be determined. Further research needs to be investigated that what is the main factors and properties of concrete cover causing the spatial corrosion distribution. Also, the spatial variability of concrete cover quality associated with steel corrosion distribution must be investigated. Since concrete cover quality totally affect the capability of chloride diffusion that generating the initiation of steel corrosion and variation in amount of steel corrosion.



Distance from left edge of the specimen A (mm)

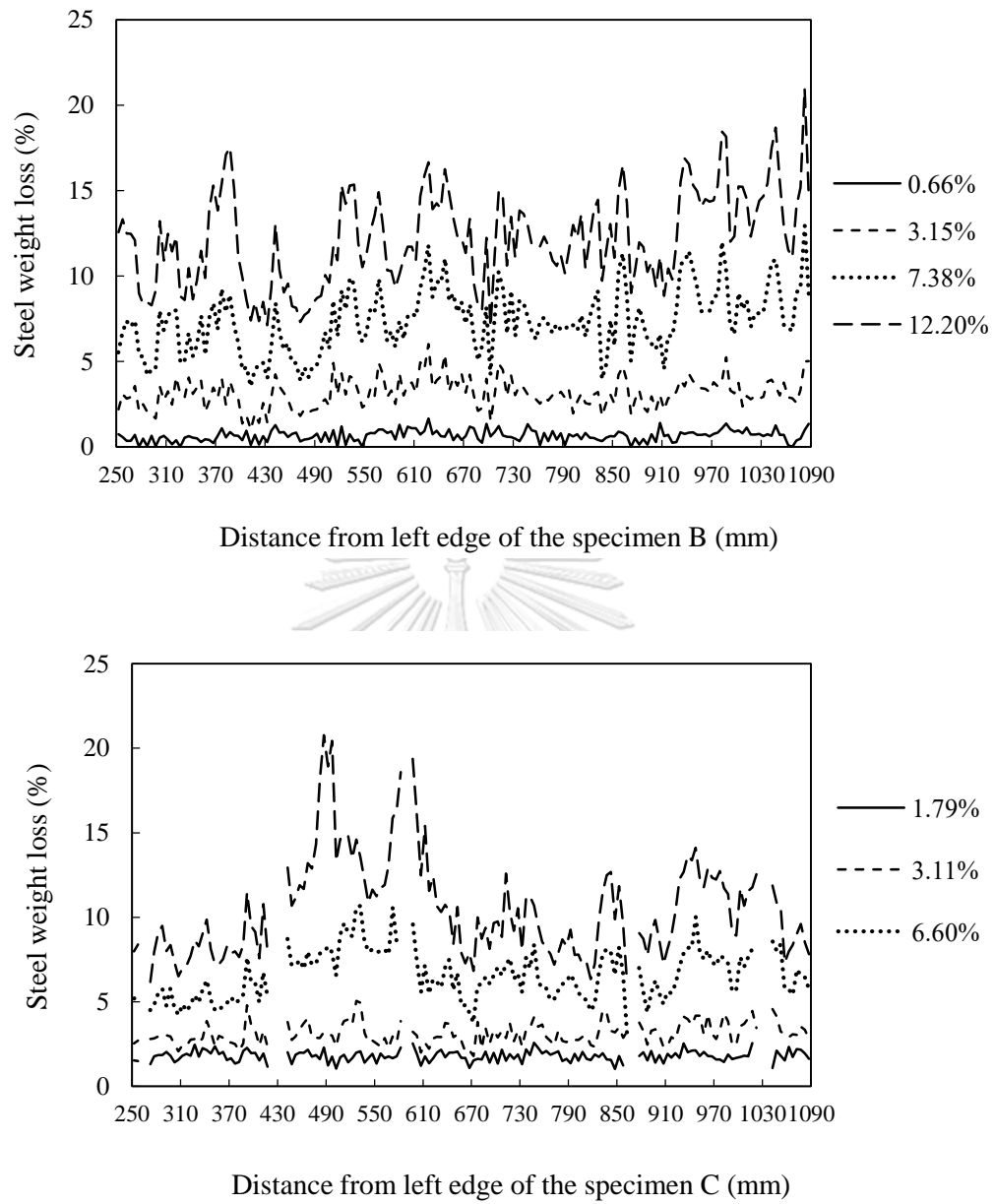


Figure 9 Spatial distributions of steel weight losses of RC specimens (Lim et al., 2016, 2017)

2.7 Effect of Steel Corrosion on Structural Capacity of RC structures

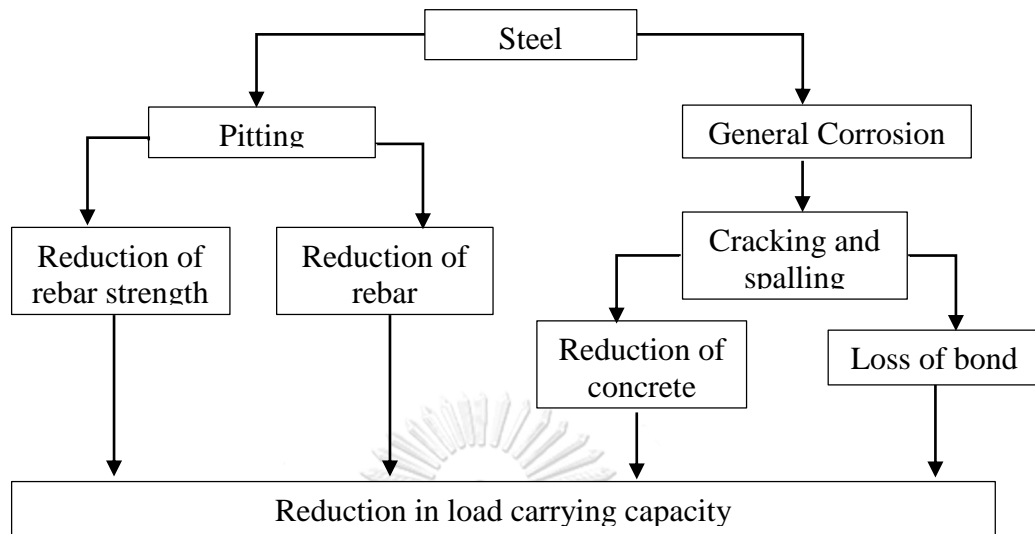


Figure 10 Effects of steel corrosion on RC members

RC structures have a limited service life. The durability of concrete structures depends on the resistance of the concrete against the chemical and physical factors to protect the embedded reinforcement against corrosion. Corrosion affects the behavior of reinforced concrete structures by loss of area in steel rebar, cracking and spalling of concrete cover and loss of bond between steel and concrete. The pitting steel corrosion leads to a reduction in the cross-sectional area of the bar resulting in a reduced load carrying capacity. The general steel corrosion results in cracking and spalling of concrete cover, which causes the loss of bond between the steel and concrete and consequently a reduction in concrete section. Figure 10 summarizes the effects of corrosion on load carrying capacity of RC member.

2.7.1 Flexural Capacity

Several studies have been proposed to investigate the effects of steel corrosion on flexural capacity of RC members. It is reported that the main reasons of degradation of flexural capacity due to steel corrosion are reduction of cross-sectional of reinforcing bars, decreasing of stiffness of concrete section due to the cracking and degradation of bond strength. Al-Sulaimani et al. (Al-Sulaimani 1990) investigated the effect of steel corrosion on the flexural strength of RC beams. It was observed that up to 1.5% corrosion level, there was no reduction in ultimate flexural strength however there was a reduction in flexural strength with further increase in corrosion levels (12% reduction at 5% corrosion level). Al-musallam et al. (Al-Sulaimani 1990) conducted experimental investigation to determine the effects of corrosion on the behavior of corroded slabs. It was found that steel corrosion changed the failure mode from flexure in the control slabs to bond-shear failure in the corroded slabs. Reduction in the ultimate flexural strength was also observed; 25% and 60% reduction in ultimate strength for 5% and 25% corrosion level, respectively. Mangat and Elgarf (Mangat 1999) investigated the effect of corrosion on flexural strength of RC beams. A significant reduction in the ultimate flexural capacity was identified (75% reduction in flexural strength for 10% steel corrosion). The models for estimating the residual flexural capacity of corroded

RC beam has been proposed (Torres-Acosta AA 2007). The average corrosion penetration, maximum concrete surface crack width, and the maximum pit depth were estimated for corroded RC beams. The obtained results showed that 1) a decreasing of 60% in the flexure capacity was observed with 10% of the ratio between average corrosion penetration and rebar radius; 2) the maximum pit depth is the most important parameter affecting flexural capacity reduction in corroded RC beam.

2.7.2 Shear Capacity

The effects of steel corrosion on shear capacity of RC members are not as well understood as the bond strength or flexural capacity. Several studies have been reported in the literature to investigate the effects of steel corrosion on shear strength of RC beams. Rodriguez et al. (Rodriguez 1997) conducted experiment to investigate the effects of steel corrosion on the load carrying capacity of reinforced concrete beams. After corroding the reinforcement (only the flexural or both the flexural and shear reinforcement) by an accelerated corrosion technique, the beams were tested in four-point bending with a shear span to height ratio of 4.0. It was observed that the mode of failure changes from bending to shear after the steel corrosion in beams with usual reinforcement and that pitting corrosion of the shear stirrups was the most significant factor in the reduction of the load carrying capacity of corroded beams. Val (Val 2007) conducted reliability analysis to investigate the effect of general and pitting corrosion on the flexural and shear behavior of reinforced concrete beams. Different corrosion rates were considered in the reliability analysis. The results of the analysis showed that higher corrosion rates had a significant effect on the behavior of corroded beams and at these corrosion rates pitting corrosion (especially pitting corrosion of stirrups) had a more pronounced effect on the behavior of the beams as compared to those with general corrosion. The results also showed that, in case of pitting corrosion, at higher corrosion rates the shear failure becomes the dominant type of failure.

The above two studies investigated the effects of general and pitting steel corrosion on the flexural and shear behavior of reinforced concrete beams. The results indicated that the reduction in shear capacity is higher as compared to reduction in flexural capacity under corrosion effects (especially pitting corrosion effects) as the beams that were designed to fail in flexure, failed in shear when subjected to corrosion effects. Cairns et al. (Cairns 1995) proposed analytical and experimental research to study shear strength of RC beams with exposed reinforcement. It was concluded that properly anchored reinforcement significantly contributed to strength of reinforced concrete even if it was exposed over the span and that the shear strength of the beams increased with exposed reinforcement. The author also proposed a method to calculate the shear strength of beams with portion of the reinforcement exposed.

A few studies have considered the effects of different levels of steel corrosion, whereas the steel corrosion induced degradation is directly associated with the steel corrosion levels. The findings were contradictory. Cairns et al. (Cairns 1995) found that shear strength increases with loss of bond between the longitudinal reinforcement and concrete while Jeppsson et al. (Jeppsson 2003) found that shear strength decreases with loss of bond between the longitudinal reinforcement and concrete. Raof and Lin (Raof 1997) reported that the increase or decrease in shear strength due to steel corrosion mainly depend on the a/d ratio of the beams. From the above it is evident that

further research must be done to investigate the effect of steel corrosion on the shear behavior of RC beams with different a/d ratios at different corrosion.

2.7.3 Bond Strength

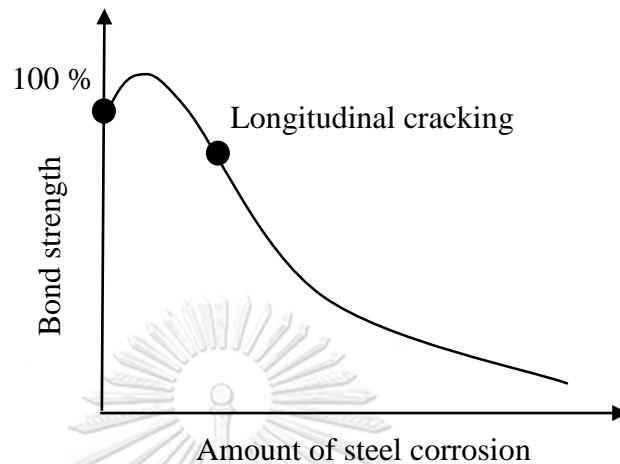


Figure 11 Effect of steel corrosion on bond strength

Bond is necessary to anchor reinforcement and to ensure composite interaction between steel and concrete. The reduction in confinement due to cracking of the concrete cover will lead to a progressive reduction in bond strength. Weakening of the bond is caused by development of a less firmly adhering interstitial layer of corrosion products between concrete and steel, and reduction in the steel ribs due to pitting. The effect of corrosion of the steel on the bond strength of reinforced concrete members has been investigated by many researchers and is relatively well understood. Several studies reported that the bond strength increases with a higher steel corrosion level until concrete cracks and then the bond strength starts decreasing with further increase in steel corrosion level (Almusallam 1996, Fang 2004, Bhargava 2007, Ouglova 2008). Figure 11 shows the typical change in bond strength with increase in steel corrosion level. It is also reported in the literature that the bond strength of unconfined steel bar is significantly lower than confined steel bar at the same steel corrosion level (Wang 2003).

2.7.4 Ductility Evaluation of Concrete Bridge Pier Subjected to Lateral Cyclic Loading

The onset of buckling of longitudinal rebars in RC bridge is a limit damage state. Severe deterioration of flexural capacity cause a rebar buckling and this require extensive repairs. Berry and Eberhand (Berry M. P. 2005) and Natio et al. derived three relationships linking plastic rotation, drift ratio, and displacement ductility with the onset of rebar buckling based on the results of plastic hinge analysis, moment curvature analysis, and effect of the confinement reinforcement. Kobayashi et al. (2006) proposed experimental results of RC columns with and without steel corrosion on longitudinal rebars subjected to cyclic loading. The result showed that cyclic loading cause a severe damage from spalling of concrete cover. Steel corrosion lead to cover cracking and debonding between cover concrete and steel rebar.

Relationship between the lateral load and displacement of RC bridge piers and predict the displacement at the onset of buckling of longitudinal rebars is presented as follow.

- Plastic Hinge Analysis

Evaluation of a displacement at the onset of a buckling of longitudinal rebar of RC column is proposed by Naito et al. (2011). Euler's critical stress of a rebar fixed between two supports is

$$\sigma_E = \frac{4\pi^2 EI}{L_B^2 A} \quad (8)$$

where E is modulus of elasticity of steel rebar; A is cross-sectional area; I is moment of inertia and L_B is buckling length of the rebar

In the RC column subjected to cyclic loading, buckling of longitudinal rebars are prevented by concrete cover and tie. Therefore, Euler's critical stress is not reached. Based on the equilibrium of moment at the midpoint of buckling length, Naito et al. (2006) presented the stress-strain relation ($\sigma - \varepsilon$) of buckling of longitudinal rebar.

$$\sigma = \frac{2(D/S)\sigma_t}{1.95N_B\sqrt{\varepsilon} + 2(D/S)} g(N_B) \quad (9)$$

$$g(N_B) = 1 + \frac{0.65\pi N_B}{16(D/S)A_r\sigma_t} (R_t + R_c) \quad (10)$$

where D is diameter of rebar; σ_t is tensile strength of rebar; A is cross-sectional area of rebar; S is tie spacing; N_B is number of spaces between ties within buckling length; and R_t and R_c are prevention force of tie and concrete cover, respectively for lateral deformation of longitudinal rebar.

$$R_t = Q_t f(N_B) \quad (11)$$

$$R_c = q_c N_B S \quad (12)$$

$$Q_t = a_t \sigma_t \quad (13)$$

$$q_c = 0.03\beta_1 d_c D \sigma_c^{2/3} \quad (14)$$

$$a_t = \begin{cases} N_t A_t / N_L & \text{if } N_L < 5 \\ N_t A_t / (0.2N_L + 4) & \text{if } N_L \geq 5 \end{cases} \quad (15)$$

$$f(N_B) = \begin{cases} (N_B^2 - 1)/N_B & \text{if } N_B \text{ is odd} \\ (N_B^2 + 2)/N_B & \text{if } N_B \text{ is even} \end{cases} \quad (16)$$

$$\beta_1 = 1 - 0.75(\varepsilon_{\max} / \varepsilon_c) \quad (17)$$

where A_t is cross-sectional area of tie; N_t is number of ties confining the longitudinal rebars perpendicular to direction of the load; N_L is number of longitudinal rebars perpendicular to direction of the load; d_c is distance from center of longitudinal rebar to the edge of cover; σ_t is yield strength of tie; σ_c and ε_c are compressive strength of concrete and strain at the compressive strength, respectively. ε_{\max} is strain at the compressive longitudinal rebars; and β_1 is reduction parameter affected by compressive strain on the reduction of compressive strength.

Buckling length of longitudinal rebar depends on the arrangement of reinforcements, cross-section size, and material properties of concrete and rebar. In the section analysis which column are subjected to axial load and cyclic load, the curvature ϕ_1 at the onset of longitudinal rebar are determined based on the numerical simulation using Equations 11 to 17 under the assumption that the stress-strain behavior of longitudinal rebar satisfies Menegotto-Pinto's model (Menegotto and Pinto, 1973).

$$\phi = -\frac{1}{180d'} \ln \left[\left(\frac{\sigma_y}{E} - \frac{\Delta\varepsilon_B}{100} \right) \left(\frac{2SN_B}{\pi D} \right)^2 - 0.0045 \right] + \frac{\Delta\varepsilon_B}{d'} \quad (18)$$

$$\Delta\varepsilon_B = \left[\frac{2(D/S)}{1.95N_B} \left(g(N_B) \frac{\sigma_t}{\sigma_y} - 1 \right) \right]^2 \quad (19)$$

where d' is distance from extreme compression longitudinal rebar to extreme tensile longitudinal rebar; and σ_y is yield strength of longitudinal rebar.

The total tip displacement of RC column, δ_u can be estimated from response to displacement at yielding δ_y and plastic deformation, δ_p . ϕ_u is ultimate curvature over the plastic hinge length, L_P . The total tip displacement is (Berry and Eberhard, 2005).

$$\delta_u = \delta_y + (\phi_u - \phi_y)L_P(h - L_P/2) \quad (20)$$

$$L_P = 0.5d + 0.05h \quad (21)$$

where h is shear span of RC column and d is effective depth of RC column.

Naito et al. (2011) presented the computed results showing the displacement at the onset of longitudinal rebar buckling presented by Equation (20) compared with the experimental results. Specimen with a large amount of steel weight loss of tie showed a brittle behavior after onset of longitudinal rebar buckling. However, the relationship between load and displacement of tip of RC column of the specimens before the onset

of rebar buckling presented ductile behavior. Therefore, regardless of amount of steel weight loss, the proposed equation can be used to predict the seismic displacement capacity accurately.

2.8 Reliability Assessment of RC Bridge Structures Subjected to Steel Corrosion

Bridge structures have played an important role for serving the economic, social and environmental welfare of nation. Bridge structures are deteriorated by aging effect (e.g., material corrosion), natural hazards (seismic hazard, airborne chloride hazard) and man-made hazard (traffic hazard). Reliability assessment has become more and more important over the past decades. It provides the significant information about the structural condition of bridge structures (Frangopol 2011). Reliability approach is one of the important parts of bridge management systems. The main objective of bridge management systems is to help engineers and other decision makers determine when and where to spend bridge fund in order to enhance public safety, preserve existing infrastructures and serve commerce (Estes 2003). Bridge structures are under deterioration due to aging, mechanical stressor, and aggressive environment. Under the combination of these factors, bridge management system associated with prediction models, inspection plan, repair, maintenance action plan, and cost models must be conducted effectively using life-cycle reliability concepts. Since the most bridge management systems decisions are made under the limited budget therefore optimization is an essential tool for proper life-cycle management (Okasha 2012). Optimization techniques are used for minimizing the life-cycle cost and maximizing the service life of structures (Barone 2013, Barone 2014).

Structural reliability methods have gained increasing prominence and are used to forecast life-cycle of structural performance over many decades of life (Estes 2003). Time-dependent reliability analysis needs a number of assumptions about loading conditions, structural resistance, and deterioration models. These models predict a future performance and are the basic for optimum inspection maintenance planning. Uncertainties associated with the prediction of structural performance, deterioration model, and inspection results should be considered in the proper life-cycle reliability assessment (Ang 2005) (Liu 2005). Although, there have been several model proposed for evaluating the structural performance of corroded RC structures.

Steel corrosion is generally considered to be the most important cause of RC bridge structure deterioration. Many studies have attempted to predict the effects of the propagation of steel corrosion on structural performance. For example, Akiyama et al. (Akiyama 2012) proposed a methodology for probabilistic hazard assessment associated with airborne chloride for estimating the time-variant steel weight loss of RC structures located in a marine environment. They found that the reliability of RC bridge structures significantly decreased as the amount of steel weight loss increased. Within the last few decades, several models used for evaluating the reliability of corroded RC structures have been proposed. The previous works on the life-cycle reliability assessment for seismic and flexural performance of RC structures are discussed as follow.

2.8.1 Seismic Reliability Assessment of RC Structures

The probabilistic assessment of RC structures under seismic hazard has been rapidly developed over the last two decades. Cornell et al. (Cornell 2002) and Yun et al. (Yun 2002) proposed a performance-based methodology for seismic risk assessment. Moreover, a structural seismic fragility curve considering the probability of exceedance of a specified damage state associated with seismic intensity has been established (Nielson 2007, Dong 2014). However, little attention has been dedicated to the assessment of the seismic reliability of corroded RC structures. The effect of steel corrosion must be considered in the life-cycle seismic reliability of a structure located in an aggressive environment because steel corrosion is the main factor decreasing structural capacity. Choe et al. (Choe 2009) analyzed the structural seismic fragility of an RC bridge subjected to corrosion. Ghosh and Padgett (Ghosh 2016) proposed time-dependent seismic fragility curves of multi-span continuous steel girder bridges accounting for variation in ground motion and corrosion parameters. However, their model associated with the deterioration of RC column due to steel weight loss needs to be improved. The effects of material corrosion on the seismic behavior of a typical RC bridge based on time-variant seismic capacity deterioration were addressed by Simon et al. (Simon 2010). These authors assumed that the steel corrosion is uniformly distributed over the entire structure and that reduced diameters of the rebar are used in the seismic analysis. This assumption is an oversimplification when estimating seismic capacity, notably ductile capacity. Berto et al. (Berto 2009) examined the seismic performance of existing RC structures affected by degradation phenomena, such as rebar diameter reduction and concrete cover degradation; however, they did not consider the interaction between the concrete and rebar degradation in the evaluation of the seismic capacity of a corroded RC structure.

Probabilistic methods for evaluating a deteriorated RC bridge subjected to chloride attacks have been proposed, and the life-cycle analysis of an RC structure based on a probabilistic framework has been presented (Prezzi 1996) (Frangopol 1997) (Val 2003). However, these frameworks did not include the structural reliability estimation for both seismic hazard and continuous deterioration. Akiyama et al. (Akiyama 2012) established a methodology for a probabilistic assessment associated with airborne chloride and Akiyama et al. (Akiyama 2010) proposed a procedure to calculate the time-variant steel weight loss for an RC structure located in a marine environment. The seismic demand depends on the results of the seismic hazard assessment, whereas the deterioration of the structural seismic capacity depends on the environmental hazard assessment. An RC structure located in a marine environment deteriorates with time due to chloride-induced corrosion of the reinforcing bars. Akiyama et al. (Akiyama 2011) presented a procedure to integrate the airborne chloride hazard into the life-cycle seismic reliability estimation for a new RC bridge pier.

2.8.2 Reliability Assessment associated with Flexural Performance of RC Structures

Within the last decades, several models used for evaluating the reliability of corroded RC girders and slabs have been proposed by many researchers. Reliability-based service life assessment of aging concrete girder was established by Mori et al. (Mori 1993). Reliability of reinforced concrete girders under the corrosion attack was proposed by Frangopol et al. (Frangopol 1997). The effects of corrosion on both

flexural and shear reliabilities of RC bridge T-girder are investigated. The results showed that under the same corrosion rate, the loss of structural reliability is generally larger than shear reliability. Stewart and Rowsky (Stewart 1998) presented time-dependent reliability of deteriorating reinforced concrete bridge decks. This study used the application of de-icing salts and atmospheric exposure in marine environment to investigate the long-term deterioration of RC bridge deck. Enright et al. (Enright 1999) proposed reliability-based condition assessment of deteriorating concrete bridge considering load distribution. They presented the influence of resistance degradation and post failure load distribution, and comparison of existing T-beam bridge reliability estimated for several system models. Saveswaran et al. (Saveswaran 2000) and Lawanwisut et al. (Lawanwisut 2001) presented reliability assessment of deteriorating RC beams. Based on the previous studies, the effect of steel corrosion on flexural performance is assumed as a uniform distribution over the entire structures by using the reduced cross-sectional area of steel rebar to evaluate the flexural capacity. This assumption is an oversimplification when estimating flexural capacity. Stewart et al. (Stewart 2004) and Stewart and Suo (Stewart 2009) presented the spatial effect of pitting corrosion on the reliability of RC beams. They strongly suggest that the inclusion of spatial variability of pitting corrosion can lead to significant decrease in flexural reliability. Darmawan and Stewart (Darmawan 2007) established time-dependent reliability analysis of corroding pre-stressed concrete bridge girders by considering the effect of pitting corrosion.

Based on the previous studies on both seismic reliability and reliability associated with flexural performance, the studies on the life-cycle reliability assessment of existing structures using monitoring and/or inspection information are scarce in the literatures. Estes and Frangopol (Estes 2003) presented updating highway bridge reliability based on bridge management systems by using visual inspection results. This study examined how visual inspection data can be used to update the reliability of bridge. Frangopol et al. (Frangopol 2008) presented bridge reliability assessment based on monitoring to demonstrate the use of monitored data for developing a prediction model. Akiyama et al. (Akiyama 2010) proposed updating the time-dependent reliability of RC bridge slab using inspection results (crack width and chloride concentration). Based on a lack of the studies on the updating life-cycle reliability of existing RC structures using inspection results, a determining that how long the corroded RC bridge structures will maintain the life-cycle reliability greater than the threshold are very difficult. The effective procedures for estimating the life-cycle reliability of existing RC structures using inspection results need to be presented.

2.9 Role of Inspection Information provided by Existing RC Structures

Inspection information from existing structures has been widely used in life-cycle engineering field. This information can provide an indication of the material deterioration of structures (Okasha 2012, Zhu 2013, Soliman 2014). Inspection and maintenance actions are necessary to reduce the uncertainties associated with prediction models (Zheng 1998). Inspection results are generally used for intervention planning (e.g., maintenance, repair, rehabilitation, or replacement) for existing structures (Frangopol 2008). Estes et al. (Estes 2003) used visual inspection results to provide an updated perspective on highway bridge reliability based on bridge management systems. Frangopol et al. (Frangopol 2008) examined the utility of monitoring data for

the development of a prediction model and presented a bridge reliability assessment based on monitoring data. Akiyama et al. (Akiyama 2010) established a procedure for updating multiple random variables based on inspection results using Sequential Monte Carlo Simulation (SMCS) and applied it to existing RC slabs in a marine environment. Although the difficulty of finding a solution using Bayesian updating depends on the relationships between observed physical quantities and the probability density functions (PDFs) of related random variables, SMCS can be applied even if nonlinear relations or non-Gaussian variables are involved.

If maintenance is not performed, structural reliability will decrease until the safety threshold is reached (Frangopol 2016). Reliability assessments that use inspection results can help determine when and where maintenance actions should be performed. Bridge components (e.g., piers, girders, decks, and abutments) are affected by multiple hazards. Therefore, the various maintenance actions and types (essential or preventive maintenance) for each bridge component must be prioritized.

Within the last decades, multiple procedures have been presented for updating the performance prediction models based on inspection results. Moan et al. (Moan 2000) proposed an approach to update the reliability of a system of fatigue critical details based on the results of the inspection of several components in the system. Akiyama et al. (Akiyama 2010) established a procedure to update the time-dependent reliability using visual inspection (i.e., crack width and chloride concentration) that is updated by sequential Monte Carlo simulation (SMCS) for an existing RC slab in a marine environment. The approaches in this field use the Bayesian updating of model parameters. Information from inspection is used to represent the likelihood function which can be combined with the prior information on model parameters to find their posterior distributions. The posterior distributions can be found expressed as (Ang 2005).

$$P(x | z) = \frac{P(x) \cdot P(z | x)}{\int P(x) \cdot P(z | x) dx} \quad (22)$$

where $P(x | z)$ is the posterior distribution of model parameters x given the additional information z ; $P(x)$ represents the prior distribution of model parameters; $P(z | x)$ is the likelihood function of obtaining information z conditioned by x ; z and x are the vectors of observed data and model parameters, respectively. By knowing the prior distributions and the likelihood function, the posterior distributions can be established using sampling approaches based on Markov chain Monte Carlo simulation. The likelihood function $P(z | x)$ in this process can be expressed by Perrin et al. (Perrin 2007)

$$P(z | x) = \prod_{i=1}^n \left[\frac{1}{\sqrt{2\pi} \cdot \sigma_e} \cdot \exp\left(-\frac{1}{2} \left(\frac{z_i - a_i}{\sigma_e}\right)^2\right) \right] \quad (23)$$

where z_i and a_i are the observed and predicted data, respectively, at the i th inspection; σ_e is a the measurement and modeling errors which is assumed to be a normal distribution with zero mean and a standard deviation. Based on the updating process

using inspection information, the updated model parameters used in prediction model can be obtained.

2.10 Threshold Reliability for Assessing the Safety Level of Existing RC Structures

Specification of the target reliability levels is one of main factor required for probabilistic assessment of existing structures used to determine the structural safety condition. It is widely known that reliability assessment for existing structures differ from design of new structures in the following aspects (Sykora et al., 2014).

- Increasing safety level for existing structures usually concern with much more costs than that of new structures.
- Remaining life of existing structures is usually shorter than standard design working life for new structures (for instance 50 or 75 years).
- Actual structural conditions can be available for existing structures by using measurement from inspection process.
- Inspections help to reduce the uncertainties about the resistance and load parameter.

For assessment existing structures, it has been reported that it would be uneconomical to define target reliability levels as same with for new structures (Vrouwenvelder 2010). This is reported by present practice in USA, Canada, and Netherland that target reliability indices for existing structures decrease by about 0.5-1.7 compared with for new structures (Maljaars 2012, Casas 2013). The target reliability levels were reported in EN 1990. It is primarily intended for design of new structures. Reliability levels are classified by using consequence of failure. EN 1990 recommends the threshold reliability index for two reference periods (1 and 50 years) as shown in Table 1.

Table 1 Reliability Classification for Different Reference Periods according to EN1990 2002

| Reliability classes | Failure consequence | Reliability index | | Examples |
|---------------------|---------------------|-------------------|----------|--------------------------|
| | | 1 year | 50 years | |
| RC3 | High | 5.2 | 4.3 | Bridges, public building |
| RC2 | Medium | 4.7 | 3.8 | Residences, office |
| RC1 | Low | 4.2 | 3.3 | Agricultural building |

Considering a reference period equal to the remaining working life, it might be understood from (EN1990 2002) that the reliability level corresponding to an arbitrary remaining working life can be derived as follow

$$\beta_{t_{ref}} = \Phi^{-1}\{[\Phi(\beta_1)]^{t_{ref}}\} \quad (24)$$

where β_1 is target reliability index provided by Table 1, t_{ref} is reference period or it can be considered as a remaining life, Φ and Φ^{-1} are cumulative distribution function of standardized normal variable and its inverse function, respectively. However, this concept seems to be hardly applicable for emergency and crisis situation. Based on Equation (24), when the reference period is very short, target reliability (β) will be dramatically increased. ISO 2394 was presented more details associated with specification of target reliability. Target reliability provided by ISO 2394 is related not only the consequence of failure but also the relative cost of safety measures as shown in Table 2.

Table 2 Threshold reliability index in accordance with ISO/DIN 2394 (1998)

| Relative Cost of Safety Measures | Consequences of Failure | | | |
|----------------------------------|-------------------------|------|----------|-------|
| | Small | Some | Moderate | Great |
| High | 0 | 1.5 | 2.3 | 3.1 |
| Moderate | 1.3 | 2.3 | 3.1 | 3.8 |
| Low | 2.3 | 3.1 | 3.8 | 4.3 |

Cost of safety measures is a cost for improving structural reliability or safety considering properties of construction material and characteristic of related failure mode. The relative cost of safety measures strongly depend on structural resistance and load effects.

Threshold reliability index might be selected independently of the reference period that seems to be more appropriate procedure than that of EN 1990. Considering Table 2, the threshold reliability for existing RC structures usually decreases as it takes more effort to increase the reliability level (Vrouwenvelder 2002). For instance; low costs of safety measures can be selected for new design state while moderate costs of safety measures might be selected for assessing the existing RC structures.

CHAPTER 3

RESEARCH OBJECTIVES

3.1 To present a novel methodology for estimating the life-cycle reliability of RC bridge structures under multiple hazards. Life-cycle seismic reliability of RC bridge pier under seismic hazard and hazard associated with airborne chloride hazard is conducted and life-cycle reliability of PC girder under traffic hazard and hazard associated with airborne chloride hazard is conducted.

3.2 To present a novel procedure to estimate the updating parameters (average and variance of steel weight loss) based on inspection results by incorporating a spatial variability of steel corrosion.

3.3 To present the updating process using SMCS for the life-cycle reliability assessment of existing RC bridge structures by using inspection data. The effects of number of inspection location on the correlations between random variables are presented.

3.4 To identify the bridge component with the lowest reliability level, time after construction at which maintenance action is required, and which hazards is the most threaten for each bridge component.

CHAPTER 4

LIFE CYCLE RELIABILITY ASSESSMENT OF EXISTING CORRODED REINFORCED CONCRETE (RC) BRIDGES UNDER MULTIPLE HAZARDS USING INSPECTION DATA

4.1 Procedures for Estimating the Life-Cycle Reliability of Corroded RC Bridges

Generally, reinforced concrete (RC) bridge are affected by range of stressors including multiple hazards, such as seismic hazard, demand from traffic load and material deterioration (concrete and steel weight loss) (Frangopol 1997). The inclusion of time-variant deterioration of structural performance and structural demand based on the multiple hazards should be considered in the life-cycle reliability assessment.

4.1.1 Flowchart for Estimating Life-Cycle Reliability of Existing RC Bridges

In this study, the analyzed RC bridge consisting of RC bridge pier and pre-stressed concrete (PC) bridge girder are considered. Seismic reliability assessment for RC pier and reliability assessment for PC girder are conducted. Figure 12 shows a flowchart presenting the life-cycle reliability assessment for RC bridge structures under multiple hazards. The flowchart has five parts, A, B, C, D and E. In Part A, the structural capacity is calculated based on a section analysis. In Part B, seismic hazards, traffic hazards, and the hazard associated with airborne chloride from marine environment are evaluated. In Part C, amount of steel weight loss in longitudinal rebar at time t after construction is calculated based on the airborne chloride hazard (environmental factor) and random variables associated with the prediction of steel weight loss (Akiyama 2010). Combining the computational results of Parts A, B and C can present the structural reliability of new RC bridges.

One of the main differences in the process of life-cycle reliability assessment for new and existing RC bridges is whether inspection results are available. In this study, inspection process is used to determine the amount of steel weight loss; additionally, random variables related to prediction of steel weight loss can be updated using Sequential Monte Carlo Simulation (SMCS) ((Akiyama 2010). In addition, the spatial variability associated with the longitudinal rebars in RC members subjected to chloride attack must be modeled. In this study, parameters to reproduce the stochastic field are determined based on the previous experimental results for visualizing the spatially distributed steel corrosion over an RC specimen using X-ray technologies (Lim 2016) (Lim 2017). This stochastic field modeling is conducted in Part D (Honjo 2013). Estimation of average steel weight loss and its variance based on the inspection results are also discussed in Part D. The statistical error depends on the number and space intervals of inspection locations. Model uncertainties associated with the prediction of steel corrosion, represented by multiple random variables can be reduced using SMCS, even when the relationship among these random variables and the measurements from the inspection results are nonlinear and non-Gaussian (Yoshida 2009, Akiyama 2010). In Part E, random variables are adjusted to be consistent with inspection results using

SMCS. Finally, the updated life-cycle reliability of existing RC bridges under multiple hazards can be estimated.

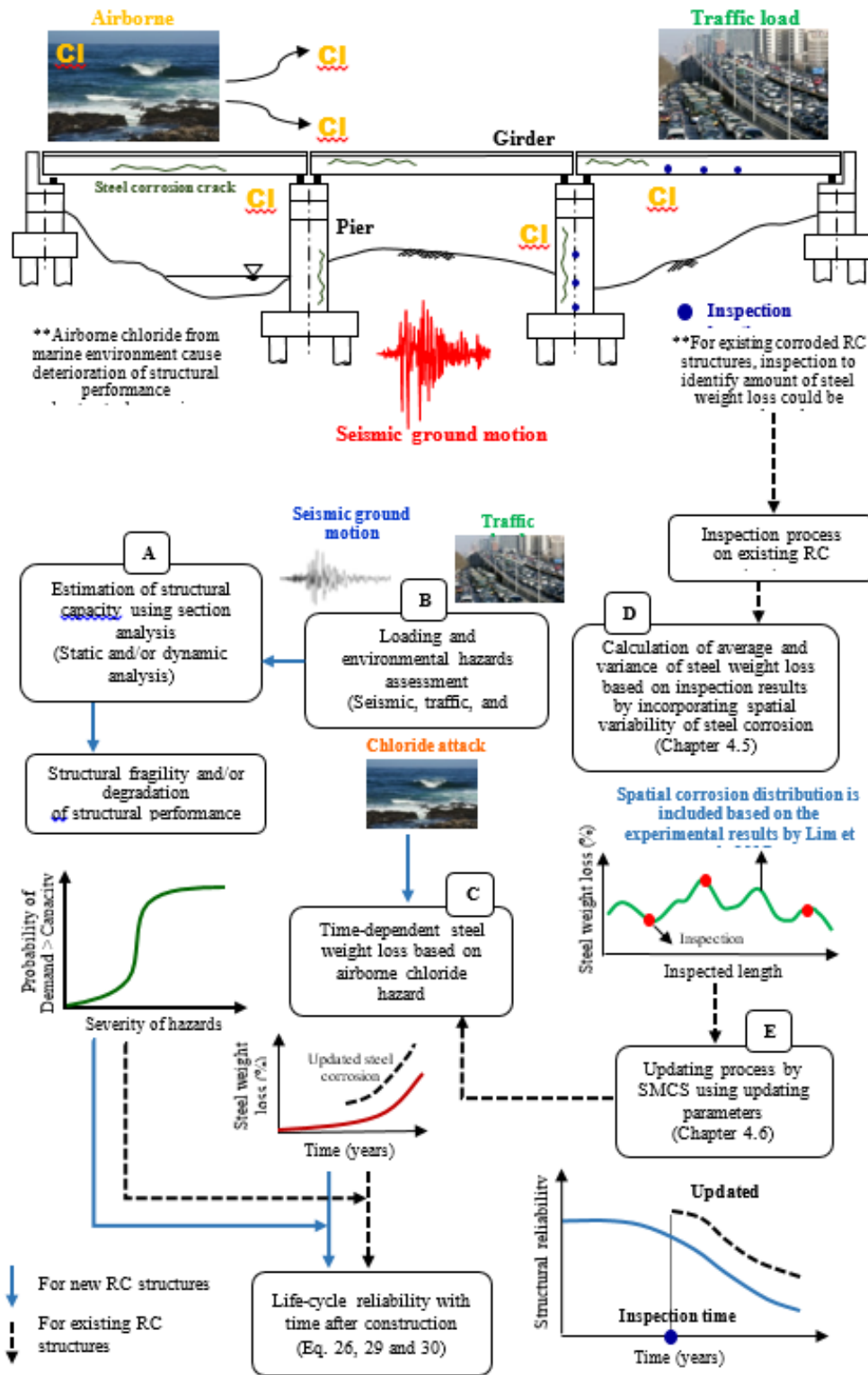


Figure 12 Flowchart for estimating life-cycle reliability of existing RC bridges

4.1.2 Life-Cycle Reliability Assessment of Existing RC Bridge Piers

The life-cycle reliability of RC structures can be estimated by combining the bridge performance assessment, hazard assessment, fragility analysis, and model to evaluate a material deterioration. The basic equations used to estimate the life-cycle reliability of RC piers and PC girders are described in the following sections.

- Basic Equations Estimating the Life-Cycle Seismic Reliability

When estimating life-cycle seismic reliability, the variability and uncertainty in earthquake occurrence, seismic ground motion, and structural capacity and demand must be considered. Given a seismic intensity S and steel weight loss C_w , the conditional annual probability of exceedance of the seismic capacity can be calculated as follows (Akiyama 2011).

$$p_{fa}(t) = P[S_{de} \geq S_{ca} | S, C_w(t)] \quad (25)$$

where S_{de} is the seismic displacement demand calculated by non-linear dynamic analysis using artificial ground motions with Takeda's hysteresis model and a single degree of freedom (SDOF); S_{ca} is the seismic displacement capacity estimated by cross-sectional analysis and plastic hinge analysis and used to assess the tip displacement of RC piers at the onset of longitudinal rebar buckling (Akiyama 2011). $P[S_{de} \geq S_{ca} | S]$ represents the general seismic fragility for which seismic displacement demand exceeds seismic displacement capacity over the total number of Monte Carlo Simulations (MCS). Buckling of longitudinal rebars is considered to be the limit state of the RC pier. Because steel weight loss causes seismic capacity deterioration and increases the seismic demand, the effect of steel corrosion must be considered in the life-cycle reliability assessment (Akiyama 2010, Akiyama 2011). When considering the probability distributions of S and C_w , the life-cycle reliability of RC bridge piers is as follows, including seismic hazards and hazards associated with airborne chlorides (Akiyama 2011).

$$p_{fa}(t) = \int_0^{100} \int_0^{\infty} \frac{dp_0(S)}{dS} \cdot P[S_{de} \geq S_{ca} | S, C_w(t)] \cdot f(C_w(t)) dS dC_w \quad (26)$$

where $p_0(S)$ is the annual probability of exceeding the prescribed value S at a specific site (i.e., the seismic hazard curve) and $f(C_w(t))$ is the probability density function (PDF) of steel weight loss expressed as a percentage.

4.1.3 Life-Cycle Reliability Assessment of Existing PC Bridge Girders

- Basic Equations Estimating Life-Cycle Reliability of PC Bridge Girders

This study calculates a performance function comparing the flexural bending capacity F_{ca} and the flexural bending demand F_{de} . Yielding of the pre-stressing strand is considered as a limit state of the PC girder. Given the traffic loading T_t and steel weight loss C_w , the conditional annual probability of exceedance of flexural bending capacity is calculated as follows:

$$p_{fa}(t) = P[F_{de} \geq F_{ca} | T_t, C_w] \quad (27)$$

$$F_{de} = L_{\max,t} + D \quad (28)$$

where F_{ca} is the flexural capacity considering steel weight loss, which is calculated by cross-sectional analysis using the reduced cross-sectional area of pre-stressing strands; F_{de} is the flexural demand at time t , estimated from the bending moment due to both the live load $L_{\max,t}$ and the dead load D . $L_{\max,t}$ is estimated by numerical simulation of traffic loading T_t based on statistical vehicle data. Traffic load simulation is conducted to evaluate the annual maximum bending moment due to traffic load acting on the girder at the mid-span. The data is contained in the traffic load simulation, which was collected using the Japanese survey traffic data system BWIM. This traffic loading simulation considers a mixture of 11 vehicle types, the axle load based on vehicle weight, the position of the axle load, and the distance from vehicle to vehicle. It is assumed that traffic congestion occurs twice a day (during the morning and evening). In addition, the uncertainties associated with the mixture of vehicle types and the vehicle-to-vehicle distances are considered during MCS. It is assumed that the statistical vehicle data is time-invariant. D is the bending moment due to the weight of the PC girders themselves, which depends on the unit weight of concrete, the section size and the span length of the PC girder. Dimensional errors associated with the cross-section of PC bridge girders are considered in calculation of the dead load D and the flexural capacity F_{ca} . During reliability analysis, the ratio of experimental to computed results for the flexural strength of post-tensioned concrete beams due to corrosion was used as the model uncertainty, as proposed by Minh et al. (Minh H 2003, Minh 2004, Minh 2006, Minh 2007)

Considering the probability distributions of T_t and C_w , the life-cycle reliability of RC bridge girders accounting for traffic hazards and hazards associated with airborne chlorides is calculated as follows.

$$p_{fa}(t) = \int_0^{100} \int_0^{\infty} P[F_{de} \geq F_{ca} | T_t, C_w(t)] \cdot g(T_t) f(C_w(t)) dT_t dC_w \quad (29)$$

where $g(T_t)$ is the PDF of the traffic load.

For the period of time after construction T , the cumulative-time failure probability p_f of both a bridge pier exposed to seismic and airborne chloride hazards (see Equation (26)) and a bridge girder exposed to traffic and airborne chloride hazards (see Equation (29)) is as follows (Akiyama 2011).

$$p_f = 1 - (1 - p_{fa}(t=1)) \cdot (1 - p_{fa}(t=2)) \cdots (1 - p_{fa}(t=T)) \quad (30)$$

Based on the cumulative failure probability p_f in Equation (30), the corresponding reliability index, β , is as follows:

$$\beta = \Phi^{-1}(1 - p_f) \quad (31)$$

where $\Phi(\cdot)$ is the cumulative distribution function of the standard normal distribution.

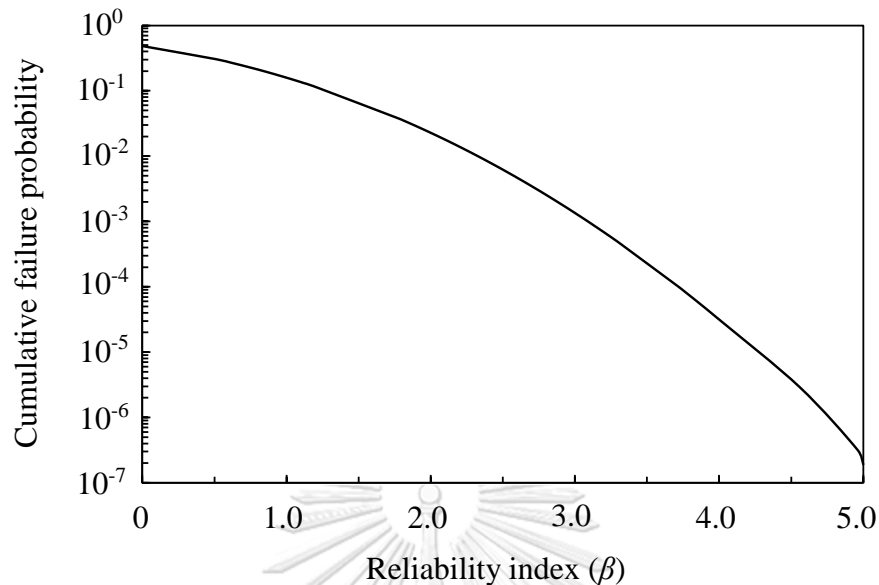


Figure 13 Relationship between cumulative failure probability (P_f) and reliability index (β)

In order to prioritize maintenance actions among bridge components that have different failure modes and are exposed to different hazards, the recovery time must be considered when defining the limit state of each component. Based on previous seismic disasters in Japan, including the 1995 Kobe earthquake and 2011 Great East Japan earthquake, it would take a similar number of days to recover the RC components if the load effects were greater than the displacement at the longitudinal rebars yielding and less than the displacement at the onset of longitudinal rebars buckling (Kobayashi 2012). Therefore, in this paper, the limit state of the RC pier was defined based on the onset of local buckling of the longitudinal rebars and the limit state of the PC girder was defined by the yielding of the pre-stressing strand. Therefore, the reliabilities of RC piers and PC girders can be compared using the same reliability threshold to identify the component with the lowest reliability, even though their failure modes differ and they are exposed to different hazards. This study provides a novel reliability framework for comparing the life-cycle reliability of various bridge components exposed to multiple hazards. These results will help prioritize maintenance actions.

4.2 Loading and Environmental Hazards Assessment (Part B in Figure 12)

In this study, it is assumed that existing RC bridges are under multiple hazards; seismic hazard, traffic hazard, and hazard associated with airborne chloride. Seismic and traffic hazard affect the whole bridge structure. However, different bridge components are more likely to fail due to the different effects that can be caused by specific hazard (Decò 2011). For instance, vertical load due to traffic hazard mainly affect bridge super-structures that mostly involve the flexural failure mode (Akgul 2002). While seismic fragility of the bridge is totally dependent on bridge sub-structure components (piers, bearings and abutments) (Padgett 2007). Therefore in this study,

load effect can be analyzed separately for RC pier and PC girder. Load effect caused by seismic and traffic hazard are considered to be statistically independent since their occurrence are independent. In addition, effect of steel weight loss due to hazard associated with airborne chloride will deteriorate the structural capacity of bridges. The detail of assessment in each hazards are described as follow.

4.2.1 Seismic Hazard Assessment

The goal of seismic hazard assessment is to ensure that a structure can withstand a given level of ground motion. There is relation between uncertainty about the location, size, and ground motion intensity of future earthquakes. Probabilistic Seismic Hazard Analysis (PSHA) aims to quantify these uncertainties and combine them to produce description of the distribution of future ground motion that may occur at a considered location. In order to assess risk to structures from ground motion, the annual probability of exceedance some level of earthquake ground motion at a specific site must be determined.

Using PSHA, all possible earthquake events and resulting ground motions are considered with probabilities of occurrence in order to find the level of ground motion intensity exceeded with some tolerably low rate. Generally, PSHA is explained briefly as following five steps.

1. Identify all earthquake sources capable of producing damaging ground motions.
2. Characterize the distribution of earthquake magnitudes (the rates at which earthquakes of various magnitudes are expected to occur).
3. Characterizing the distribution of distances from source to specific site associated with potential earthquakes.
4. Predict the resulting distribution of ground motion intensity as a function of earthquake magnitude, distance, etc.
5. Combine uncertainties in earthquake size, location and ground motion intensity, using a calculation known as the total probability theorem.

It is assumed that earthquakes occur randomly and independently. The annual probability that intensity Γ at a specific site will exceed a value γ is (Kameda and Nojima, 1988).

$$p_0(\gamma) = 1 - \exp\left[-\sum_{k=1}^n v_k q_k(\gamma)\right] \cong \sum_{k=1}^n v_k q_k(\gamma) \quad (32)$$

where n is the number of potential earthquake sources around the specific site, v_k is the earthquake occurrence rate at source k with upper and lower bound magnitudes, m_{uk} and m_{lk} , respectively, and $q_k(\gamma)$ is the probability of earthquake occurrence that Γ exceed γ at source k , as follows

$$q_k(\gamma) = \int_{m_{lk}}^{m_{uk}} \int_{r_k}^{r_k} P(\Gamma > \gamma | m, r) f_{Mk}(m) f_{Rk}(r) dm dr \quad (33)$$

where $f_{Mk}(m)$ is the probability density function (PDF) of magnitude M of possible earthquake at source k , $f_{Rk}(r)$ is the PDF of distance R with upper and lower level, r_{uk} and r_{lk} , respectively from specific site to rupturing fault at source k , and $P(\Gamma > \gamma | m, r)$ is the probability of Γ exceed γ given $M = m$ and $R = r$.

Attenuation relationship is important factor for PSHA. When the attenuation uncertainty is involved, the random intensity is expressed as follow.

$$\Gamma = U\gamma^*(m, r) \quad (34)$$

where $\gamma^*(m, r)$ is the attenuation relation represented as a function of m and r , and U is the lognormal random variable representing attenuation uncertainty with median of 1.0 and coefficient of variation. $P(\Gamma > \gamma | m, r)$ in Equation (35) can be expressed as

$$P(\Gamma > \gamma | m, r) = P(U\gamma^*(m, r) > \gamma) = P\left(U > \frac{\gamma}{\gamma^*(m, r)}\right) \quad (35)$$

4.2.2 Hazard Associated with Airborne Chlorides

Environmental hazard should be quantitatively assessed and results of assessment should be taken into consideration about durability design of RC structures. There is a lack of research on marine environment hazard assessment. This is because the data on coastal atmospheric exposure is very limited. Probabilistic methods for evaluation of deterioration of RC bridges subjected to chloride attacks have been proposed (Prezzi 1996, Val 2003). The effects of airborne chlorides should be modelled as a spatial-temporal variation into structural design. Observed values in Japan (PWRI 1988) are used to determine the attenuation relationship between the amount of airborne chlorides (C_{air}) and the distance from the coastline (d). There are 34 stations for collecting data on C_{air} located all over Japan as shown in Figure 14.

Generally, in Japan, the wind usually blows from west to east. Structures near east sea of Japan have strong suffered from severe damage due to airborne chlorides. The time period for collecting airborne chloride samples used in current study is three years. Wind speed, ratio of sea wind (defined as the percentage of time during one day when the wind is blowing from sea toward land), and the distance from the coastline, affect the amount of airborne chlorides. The attenuation of C_{air} (mdd, i.e. 100mg/m²/day) in the lateral direction can be expressed as (Akiyama 2012).

$$C_{air} = x_2 \cdot 1.29 \cdot r \cdot (x_1 \cdot u^{0.386}) \cdot d^{-0.952} \quad (36)$$

where r is the ratio of sea wind, u (m/sec) is the average wind speed during the observation period, and d (m) is the distance from the coastline. The comparison of observed values with predicted values by Equation (36) is shown in Figure 15. The ratio of sea wind r and the speed of wind u used in Equation (36) were obtained from the meteorological data collected

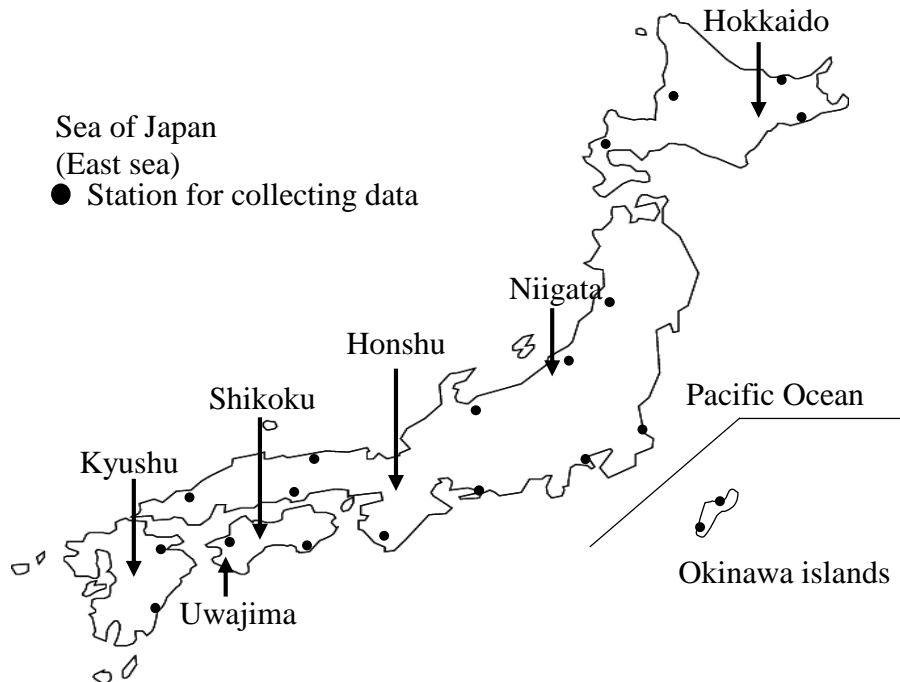


Figure 14 Data collection locations to observe amount of airborne chloride in Japan (Akiyama 2012)

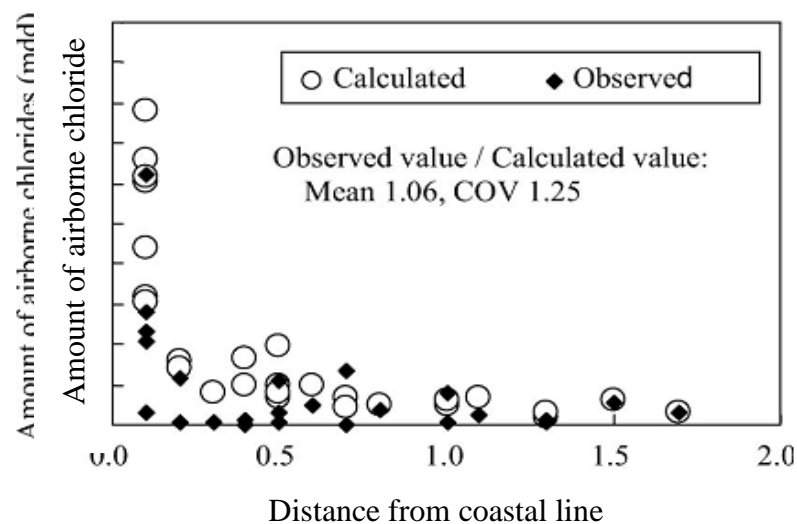


Figure 15 Relationship between amount of airborne chlorides (mdd) and distance from coastal line (km) (Akiyama 2012)

Since the data on airborne chlorides are very limited, it is difficult to consider the effect of geological formation around structures, precipitation, and the differences in coastal topography (e.g. sand beach and reef) on the amount of airborne chlorides collected at each location. Also, Equation (36) cannot be applied for a splash zone. In order to reduce the uncertainty involved in the prediction of airborne chlorides, it is

necessary to include additional parameters in the attenuation equation. The probability that C_{air} at a specific site will exceed an assigned value c_{air} is

$$q_s(c_{air}) = \int_0^{\infty} \int_0^{\infty} P(C_{air} > c_{air} | u, r) f_u(u) \cdot f_r(r) dudr \quad (37)$$

where $f_u(u)$ and $f_r(r)$ are the probability density functions (PDF) of u and r , respectively, and $P(C_{air} > c_{air} | u, r)$ is the probability of $C_{air} > c_{air}$ given u and r . The statistics of wind speed and the ratio of sea wind for the three years of C_{air} collection were obtained from meteorological data. The uncertainty in r is small compared to that in u and, for this reason, it can be neglected. Considering model uncertainty, the attenuation can be expressed as (Akiyama 2012).

$$C_{air} = U_R \cdot (1.29 \cdot r_0 \cdot u^{0.386} \cdot d_0^{-0.952}) \quad (38)$$

where U_R is a lognormal random variable representing model uncertainty shown in Figure 15. Then, Equation (37) can be expressed as (Akiyama 2012)

$$q_s(c_{air}) = \int_0^{\infty} P\left(U_R > \frac{C_{air}}{1.29 \cdot r_0 \cdot u^{0.386} \cdot d_0^{-0.952}}\right) \cdot f_u(u) du \quad (39)$$

4.2.3 Traffic Hazard Assessment

Assessment of highway bridge structures requires accurate prediction of the live load effects due to the traffic condition that a structure may be expected to resist during its entire life. Traffic load are the most common type of hazard for bridge super structure because it is the basic type of loading that engineer need to deal with during the design process.

In this study, the traffic load simulation proposed by Matsuzaki et al. (Matsuzaki 2010) is conducted to evaluate the annual maximum bending moment due to traffic load acting on the PC bridge girder at the mid span. The actual data is contained in the traffic load simulation which is collected using a survey traffic data system BWIM. This traffic loading simulation is analyzed by considering the mixing rate of vehicle types, axle load based on weight of vehicles, positions of axle load, and distance between vehicle to vehicle. Congestion condition of traffic is assumed twice a day (Morning and evening). In addition, uncertainties of mixing rate of vehicle types and vehicle-to-vehicle distance are created by MCS. Although, structural bridge members may fail in different modes under traffic loads, only the flexural failure mode is considered in this paper with respect to PC bridge girder.

Based on vehicle loading distribution obtained by traffic simulation, method of Courbon theory is used to evaluate the effect of bending moment into the target bridge girder. The effects of vehicle loading distribution differently affect the bending moment value due to positions of girder (exterior or interior girder).

4.3 Prediction of Structural Capacity using Section Analysis (Part A in Figure 12)

4.3.1 Buckling Analysis of Corroded RC Bridge Piers

An analytical method to evaluate the seismic fragility of an RC pier with various amounts of steel weight losses has been proposed by (Akiyama 2011).

$$P[D_e \geq C_a \mid \Gamma = \gamma, C_w = c_w(t)] = P\left[\frac{D_e(\Gamma = \gamma, C_w = c_w(t))}{C_a(C_w = c_w(t))}\right] \quad (40)$$

The seismic fragility is estimated from the ratio of the number of times that the seismic displacement ductility demand $D_e(\Gamma = \gamma, C_w = c_w(t))$ exceeds the seismic displacement ductility capacity $C_a(C_w = c_w(t))$ to the total number of Monte Carlo simulations. $D_e(\Gamma = \gamma, C_w = c_w(t))$ is the maximum lateral displacement at the tip of the pier and is calculated by a nonlinear dynamic analysis using artificial ground motions. The details associated with the generation of the artificial ground motions are provided in Akiyama et al. (Akiyama 2014). $C_a(C_w = c_w(t))$ is the lateral displacement δ_u at the onset of the longitudinal rebar buckling. Because rebar buckling requires extensive repairs, this displacement is a key damaged state. $C_a(C_w = c_w(t))$ is calculated based on the results of the plastic hinge analysis, the moment-curvature analysis, and the expected influence of the confinement reinforcement (Naito 2011). When the average steel weight loss in a plastic hinge is estimated, the seismic ductility capacity can be calculated as follows

$$\delta_u = \delta_y + (\phi_u - \phi_y)L_P(h - L_P/2) \quad (41)$$

$$L_P = 0.5d + 0.05h \quad (42)$$

where δ_y and ϕ_y are the lateral displacement and curvature at yielding, respectively, calculated by a section analysis using a reduced cross sectional area of the longitudinal rebar; ϕ_u is the ultimate curvature estimated by the displacement ductility evaluation method using the stress-strain relationship of the buckling behavior of the longitudinal rebar in the plastic hinge proposed by Naito et al. (2011). L_P in Equation (42) is the equivalent plastic hinge length proposed by Mattock (Mattock 1965); h is the shear span of the RC column; and d is the effective cross-sectional depth.

Based on the comparison of the experimental and computational results of corroded RC columns subjected to cyclic loading, Akiyama et al. (Akiyama 2011) confirmed that the accuracy of the results of corroded columns is approximately the same as that of non-corroded columns. To ensure the computational accuracy of δ_u , the average steel weight loss in the plastic hinge of an RC bridge pier must be estimated correctly. The average steel weight losses in the plastic hinge are measured after the longitudinal rebar was dismantled from the specimen to remove the corrosion products; this average steel weight loss was used when comparing the experimental and computational results. For an existing RC bridge pier, this must be estimated based on the discrete inspection results associated with the steel weight loss.

4.3.2 Degradation of Flexural Capacity of PC Bridge Girder

The flexural capacity F_{ca} of PC girder in Equation (27) is calculated based on section analysis using reduced cross-sectional of pre-stressing strands. The flexural capacity decreases with the time after construction due to the increasing of weight loss of pre-stressing strands. In this study, uncertainties of dimensional error are considered to estimate the flexural capacity. In addition, the ratio of experimental results to computed results of flexural strength of post-tensioned concrete beam due to corrosion, proposed by Minh et al. (Minh H 2003) (Minh 2004) (Minh 2006) (Minh 2007), is used as model uncertainties for estimating the flexural capacity due to steel weight loss.

4.4 Hazard Assessment Associated with Airborne Chloride and Estimation of Time-Variant Steel Weight Loss (Part C in Figure 12)

In a marine environment, various factors are related to the material deterioration mechanism of RC structures. The precise influences of these factors are difficult to predict because they vary in time and space. Therefore, a long-term structural performance analysis must follow reliability concepts and methods (Ellingwood 2005, Frangopol 2011). Akiyama et al. (2010) proposed a probabilistic model of the hazards associated with airborne chlorides by considering the spatial-temporal variation effects. The results of the hazard assessment associated with airborne chlorides depend on wind speed on the location analyzed, ratio of sea wind (defined as the percentage of time during one day during which the wind is blowing from the sea towards the land), and the distance from the coastline. Using the hazards associated with airborne chloride, the steel weight loss $W(t)$ given the corrosion resulting from chlorides at time t after construction is estimated using nine random variables (Akiyama 2010). $W(t)$ can be expressed using following Equations (43) to (53).

$$C_{air} = x_2 \cdot 1.29 \cdot r \cdot (x_1 \cdot u^{0.386}) \cdot d^{-0.952} \quad (43)$$

$$C_0 = x_3 \cdot 0.988 C_{air}^{0.379} \quad (44)$$

$$q = -6.77(W/C)^2 + 10.10(W/C) - 3.14 \quad (45)$$

$$D_c = x_7 \cdot 10^q \quad (46)$$

$$\text{Steel corrosion initiation time: } t_1 = \frac{1}{4D_c} \left[\frac{0.1(c + x_6)}{\text{erf}^{-1}\left(1 - \frac{x_4 C_T}{x_5 C_0}\right)} \right]^2 \quad (47)$$

$$Q_{cr}(c) = \eta(W_{c1} + W_{c2}) \quad (48)$$

$$W_{c1} = \frac{\rho_s}{\pi(\gamma - 1)} \left[\alpha_0 \beta_0 \frac{0.22((2(c + x_6) + \phi)^2 + \phi^2)}{E_c(c + x_6 + \phi)} f_c'^{2/3} \right] \quad (49)$$

$$W_{c2} = \alpha_1 \beta_1 \frac{\rho_s}{\pi(\gamma-1)} \cdot \frac{(c+\phi)}{(5c+3\phi)} w_c \quad (50)$$

$$f_c' = -20.15 + 21.0/(W/C) \quad (51)$$

$$\text{Steel corrosion crack occurrence time: } t_2 = t_1 + \frac{x_8 Q_{cr}(c)}{x_9 V_1} \quad (52)$$

$$\text{Steel weight loss } W(t) = \begin{cases} 0.0; & t_1 \geq t \\ \frac{4}{\phi \rho_s} (t-t_1) V_1 x_9; & t_1 \geq t \geq t_2 \\ \frac{4}{\phi \rho_s} (t_2-t_1) V_1 x_9 + (t-t_2) V_2 x_9; & t > t_2 \end{cases} \quad (53)$$

where C_{air} (mdd=100 mg/mm²/day) is the airborne chloride; u (m/s) is the wind speed; d (m) is the distance from the coastline; r is the ratio of the sea wind; C_0 (kg/m³) is the surface chloride content; C_T (kg/m³) is the critical threshold of the chloride concentration; c (mm) is the concrete covering; t (year) is the time after construction; W/C is the water cement ratio; erf is the error function; D_c is the coefficient of diffusion of chloride; ρ_s is the steel density (7.85 mg/mm³); γ is the expansion rate of the volume of corrosion (3.0); f_c' (MPa) is the concrete strength; w_c is the crack width due to the corrosion of the steel rebar (0.1 mm); E_c (MPa) is the modulus of elasticity of concrete; ϕ (mm) is the diameter of the steel rebar; V_1 (mg/mm²/year) is the steel corrosion rate before the corrosion crack occurrence (Nakagawa 2004); Q_{cr} (kg/m³) is the critical threshold of corrosion associated with crack initiation; η is the correction factor; V_2 (mg/mm²/year) is the steel corrosion rate after corrosion cracking occurrence (Nakagawa 2004); and α_0 , α_0 , β_0 and β_1 are the coefficients related to the effect of the concrete cover, steel bar diameter and concrete strength, respectively (Qi 2001).

The nine random variables, x_i ($i=1, 2, \dots, 9$), associated with the prediction of the steel weight loss with time t after the construction are summarized in Table 3. Because x_2 , x_3 , x_5 , x_7 , x_8 and x_9 have large COVs, a lognormal distribution should be modeled instead of normal distribution (Ang 2005).

Table 3 List of random variables

| Random variables | | Distribution | Mean | COV | Reference |
|--|-------|--------------|----------|--------|--|
| Wind speed | x_1 | Normal | 1.00 | 0.0715 | Meteorological data |
| Attenuation of C_{air} | x_2 | Lognormal | 1.06 | 1.25 | PWRI (1988) |
| C_0 - C_{air} equation | x_3 | Lognormal | 1.43 | 1.08 | PWRI (1988) |
| Critical threshold chloride concentration at the occurrence of steel corrosion (C_T) | x_4 | Normal | 1.00 | 0.375 | Val and Stewart (2003) Matsushima et al. (1998) |
| Estimation by the diffusion equation | x_5 | Lognormal | 1.24 | 0.906 | PWRI (1988) |
| Construction errors in the concrete cover | x_6 | Normal | + 8.5 mm | 16.6* | Maeda et al. (2004) |
| Diffusion coefficient (D_c) | x_7 | Lognormal | 1.89 | 1.87 | Maeda et al. (2004) |
| Critical threshold of the corrosion amount at crack initiation (Q_{cr}) | x_8 | Lognormal | 1.00 | 0.352 | Matsushima et al. (2004) Tanaka et al. (2006) Yokota et al. (2004) |
| Steel corrosion rate | x_9 | Lognormal | 1.00 | 0.580 | Nakagawa et al. (2004) |

* Standard deviation.

The statistical information of x_6 (Kawamura 2004) was investigated from the differences between specified concrete cover and measured concrete cover from real structures; It was reported that the standard deviation of x_6 is independent of the design concrete cover.

4.5 Estimation of Average and Variance of Steel Weight Loss by Incorporating a Spatial Variability of Steel Corrosion

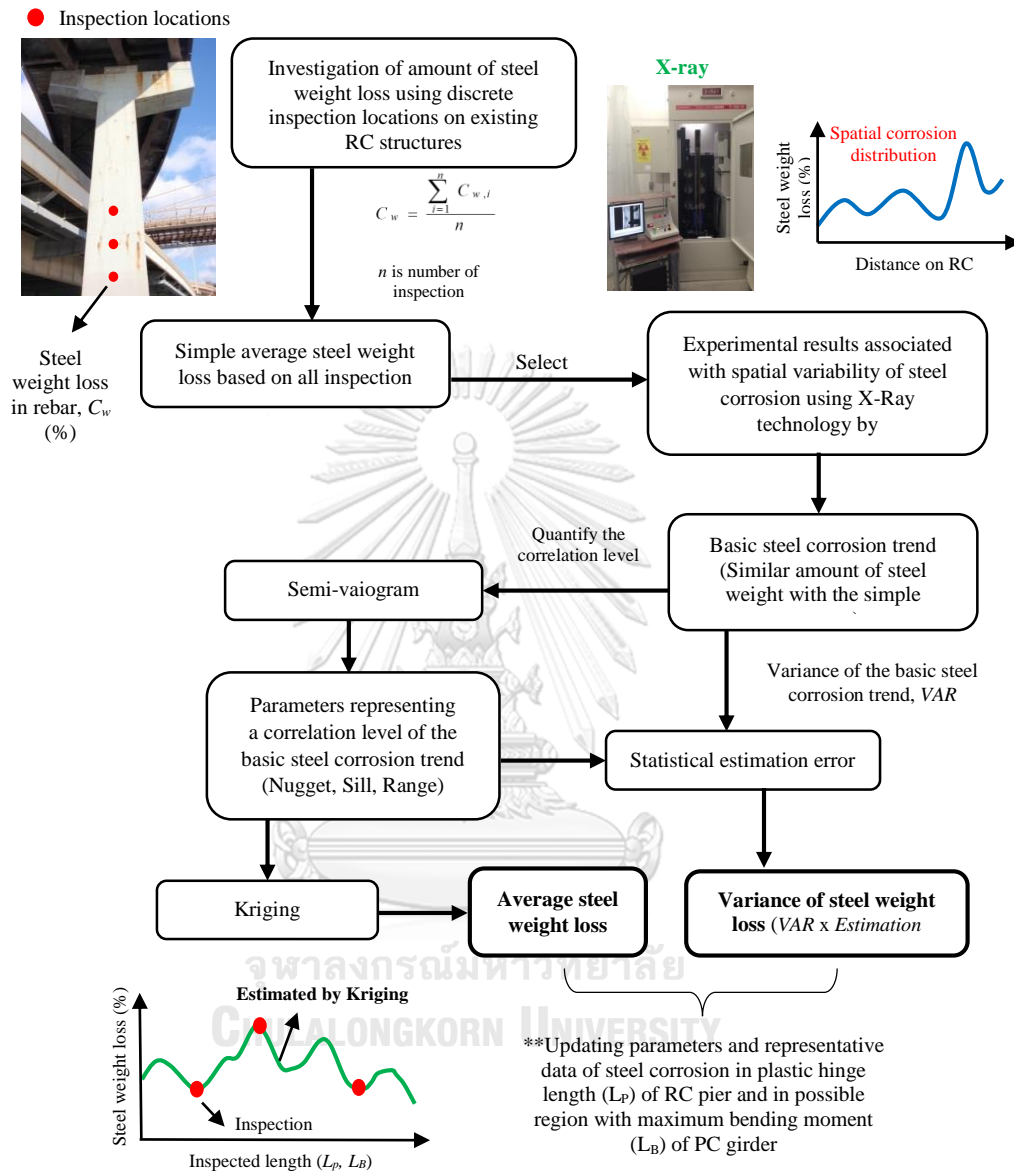


Figure 16 Estimation of the average steel weight loss and variance using discrete inspection results (adapted and extended from Yanweerasak et al. (Yanweerasak 2016))

The average steel weight loss in the plastic hinge of an RC bridge pier and the variance associated with the estimation of the average steel weight loss are calculated following the procedure shown in Figure 16. These values can be estimated by a semi-variogram calculation, a Kriging interpolation, or the statistical estimation error process (Honjo 2013) depending on the number and spatial interval of inspection locations. The parameters used to reproduce the spatial distribution of the steel corrosion are determined based on the experimental results to visualize the steel corrosion distribution in RC specimens using X-ray techniques.

4.5.1 Visualization of Corroded Rebars in RC Member by Digital Image Processing of X-ray Photogram (Part D in Figure 12)

For existing RC structures located in an aggressive environment, the effect of spatial steel corrosion distribution over the length of reinforcing bars on the structural performance must be considered. The spatial variability in the steel corrosion must be integrated into the estimation of the structural capacity. When the parameters to reproduce the spatial distribution of the steel corrosion are provided on several inspection locations, the spatial distributions of steel corrosion in an existing RC structure can be estimated by the statistical estimation error process (Honjo and Otake, 2013). Recently, X-ray techniques have been applied to visualize concrete cracking in order to investigate the behavior of the fracture process zone in the concrete (Otsuka and Date, 2000). Lim et al. (2016, 2017) presented the experimental results of the visualization of steel corrosion in RC members using X-ray technologies to understand the non-uniform steel corrosion distribution over the RC component. Figures 17 and 18 show the X-ray apparatus and RC specimens, respectively (Lim 2016, Lim 2017). An RC beam was corroded by electrical corrosion. As indicated in Figure 18, the locations for taking X-ray images photograms start from distances of 250 to 1090 mm with 14 times of 60 mm interval from the left side of the specimen.

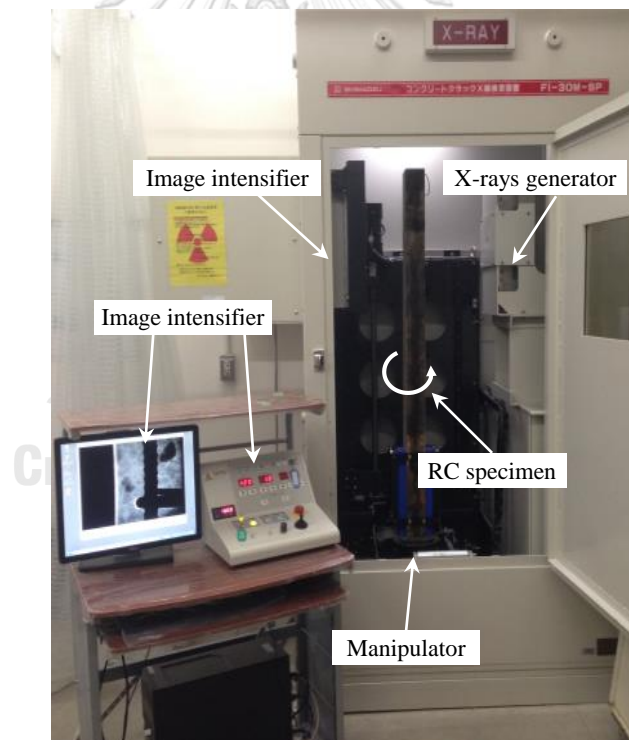


Figure 17 X-ray configuration

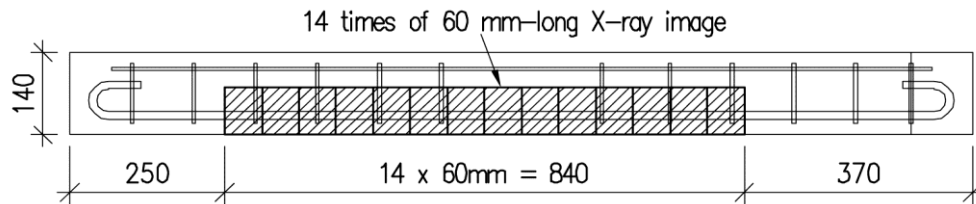


Figure 18 Configuration of the RC beam specimen for capturing the X-ray picture (Lim 2016, Lim 2017)

The estimation of steel weight loss in RC specimen using X-Rays technology based on the experiment are described as follow.

a) Processing of taking the X-ray

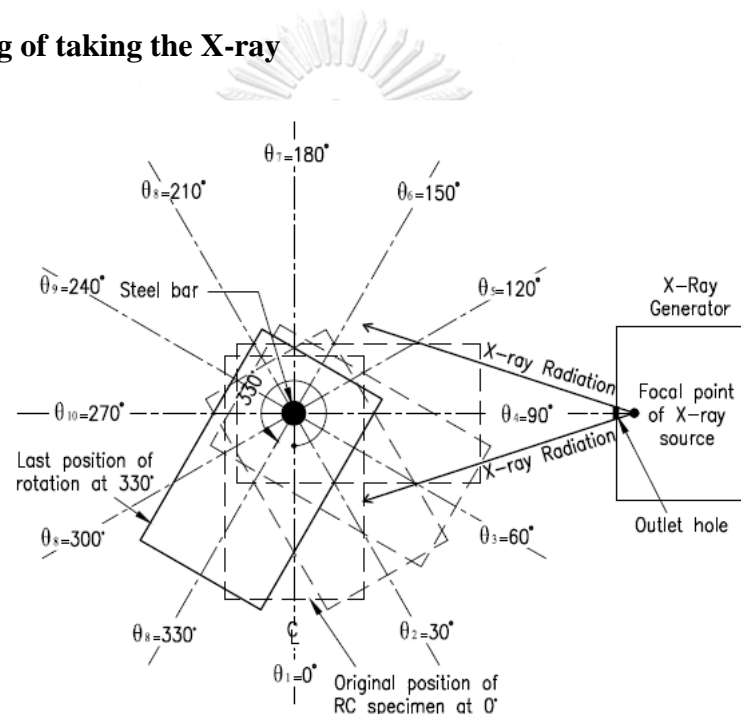


Figure 19 Process of taking X-ray from different viewing angles (Lim 2017)

X-ray configuration shown in Figure 17 was used to visualize and capture images of the non-corroded and corroded areas of the steel bar inside the RC specimen from different viewing angles. The images of the steel bar from viewing angles of 0° , 30° , 90° , 150° , 180° , 210° , 270° , and 330° were taken as shown in Figure 19. At each angle, the total length along the specimen that was taken by the X-ray was 840 mm, which required 60 mm-long images to be captured 14 times. The first step was setting up the specimen in an appropriate position. The specimen was set up between the X-ray intensifier and generator in the X-ray chamber onto a manipulator, which can be used to translate or rotate the specimen to the desired positions by controlling the operation panel. Then, the specimen was rotated to the angle 0° and horizontally adjusted into the position where the center of the steel bar was aligned with the middle point of the X-ray source outlet. This setting made the center of the steel bar fixed as the center point

of rotation of the specimen. In the vertical direction, the specimen was then adjusted up or down against the X-ray radiation source to obtain the starting position from the base of the specimen on the computer screen.

After setting up the specimen, the radiography-image acquisition by attenuating the primary X-ray with materials of different densities and thicknesses could proceed. The chosen X-ray tube and current depend on different source-to-specimen distances and thicknesses of concrete because the specimen was rotated to different viewing angles: 120 kV, 1.2 mA for the viewing angles of 0°, 30°, 150°, 180°, 210°, 300°, and 330° and 145 kV, 1.2 mA for viewing angles of 90° and 270°. Starting from the base of the specimen (location 1 at 370 mm) and a viewing angle of $\theta_1 = 0^\circ$, the RC specimen was translated vertically with an increment of 60 mm 14 times, which was supplied by the X-ray generator. The radiation penetrated through the RC specimen to visualize composition details of various densities in the form of attenuated X-ray radiation onto a detector of the image intensifier. After the attenuated X-rays were converted into visible light on a fluorescent screen, the equipped couple-charged device (CCD) camera unit, whose capture command was linked to and controlled by a computer software program, was used to capture and store them as digital values. These digital values comprise a 1024 x 768 pixels grey-scale image.

The same process was performed repeatedly to capture images from the remaining viewing angles. The viewing angles of 0°, 30°, 150°, 180°, 270°, 300°, and 330° refer to those steel bar views at which the specimen was rotated to the positions of angles $\theta_1, \theta_2, \theta_3, \theta_4, \theta_5, \theta_6, \theta_7, \theta_8, \theta_9, \theta_{10}, \theta_{11},$ and θ_{12} , respectively.

b) Analysis of X-ray Images

The obtained X-ray photograph is an 8-bit grey-scale image consisting of 256 color numbers, which represents the degrees of greyness that ranges from 1 (pure black) to 256 (pure white). When it is magnified in high orders, the image displays its dark pixel composition or low values of intensity produced by the steel bar, and brighter pixels or higher values of intensity produced by the concrete component. This result occurs because the steel bar has a higher density than the concrete. Therefore, the steel bar always appears darker or has smaller pixel values than the concrete on the X-ray image. The X-ray image provides such useful details of contrasting characteristics between the dense and less dense compositions of material that it can be used to differentiate areas of the weight loss of steel bar (dense material) from those with corrosion products and concrete (less dense material).

c) X-ray Image Enhancement

In general, the original images at 0° and 180° provided the clearest views, followed by images at 30°, 150°, 210°, and 330°; the worst images were obtained at 60°, 90°, 120, 240, 270, and 300°. This result occurred because of the differences in thickness of the concrete through which the X-ray radiation penetrated when the specimen was rotated at a particular angle. The image was enhanced before the analysis so that the detailed information on the image could be easily obtained. In the enhancing process, the fine details of the image were revealed or the blurred regions were reduced using a filtering technique to accentuate the intensity changes and make the high-contrast edges visible. Visualizing the high-contrast edges between the steel bar and

concrete composite allows the area shapes of the concrete composite and steel bar to be easily distinguished.

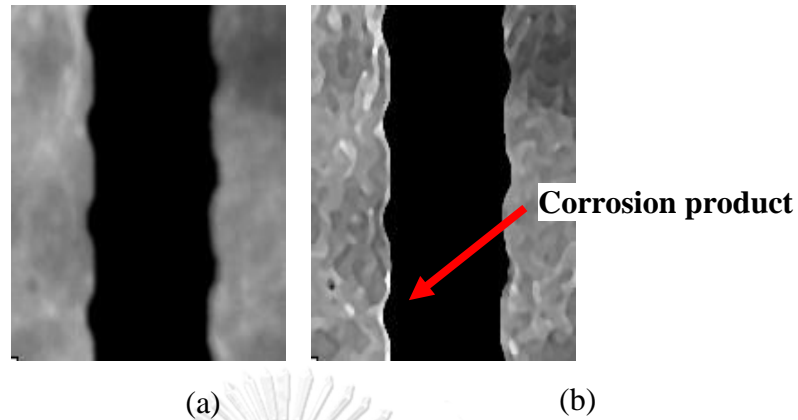


Figure 20 X-ray image of the corroded steel bar at $\theta_1 = 0^\circ$ (a) before and (b) after enhancement

d) Analysis Procedure

The pixel values of the reinforcing bars are smaller than those of concrete and steel corrosion products. The X-ray image is divided into grids of pixels, which are a mesh of small square elements. This allows the software to perform a counting the total number of pixels of each brightness intensity. Therefore, it is possible to select, count, and classify the number of pixels that are produced in the area of corroded steel bar by specifying a narrow range of the lowest of pixels as possible representing only the steel bar. To facilitate the analysis of digital data on the image, the original 60 mm-image of all viewing angles is sliced into twelve 5-mm as shown in Figure 21.



Figure 21 X-ray image of a 5-mm (a) non-corroded bar and (b) corroded bar

e) Formulation of Estimating Amount of Steel Weight Loss

For calculating the steel weight loss, the X-ray images from viewing angles of 0° , 30° , 90° , 150° , 180° , 210° , 270° , and 330° were used because these angles provided interpretable information. After the number of pixels of non-corroded and corroded steel bar has been counted, the total area is calculated by simply multiplying the number of pixels with the unit area per pixel, as:

$$A_{\theta_n} = P_{\theta_n} \times A_p \quad (54)$$

$$A'_{\theta_n} = P'_{\theta_n} \times A_p \quad (55)$$

where A_{θ_n} and A'_{θ_n} are the areas of the original steel bar before corrosion and the corroded steel bar at any viewing angle θ_n , respectively; the subscript $n = 1, \dots, k$, where $k = 8$ is the number of viewing angles; P_{θ_n} and P'_{θ_n} are the number of pixels of area of original steel bar and corroded steel bar, respectively at any viewing angles; and A_p is the unit area per pixel on the image. The unit area in pixel on the image can be converted into millimeters by calibrating the known height of the image (60 mm), which is measured while the X-ray photogram is being taken. Then, the volume of the steel bar before and after corrosion can be calculated as follows

$$V_{\theta_n} = \frac{\pi (A_{\theta_n})^2}{4L} \quad (56)$$

$$V'_{\theta_n} = \frac{\pi (A'_{\theta_n})^2}{4L} \quad (57)$$

where V_{θ_n} and V'_{θ_n} are the volumes of the original and corroded steel bars, respectively, at a viewing angle θ_n , $\pi = 3.14$ and L is the length of the steel bar in the image which is 5 mm in this calculation. The steel weight loss per L (mm) length of the steel bar is determined by taking the average of each of steel weight loss for each viewing angle as follows

$$R_w = \frac{1}{k} \sum_{n=1}^k \frac{(V_{\theta_n} - V'_{\theta_n})}{V_{\theta_n}} \times 100 \quad (58)$$

where R_w is steel weight loss per L (mm) length of steel bar, θ_n denotes the viewing angles ($\theta_n = \theta_1, \dots, \theta_8$, where $n = 1, \dots, k$), and k is the number of viewing angles ($k = 8$ for eight different viewing angles).

The X-ray application as a non-destructive method allows for the continuous inspection of the area of the corroded steel bar inside the concrete, which can help to increase the degree of accuracy in estimating steel weight loss. Lim et al. (2017) reported the employed method to estimate the steel weight loss using X-ray images from different viewing angles is accurate and the X-ray technology is a convenient method to estimate steel weight loss inside concrete. However, the differences between steel weight losses estimated by X-ray image and measured by actual steel weight loss is approximately 3%.

Steel corrosion trend taken by X-ray photogram as shown in Figures 22 to 26 could be used to reproduce spatial variability of steel corrosion to estimate the average and variance of steel weight loss. Figures 22 to 26 demonstrate the relationship between the distance from the left edge of the specimen and the local steel weight loss of the longitudinal rebar. The local steel weight loss was calculated by the volume of the sound rebar estimated by X-ray. The difference between the maximum and minimum steel weight loss ranges from 10 to 15%, independent of the steel corrosion level. Based on the experimental result, the parameters to reproduce spatially distributed steel corrosion can be determined.

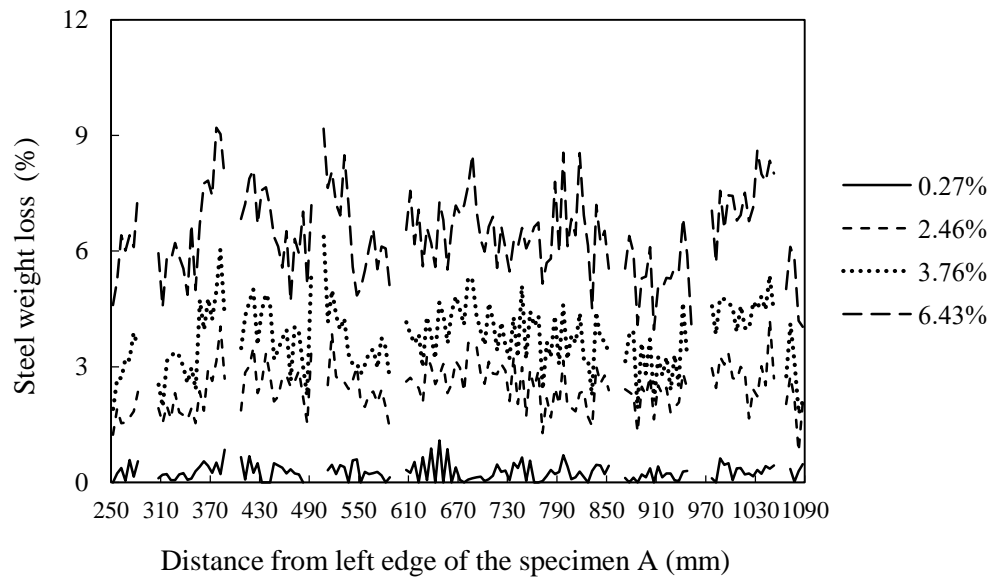


Figure 22 Steel weight losses along the length of specimen A

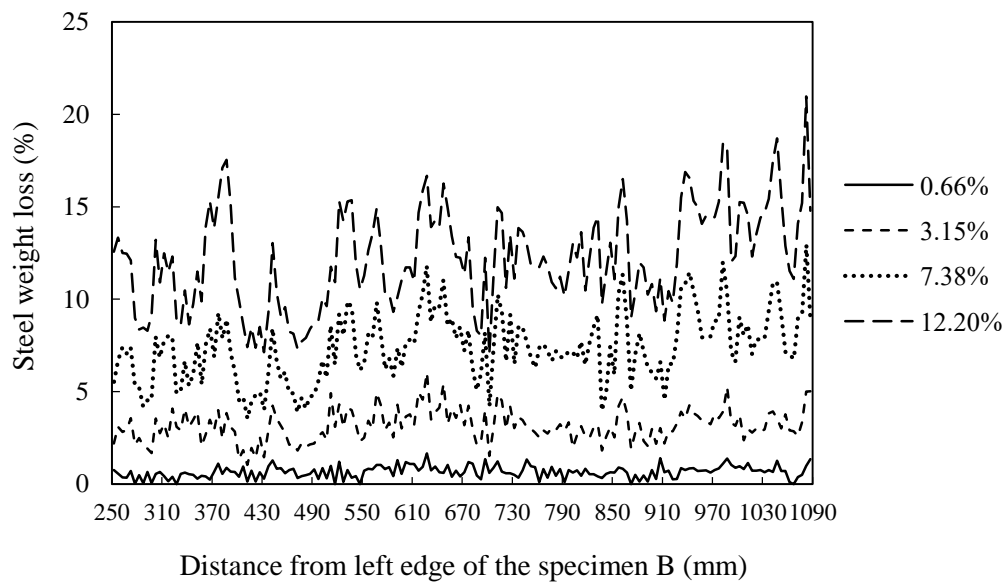


Figure 23 Steel weight losses along the length of specimen B

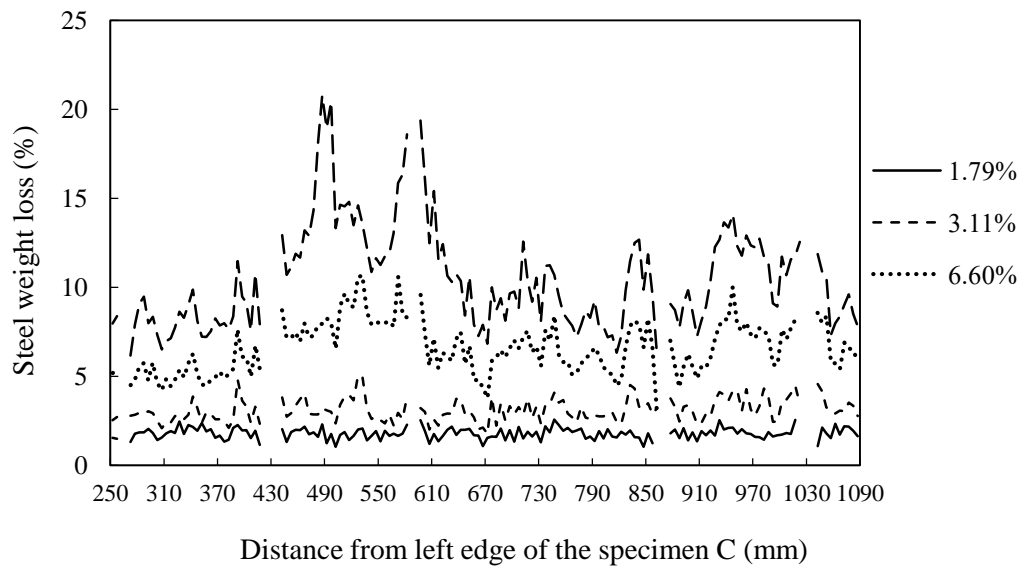


Figure 24 Steel weight losses along the length of specimen C

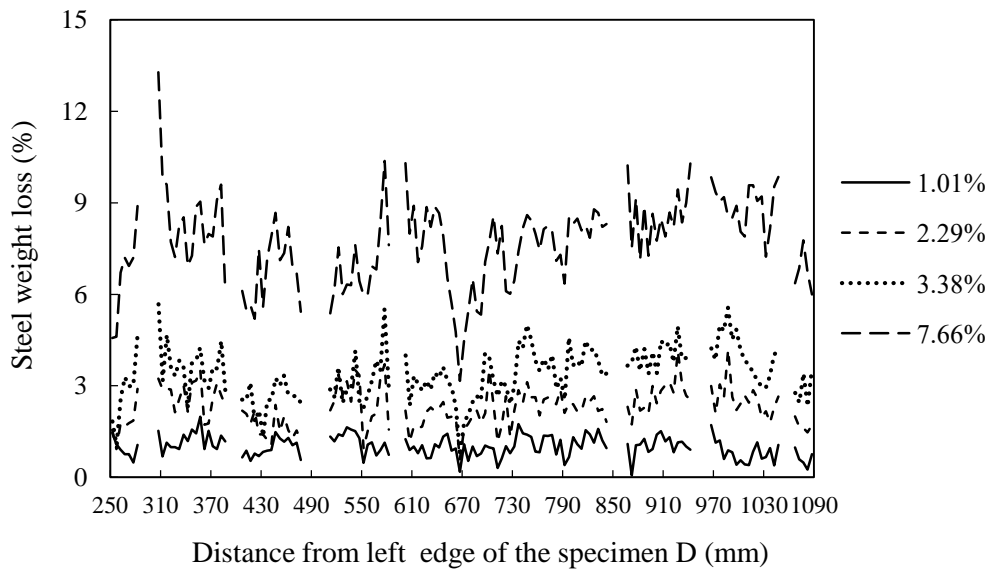


Figure 25 Steel weight losses along the length of specimen D

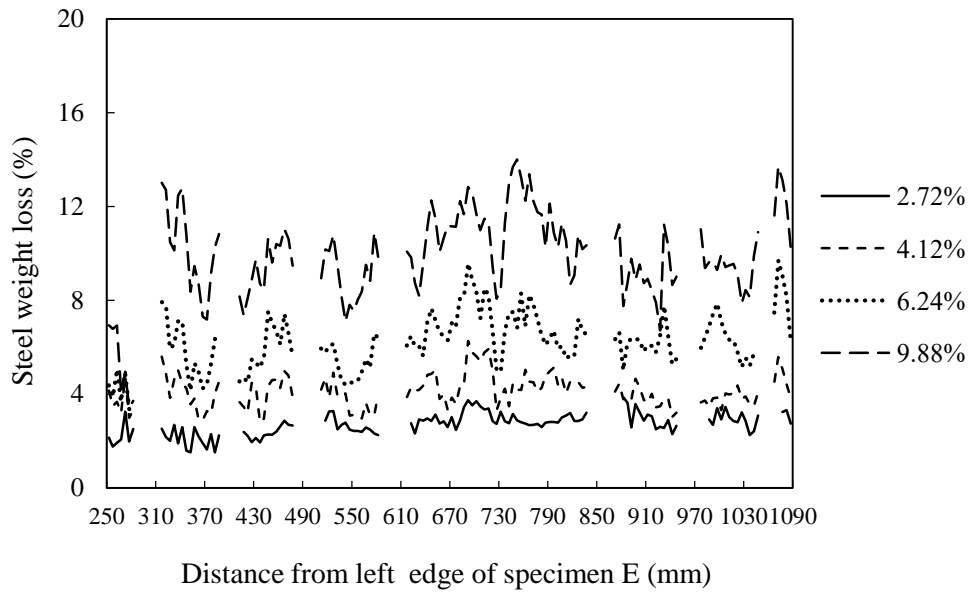


Figure 26 Steel weight losses along the length of specimen E

4.5.2 General Procedure to Estimate Average and Variance of Steel Weight Loss Based on Inspection Result

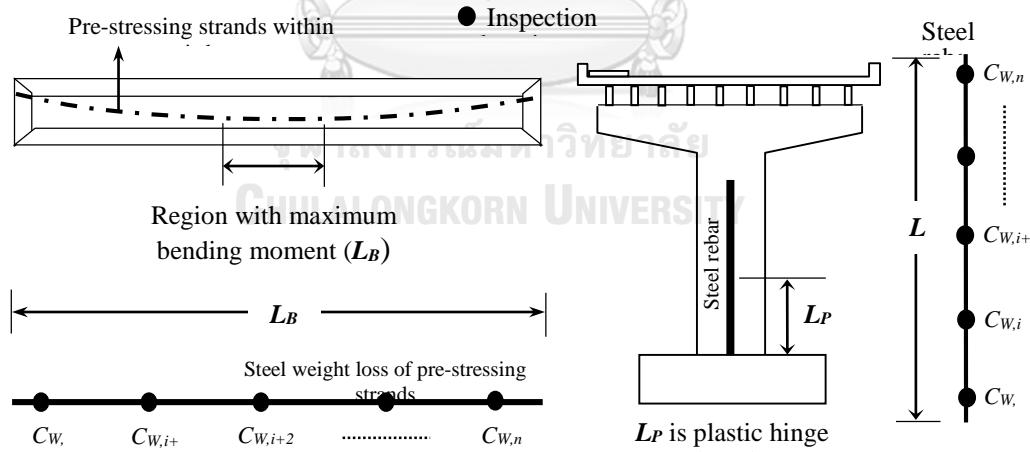


Figure 27 Inspection locations of steel weight loss along a plastic hinge of an RC pier and the region of a PC girder with the maximum bending moment

To accurately estimate the seismic capacity of corroded RC piers, and flexural capacity of corroded PC girders, the average of steel weight loss over the plastic hinge of RC piers and region of PC girder with maximum bending moment must be estimated. Seismic ductility capacity and energy dissipation of RC piers strongly depend on the amount of steel weight loss in the plastic hinge (L_p) as shown in Figure 27. For the PC

girder, maximum bending moment due to self-weight and traffic load are always occurred at the mid span of the girder if simple support girder is assumed. However, due to the traffic loading simulation by considering distribution of vehicles, it causes a slight movement of positions of maximum bending moment from the mid-span in both left and right side. Therefore, flexural bending capacity of PC girder due to the weight loss of pre-stressing strands at the maximum bending moment region (L_B) shown in Figure 27 should be considered. In addition, the variance associated with the average steel weight loss must be evaluated. The average and variance of steel weight loss provided by inspection result are estimated according to the procedure presented in Figure 16, and detail in each steps are explained as follows.

Step1: Estimation of the steel weight loss (C_w) from the inspection results.

From the inspection process, the steel weight loss of the existing RC piers and pre-stressing strands of PC girders can be determined as shown in Figures 27. The simple average of the steel weight loss from all inspection locations can be simply calculated as

$$C_{w,avg} = \frac{\sum_{i=1}^n C_{w,i}}{n} \quad (59)$$

where $C_{w,avg}$ is average steel weight loss from all inspection locations. $C_{w,i}$ is steel weight loss at each inspection location. n is number of inspection locations.

Step2: Selection of the steel corrosion trend from the experimental results provided by Lim et al. (Lim 2017)

The parameters to reproduce the spatial variability of the steel corrosion inside an RC member can be determined using the experimental distribution of the steel weight loss over the RC specimen, as shown in Figures 22 to 26. When the simple average steel weight loss from Step 1 is provided, the basic steel corrosion trend is selected from the experimental results, which has a similar amount of steel weight loss as $C_{w,avg}$, to estimate the spatial variability parameters using the semi-variogram calculation.

Step3: Quantifying the spatial correlation of the selected basic steel corrosion trend using the semi-variogram

The semi-variogram process is a useful tool for quantifying and characterizing a spatial correlation of any series of data. The semi-variance, $\gamma_z(h)$, is defined as (Goovaerts 1997) (Olea 1999) (Mount 2008).

$$\gamma_z(h) = \frac{1}{2N(h)} \sum_{N(h)} [\chi(s+h) - \chi(s)]^2 \quad (60)$$

where h is the lag vector representing the separation between two spatial locations; $N(h)$ is the number of pairs separated by lag h ; s is the vector of spatial coordinates with components x and y ; $\chi(s)$ is the variable under consideration as a function of the spatial location; and $\chi(s+h)$ is the lagged version of the variable under consideration.

Figure 28 shows an example of the relationship between the semi-variance and the lag distance computed by Equation (60). Kriging considers the degree of variation between the inspection locations and requires parameters represented to its spatial variability. Thus, the basic steel corrosion trend must be estimated by variogram to identify the parameters including sill, range and nugget. The sill is a variance in which the experimental variogram data appears to level off. The range indicates the distance after which the data are no longer correlated. The nugget is the semi-variance value at the origin referring to the variability of all data.

Given that the Kriging interpolation requires the parameters representing the characteristics of the trend variation, the semi-variogram process must be conducted to obtain the three parameters (i.e., nugget, sill, and range).

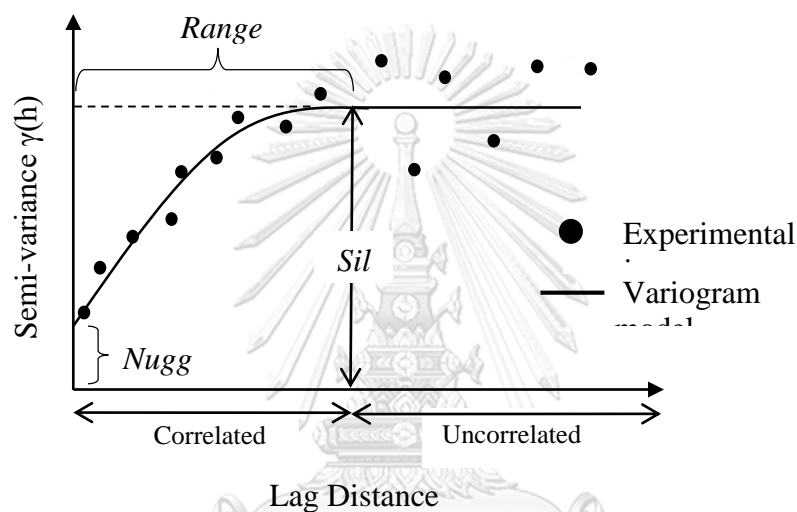


Figure 28 Relationship between the semi-variance and lag distance (Yanweerasak 2016)

Step 4: Conducting the Kriging interpolation and statistical estimation error process.
 - Kriging interpolation

Kriging is a geo-statistical interpolation technique that considers the degree of variation between known data points when the values of the unknown data points must be estimated. Kriging estimation is a weighted linear combination of the known sample values around the estimated points. Kriging interpolation attempts to minimize the error variance and defines the mean of the prediction errors as zero to exclude over- or under-estimations. The Kriging calculation depends on the semi-variogram parameters used to weight nearby inspection locations when interpolating and also provides a model of the directional trends of the data. The basic Kriging equation is (Goovaerts 1997) (Olea 1999) (Mount 2008).

$$Z^*(u) - m(u) = \sum_{\alpha=1}^{n(u)} \lambda_{\alpha} [Z(u_{\alpha}) - m(u_{\alpha})] \quad (61)$$

where u and u_α are the location vectors for the estimation point and neighboring data points indexed by α , respectively; $n(u)$ is the number of data points used to estimate $Z^*(u)$; $m(u)$ and $m(u_\alpha)$ are the expected mean value of $Z(u)$ and $Z^*(u)$, respectively; λ_α the Kriging weight designated to datum $Z(u_\alpha)$ to estimate location u , same datum will receive different weight for different estimation location. Kriging weight λ_α are derived from semi-variogram which should characterize residual component; and $Z(u)$ is the random field.

The Kriging calculation depends on the semi-variogram parameters used to weight nearby inspection locations. An example of the relationship between the steel weight loss and the inspected length (i.e., plastic hinge length and maximum bending moment region shown in Figure 27) calculated by Kriging is presented in Figure 29. The average steel weight loss can be calculated based on the Kriging trend.

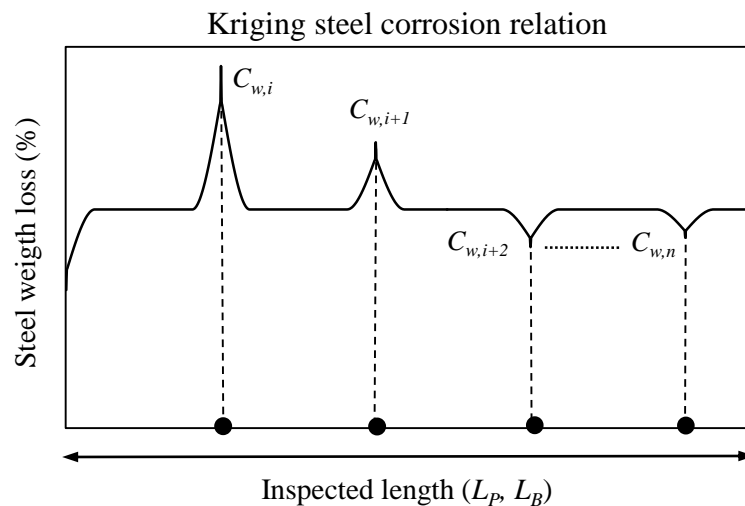


Figure 29 Relationship between the steel weight loss (%) and inspected length

- Statistical error estimation theory

Structural performance is controlled by the mean and the variance of the local average. The local average can be obtained through observational data at the discrete sites. A procedure to conduct statistical error estimation to obtain the variance of the local average of the geotechnical parameters was previously proposed (Honjo 2013). The spatial variability of the geotechnical parameters can be evaluated by the mean and variance of the local average. A geotechnical reliability analysis must be considered to determine the statistical error involved in the estimation because select parameters are predicted by the limited number of measurements at discrete sites. In this study, the procedure for the statistical error estimation is applied in the one-dimensional spatial variability associated with steel weight loss over the longitudinal rebar axis of a RC piers and pre-stressing strands of PC girders.

The method for evaluating the variance of a local average assumes that a layer under the consideration length is homogeneous and that the structural parameter (steel corrosion) can be described by superposing the trend and random component as follows

$$Z(x) = \mu_Z(x) + \varepsilon(x) \quad (62)$$

where Z is the structural parameter in the random field; x is the spatial coordinate; μ_Z is the mean value of Z ; ε is the random component of the random field with a mean of 0 and a variance of σ_Z^2 .

The autocorrelation function can be provided as $\rho(\Delta x/\theta)$, where θ is the autocorrelation distance. To evaluate the statistical estimation error of the local average, the spatial distribution of the steel corrosion trend is modelled by the random field. When the random field is assumed to be Gaussian, $\varepsilon(x) \sim N(0, \sigma_Z^2, \theta)$ is defined. In this study, σ_Z^2 is defined as the variance in the basic steel corrosion trend and autocorrelation distance, and θ is the range parameter provided by the semi-variogram process.

- *Local average and variance function*

The local average of the random field is

$$Z_v(x) = \frac{1}{V} \int_{x-V/2}^{x+V/2} Z(u) du \quad (63)$$

where x is the central coordinate of the local average and V is the target length over which the local average (inspection locations) is measured.

The mean of the local average coincides with that of the original random field when stationary behavior is assumed; for this study, the mean is provided by Kriging interpolation. The variance of the local average can be computed by the variance function, $\Gamma^2(V/\theta)$, which is a function of σ_Z^2 and V/θ .

$$E[Z_v(x)] = E\left[\frac{1}{V} \int_{x-V/2}^{x+V/2} Z(u) du\right] = \mu_Z \quad (64)$$

$$\sigma_{Z_v}^2 = E[(Z_v(x) - \mu_Z)^2] = \frac{\sigma_Z^2}{V^2} \int_{x-V/2}^{x+V/2} \int_{x-V/2}^{x+V/2} \rho(|u-v|) dudv = \sigma_Z^2 \Gamma^2\left(\frac{V}{\theta}\right) \quad (65)$$

Once the autocorrelation function is determined, $\Gamma^2(V/\theta)$ can be obtained. The exponential-type autocorrelation function can be given as

$$\rho(\Delta x) = \exp[-\Delta x / \theta] \quad (66)$$

$$\Gamma^2\left(\frac{V}{\theta}\right) = \left(\frac{\theta}{V}\right)^2 [2\left(\frac{V}{\theta}\right) - 1 + \exp\left(-\frac{V}{\theta}\right)] \quad (67)$$

The variance of the local average is obtained by

$$\sigma_{z_v}^2 = \sigma_z^2 \left[\Gamma^2\left(\frac{V_1}{\theta_1}\right) \Gamma^2\left(\frac{V_2}{\theta_2}\right) \Gamma^2\left(\frac{V_3}{\theta_3}\right) \right] \quad (68)$$

This variance is obtained by multiplying the variance of the basic steel corrosion trend from Figures 22 to 26 by the statistical estimation error. V_2 , V_3 and θ_2 , θ_3 shown in Equation (68) could be used for multi-dimensional cases. Since the correlation function is assumed to be separable, the theory developed in one-dimensional can be easily extended to multi-dimensional cases therefore variance function can be separated to evaluate the variance of the local average. The variance depends on the number of inspections, the space interval between inspection locations, and the correlation level of a basic steel corrosion trend.

4.6 Updating Based on Inspection Result by using SMCS

The seismic reliability of RC piers and reliability of PC girders can be estimated using Equations (26), (29), and Equation (30), respectively. Because inspection data are obtained from existing RC bridges, the means and COVs of the involved random variables can be updated. In this paper, the nine random variables listed in Table 3 are used to calculate the time-variant steel weight loss. All random variables associated with the inspection results can be updated simultaneously by SMCS process. The details of the SMCS procedure and how the updated random variables are applied to the reliability analysis can be found in (Yoshida 2009). Figure 30 shows the flowchart of reliability estimation by using SMCS. When steel weight loss was provided by inspection process, the observational equation based on inspection data is presented in Equation (69). The corresponding values are estimated by random variables, and the observation noise is required in the SMCS. The observational equation in this study is

$$W_{updated} = W_{predicted} + v \quad (69)$$

where $W_{updated}$ is the average steel weight loss obtained by the Kriging trend based on inspection results; $W_{predicted}$ is the steel weight loss at t years estimated by Equations (43) to (53); and v is the observation noise with a standard normal distribution. Because v depends on the magnitude of the measuring error, this value is assumed to be equal to the variance associated with the estimated steel weight loss from inspection process described by the statistical error estimation theory. When the average steel weight loss is estimated using a limited number of inspection results, the variance will increase. In this case, the variances associated with random variables after updating are approximately the same as those prior to updating.

Average steel weight losses and variances are representative data of the current state of the steel weight loss in the plastic hinge (L_P) of RC piers and region with maximum bending moment (L_B) of PC girders. The data include the effects of the spatial steel corrosion distribution and the estimation error given the limited inspection locations. The data are used to update the related random variables using SMCS. This method decreases the epistemic uncertainties associated with the prediction of the steel weight loss. Based on the updated random variables, the updated time-variant steel

weight losses and updated life-cycle reliability for an existing RC bridge structures can be obtained.

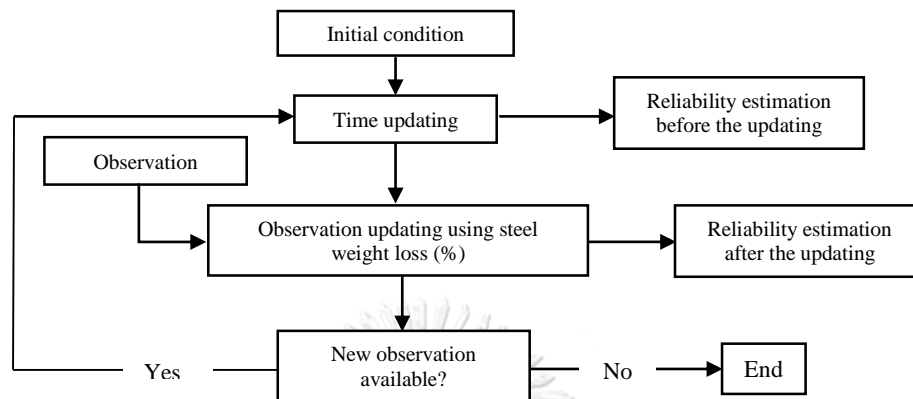


Figure 30 Flowchart of reliability estimation using SMCS (Akiyama 2010) (Yoshida 2009)

CHAPTER 5

ILLUSTRATIVE EXAMPLE

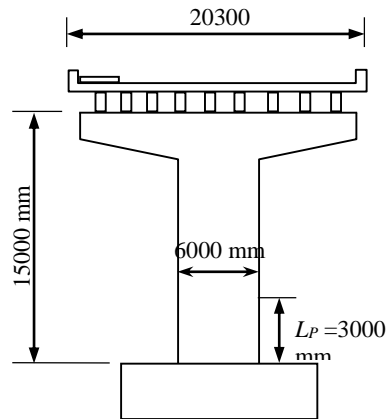
It is assumed that the RC bridges analyzed here were exposed to multiple hazards including seismic hazards, traffic hazards and hazards associated with airborne chloride. Seismic and traffic hazards affect the entire bridge structure. However, certain bridge components are more likely to fail because of specific hazards. This study estimates the life-cycle reliability of RC piers under seismic and airborne chloride hazards and PC girders under traffic and airborne chloride hazards.

5.1 Analyzing the Configuration of an RC Pier and a PC Girder

Figures 31 and 32 show the configurations of the RC pier and PC girder, respectively from a hypothetical RC bridge analyzed to exemplify the techniques discussed in this paper. Seismic fragility of RC pier modeled as SDOF was estimated based on the results of Akiyama et al. (Akiyama 2011). The bridge was designed according to the Design Specifications for Highway Bridges (DSHB) of the Japan Road Association (2002). The reliabilities of the RC bridge pier and PC girder were estimated using Equations (12) and (15), respectively

In field investigations of existing bridge piers, corrosion cracks and minor cover spalling are observed after approximately 30 years. Therefore, it is assumed that inspections for steel weight loss were conducted 30 years after construction of the RC pier and PC girder. Steel weight loss at the plastic hinge of the RC pier was inspected. The plastic hinge length L_P is equivalent to the plastic hinge length proposed by Mattock (Mattock 1965). Akiyama et al. (Akiyama 2011) reported that L_P does not vary with the amount of steel weight loss. The region with the maximum bending moment, L_B , was determined based on the distribution of traffic loading. The girder span length was 30 m. A simple support was assumed to connect the RC pier and PC girder, as shown in Figure 32. Therefore, even if the girder had deteriorated, this would not induce additional demands on the pier; similarly, if seismic excitation had occurred, this would not induce additional flexural demand on the girder. The bridge had ten girders and four traffic lanes. Based on the vehicle loading distribution determined by traffic simulation, Courbon's method theory was used to evaluate the effect of the transverse bending moment distribution on the target girder. For the bridge girder analyzed in this study, the exterior girder always experiences greater flexural demand (lower reliability) compared to the interior girders; therefore, the reliability of the exterior PC girder was analyzed. However, further research is needed to estimate the reliability considering the series-parallel system of the girders.

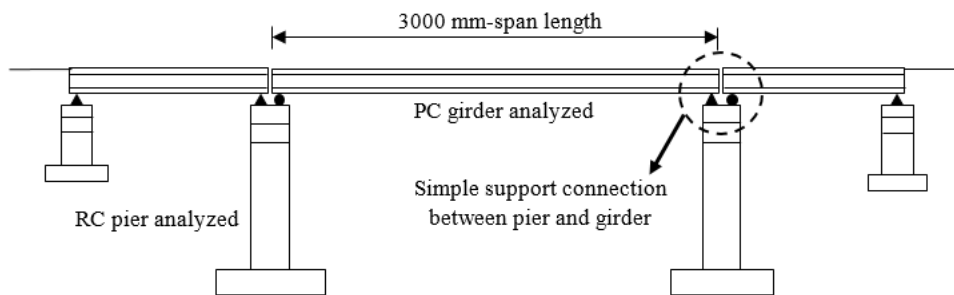
For the corrosion model of the pre-stressing strand, a uniform cross-sectional area was assumed, although spatial distribution over the girder was considered. In addition, it was assumed that chloride could only penetrate from the bottom of the girder.



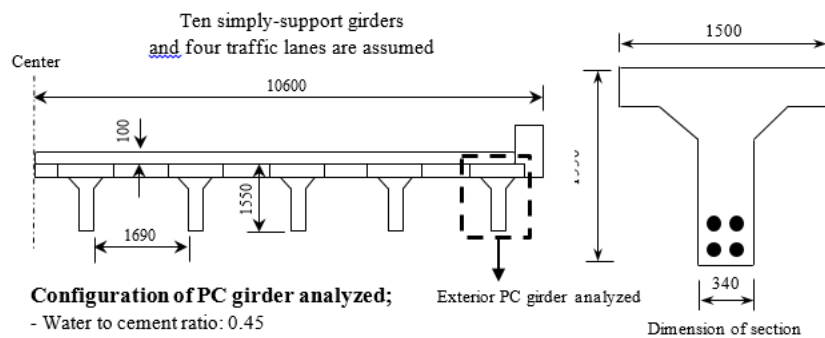
Configuration of RC pier analyzed;

- Dimension of section: 6000x3000 mm
- Longitudinal reinforcement ratio: 1.02%
- Volumetric ratio of ties: 0.53%
- Natural period: 0.61 sec
- Water to cement ratio: 0.45
- Concrete cover: 100 mm
- Plastic hinge length (L_p): 3000 mm

Figure 31 Structural details of the RC pier analyzed in this study



* *Based on the simple support connection, if the PC girder is deteriorated, this will not induce any additional demand in the RC pier and the PC girders are not affected by seismic excitation



Configuration of PC girder analyzed;

- Water to cement ratio: 0.45
- Concrete cover: 50 mm
- Pre-stressing strand type: 4 groups of SWPR7B 16S12.7mm
- Region with maximum bending moment (L_b): 5000 mm at mid-span

Figure 32 Structural details of the PC girder analyzed in this study

5.2 Structural Fragility and Degradation of Structural Performance

5.2.1 Seismic Fragility of the RC Pier with the Various Amount of Steel Weight

Loss

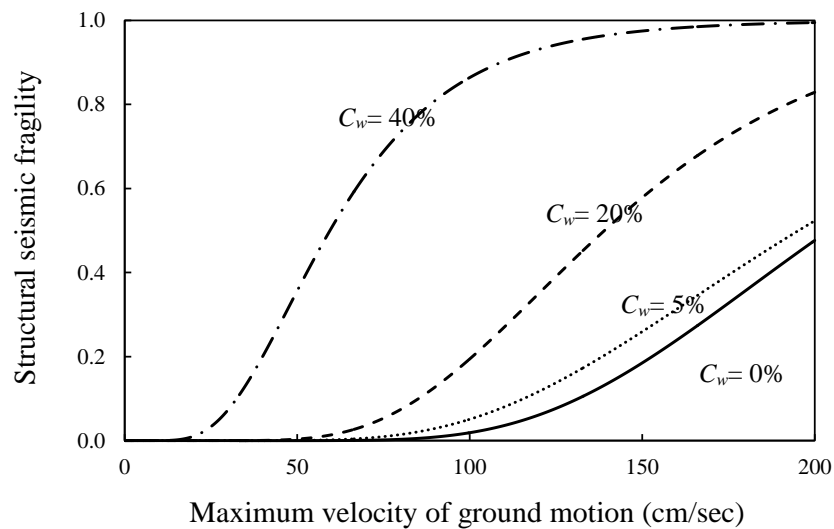


Figure 33 Seismic fragility curves of the RC pier with the various amount of steel weight losses

The seismic fragility curves of the RC pier, shown in Figure 32, were estimated by considering the reduced cross-sectional area of the steel rebar, cracking of the concrete cover due to expansion from steel corrosion and degradation of the bond between the concrete and steel. These effects decrease the ability of the ties and concrete covers to prevent lateral deformation of longitudinal rebar and reduce ductility. Akiyama et al. (Akiyama 2011) describe the process of evaluating the relationship between the moment and the curvature at the onset of buckling for longitudinal rebar of corroded RC columns, considering how steel corrosion reduces the prevention force exerted by ties and concrete covers.

Figure 33 shows the fragility curves associated with the relationship between the seismic intensity S (the maximum velocity of the ground motion) and the conditional probability $P[S_{de} \geq S_{ca}/S, C_w]$ of the RC pier with a steel weight losses, C_w , of 0, 10, 20, 30, and 40%. The RC pier's behavior was only calculated for the longitudinal direction of the bridge. Details of the generation of ground motions used in this study are provided by Akiyama et al. (Akiyama 2011). The fragility curves for greater amounts of steel weight loss shift to the left relative to those for smaller steel weight losses.

5.2.2 Flexural Degradation of the PC girder Due to Steel Weight Loss

Based on the results of cross-sectional analysis using the reduced cross-sectional area of pre-stressing wire strands in the PC girder, Figure 34 shows the relationship between the flexural bending capacity (MN·m) and weight loss for pre-stressing wire strands (%). Greater weight loss in pre-stressing wire strands decreases the flexural capacity.

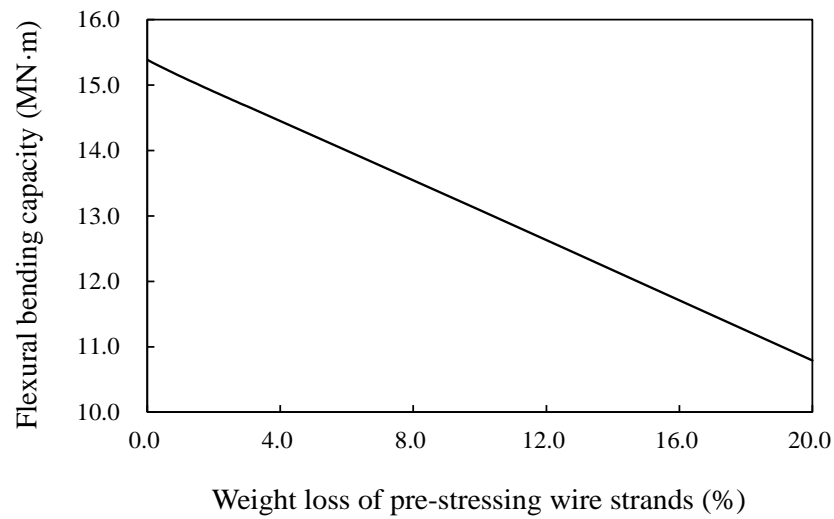


Figure 34 Flexural degradation of the PC girder due to steel weight losses

5.3 Results of Hazard Assessment

5.3.1 Seismic Hazard

The relationship between annual probability of exceedance and maximum ground motion velocity (cm/sec) between three cities in Japan (cases studies) are shown in Figure 32 known as a seismic hazard curve. It is used to estimate the seismic demand of RC pier. Based on Figure 35, the differences in seismic intensity among three cities are explicitly observed.

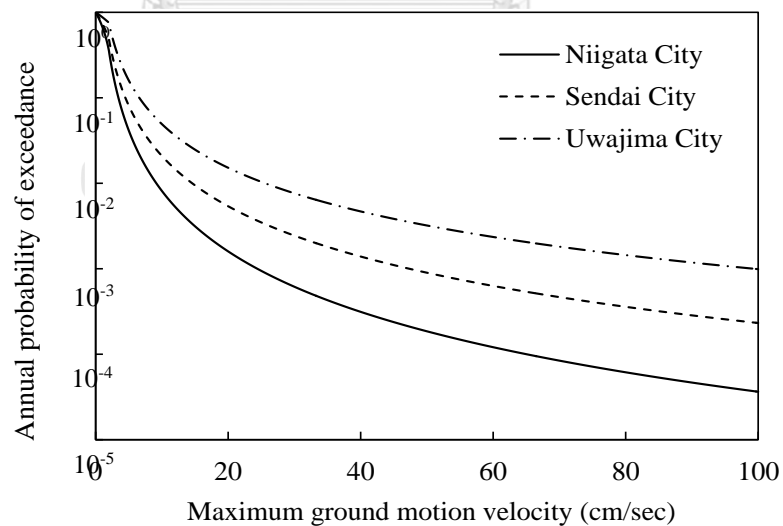


Figure 35 Seismic hazard curves of Niigata City, Sendai City, and Uwajima City

5.3.2 Hazard Associated with Airborne Chloride

Steel weight loss can be estimated based on the amount of airborne chloride (Akiyama 2010). In this study, the parameters to estimate the amount of airborne chloride in marine environment are average of wind speed, COVs of average of wind speed, ratio of sea wind, and distance from coastal line. As expressed in Equation (43), the amount of airborne chloride in each city can be estimated by using parameter shown in Table 4. Based on amount of airborne chloride, the steel weight loss can be estimated using Equations (43) to (53) and random variables listed in Table 3.

Table 4 Lists of parameters for predicting amount of airborne chloride

| Locations | Average of wind speed (m/s) | COVs of average of wind speed | Ratio of sea wind |
|--------------|-----------------------------|-------------------------------|-------------------|
| Niigata City | 3.69 | 0.072 | 0.125 |
| Sendai City | 3.42 | 0.173 | 0.251 |
| Uwajima City | 2.38 | 0.167 | 0.169 |

5.3.3 Traffic hazard

Figure 36 show the relationship between cumulative probability density function (CDF) and annual maximum bending moment for the PC girder estimated by traffic loading simulation using statistics of vehicles. Severe and mild traffic conditions are estimated using a different mixing rate of vehicles. The effect of difference in traffic loadings on the reliability of PC girder are discussed in this paper. Using this CDF, $L_{max,i}$ in Equation (14) can be calculated.

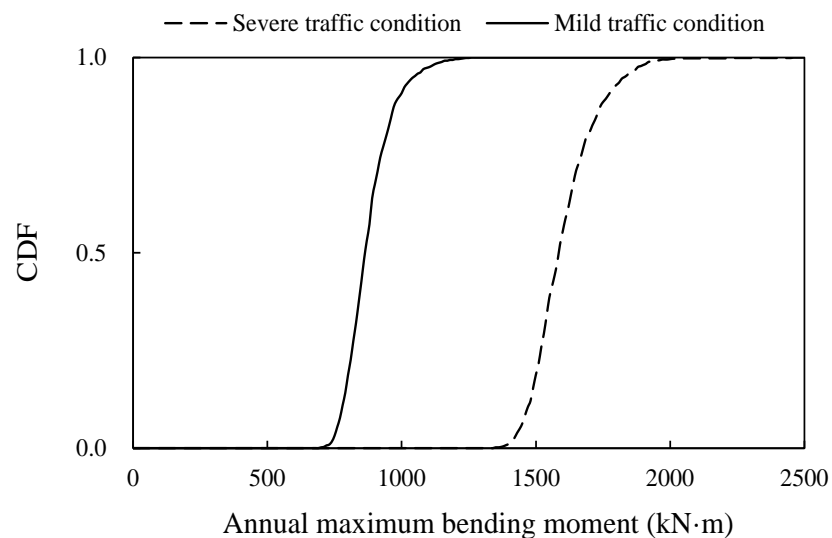


Figure 36 CDF of an annual maximum bending moment due to traffic loading simulation

5.4 Assumed Inspection Results

As an illustrative example, all cases study are considered to investigate the effects of the differences in the seismic hazard (depend on the city), traffic hazard (severe and mild conditions), airborne chloride hazard (distance from coastal line, $d=0.1$ and 0.5 km), the number of inspection locations, the magnitude of measured steel weight loss, and the frequency of inspection on the life-cycle reliability of existing RC bridge. Table 5 to 10 presents the detail of all the cases study. Figures 37 to 42 show the assumed inspection results and the location of inspection. It is assumed that inspection results can be obtained from the existing RC bridge pier, and exiting PC bridge girder simultaneously to compare the life-cycle reliability level after updating. The magnitudes of steel weight loss provided by inspection process in this study are assumed. However, in reality the magnitude of steel weight loss can be obtained on site. Coring test must be conducted at designed inspection locations to remove the cover concrete until surface of steel rebar can be seen. Then, magnifying glass with small camera will be used to take picture to observe the surface condition of steel rebar. Finally, image analysis will be conducted to estimate the amount of steel weight loss. Even though, this method can observe the steel weight loss only one side of steel rebar. Field investigations of existing bridge piers have reported that corrosion cracks and minor cover spalling occur after approximately 30 years in Japan (Ministry of Land, Infrastructure, Transport and Tourism: Annual Report on Bridge Maintenance, 2017). This is the reason why year of inspection in this study was mostly assumed to be 30 and 35 year.

Based on the buckling analysis of longitudinal rebar in the RC bridge pier, the plastic hinge length, L_p , is assumed to be 3000 mm. It is assumed that inspection process to investigate the amount of steel weight losses are taken within the plastic hinge length. For the PC girder, it is assumed that the inspection process is taken at the possible region with maximum bending moment estimated by computational analysis based on distribution of traffic loading. It is assumed to be 5000 mm at the interval of mid-span of PC bridge girder.

Abbreviations of cases study are used. N, S, and U stand for Niigata, Sendai, and Uwajima city, respectively. P and G stand for pier and girder, respectively. For example NG1 stand for the Case 1 of girder in Niigata City. SP2 stand for Case 2 of pier in Sendai City.

5.4.1 Inspection Results for Niigata City

Table 5 Details of the inspection process of the RC pier in Niigata City

| Case | Year of inspection | Distance from the coastline (d) | Number of inspection locations | Average steel weight loss of inspection results ($C_{w,avg}$) | Basic steel corrosion trends |
|------|--------------------|-------------------------------------|--------------------------------|---|------------------------------|
| NP1 | - | 0.1 km | No inspection result | | |
| NP2 | - | 0.5 km | No inspection result | | |
| NP3 | 30 | 0.1 km | 3 | 1.50 % | Figure 24 |
| NP4 | 30 | | 5 | 1.54 % | |
| NP5 | 30 | | 2 | 1.31 % | |
| NP6 | 30 | 0.5 km | 3 | 0.66 % | Figure 23 |
| NP7a | 30 | 0.1 km | 3 | 1.50 % | Figure 24 |
| NP7b | 35 | | | 4.49 % | Figure 26 |

Distance along the plastic hinge length ($L_P = 3000$ mm)

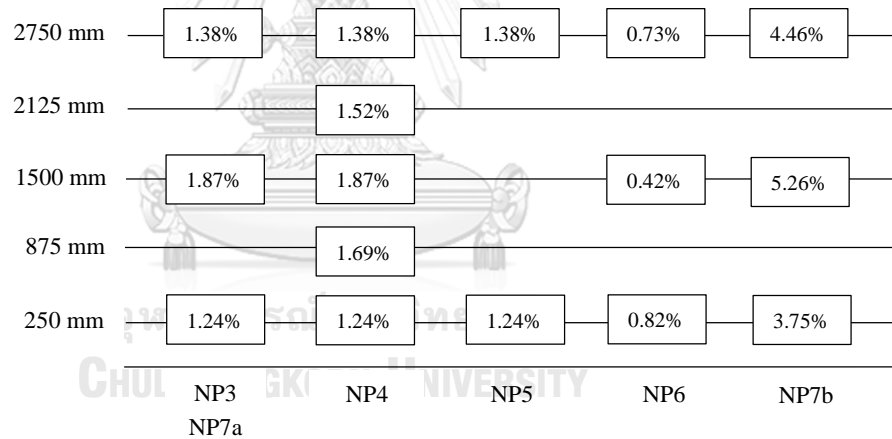


Figure 37 Amount of steel weight loss in each inspection location for the RC pier in Niigata City

Table 6 Details of the inspection process of the PC girder in Niigata City

| Case | Year of inspection | Traffic loading conditions | Distance from the coastline (d) | Number of inspection locations | Average steel weight loss of inspection results ($C_{w,avg}$) | Basic steel corrosion trends |
|------|--------------------|----------------------------|-------------------------------------|--------------------------------|---|------------------------------|
| NG1 | - | Severe | 0.1 km | | No inspection result | |
| | | Mild | | | | |
| NG2 | - | Severe | 0.5 km | | No inspection result | |
| | | Mild | | | | |
| NG3 | 30 | Severe | 0.1 km | 3 | 2.41 % | Figure 22 |
| | | Mild | | | | |
| NG4 | 30 | Severe | | | | |
| NG5 | 30 | Severe | | 2 | 2.19 % | |
| NG6 | 30 | Severe | 0.5 km | 3 | 1.69 % | Figure 23 |
| | | Mild | | | | |
| NG7a | 30 | Severe | 0.1 km | 3 | 2.41 % | Figure 22 |
| NG7b | 35 | | | | 6.18 % | Figure 26 |

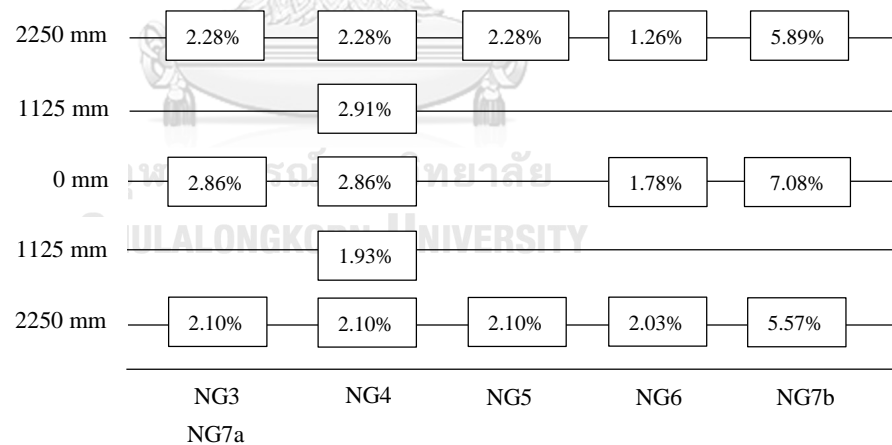
Distance along the region with maximum bending moment ($L_B = 5000$ mm)

Figure 38 Amount of steel weight loss in each inspection location for the PC pier in Niigata City

5.4.2 Inspection Results for Sendai City

Table 7 Details of the inspection process of the RC pier in Sendai City

| Case | Year of inspection | Distance from the coastline (d) | Number of inspection locations | Average steel weight loss of inspection results ($C_{w,avg}$) | Basic steel corrosion trends |
|------|--------------------|-------------------------------------|--------------------------------|---|------------------------------|
| SP1 | - | 0.1 km | No inspection | | |
| SP2 | - | 0.5 km | No inspection | | |
| SP3 | 30 | 0.1 km | 3 | 1.14 % | Figure 25 |
| SP4 | 30 | 0.5 km | | 0.45 % | Figure 22 |
| SP5a | 30 | 0.1 km | | 1.14 % | Figure 25 |
| SP5b | 35 | | | 3.47 % | |

Distance along the plastic hinge length ($L_P = 3000$ mm)

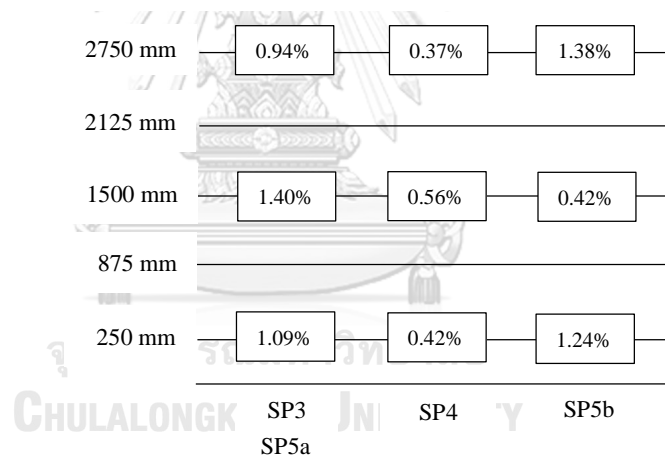


Figure 39 Amount of steel weight loss in each inspection location for the RC pier in Sendai City

Table 8 Details of the inspection process of the PC girder in Sendai City

| Case | Year of inspection | Traffic loading conditions | Distance from the coastline (d) | Number of inspection locations | Average steel weight loss of inspection results ($C_{w,avg}$) | Basic steel corrosion trends |
|------|--------------------|----------------------------|-------------------------------------|--------------------------------|---|------------------------------|
| SG1 | - | Severe | 0.1 km | | | No inspection result |
| | | Mild | | | | |
| SG2 | - | Severe | 0.5 km | | | No inspection result |
| | | Mild | | | | |
| SG3 | 30 | Severe | 0.1 km | | 1.87 % | Figure 24 |
| | | Mild | | | | |
| SG4 | 30 | Severe | 0.5 km | 3 | 1.03 % | Figure 25 |
| | | Mild | | | | |
| SG5a | 30 | Severe | 0.1 km | | 1.87 % | Figure 24 |
| SG5b | 35 | | | | 4.14 % | Figure 26 |

Distance along the region with maximum bending moment ($L_B = 5000$ mm)

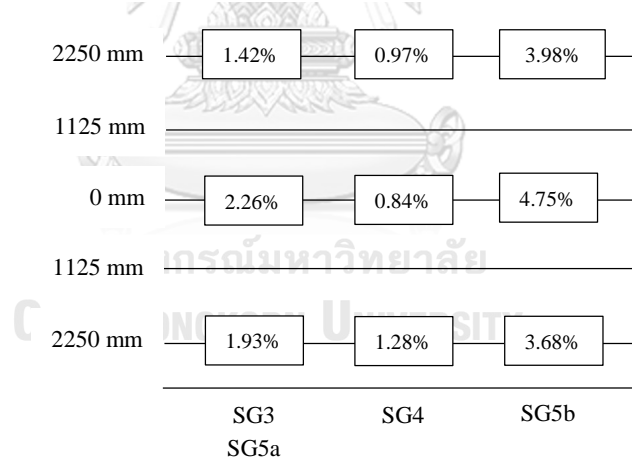


Figure 40 Amount of steel weight loss in each inspection location for the PC girder in Sendai City

5.4.3 Inspection Results for Uwajima City

Table 9 Details of the inspection process of the RC pier in Uwajima City

| Case | Year of inspection | Distance from the coastline (d) | Number of inspection locations | Average steel weight loss of inspection results ($C_{w,avg}$) | Basic steel corrosion trends |
|------|--------------------|-------------------------------------|--------------------------------|---|------------------------------|
| UP1 | - | 0.1 km | No inspection result | | |
| UP2 | - | 0.5 km | No inspection result | | |
| UP3 | 30 | 0.1 km | 3 | 0.65 % | Figure 23 |
| UP4 | 30 | 0.5 km | | 0.26 % | Figure 22 |
| UP5a | 30 | 0.1 km | | 0.65 % | Figure 23 |
| UP5b | 35 | | | 1.83 % | Figure 24 |

Distance along the plastic hinge length ($L_P = 3000$ mm)

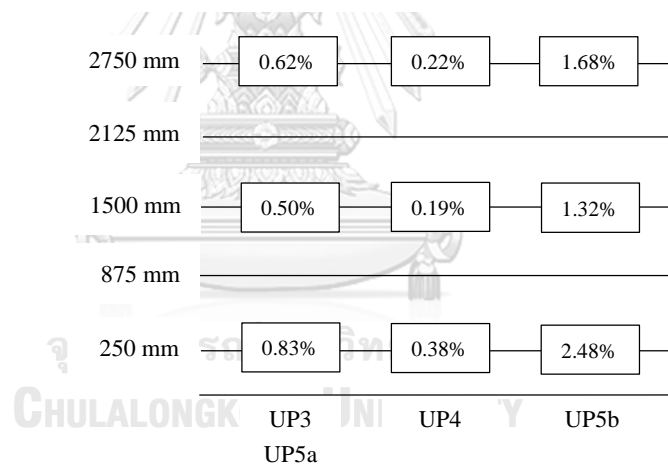


Figure 41 Amount of steel weight loss in each inspection location for the RC pier in Uwajima City

Table 10 Details of the inspection process of the PC girder in Uwajima City

| Case | Year of inspection | Traffic loading conditions | Distance from the coastline (d) | Number of inspection locations | Average steel corrosion of inspection results ($C_{w,avg}$) | Basic steel corrosion trends |
|------|--------------------|----------------------------|-------------------------------------|--------------------------------|---|------------------------------|
| UG1 | - | Severe | 0.1 km | 3 | No inspection result | |
| | | Mild | | | | |
| UG2 | - | Severe | 0.5 km | | No inspection result | |
| | | Mild | | | | |
| UG3 | 30 | Severe | 0.1 km | | 1.02 % | Figure 25 |
| | | Mild | | | | |
| UG4 | 30 | Severe | 0.5 km | 0.57 % | Figure 23 | |
| | | Mild | | | | |
| UG5a | 30 | Severe | 0.1 km | 1.02 % | Figure 25 | |
| UG5b | 35 | | | 2.23 % | | |

Distance along the region with maximum bending moment ($L_B = 5000$ mm)

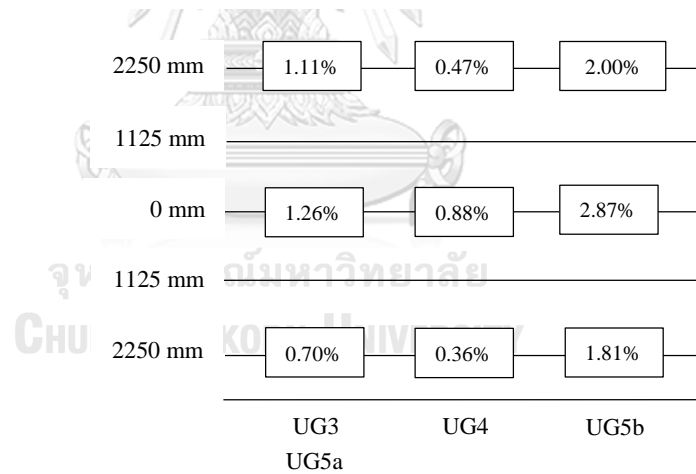


Figure 42 Amount of steel weight loss in each inspection location for the PC girder in Uwajima City

5.5 Results and Discussion

5.5.1 Life-cycle Reliability Assessment without Inspection Results

a) Results of life-cycle seismic reliability of the RC pier

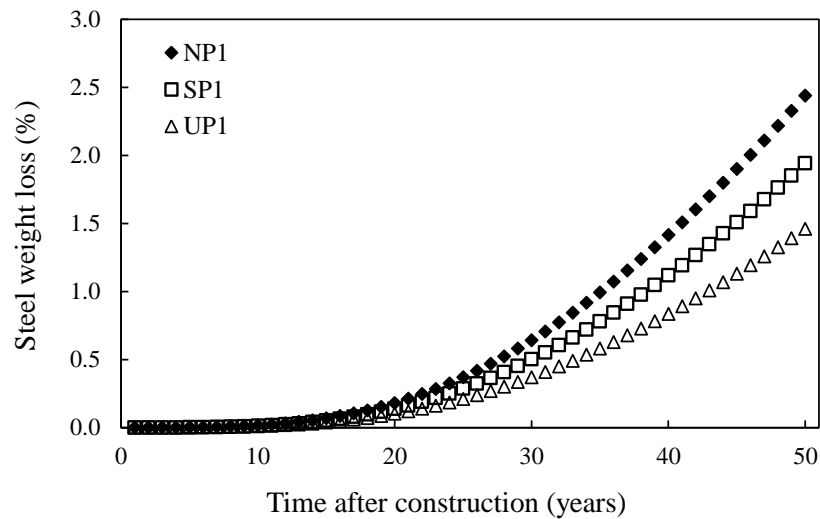


Figure 43 Relationship between the steel weight loss (%) and the time after construction (years) for RC pier at $d=0.1$ km

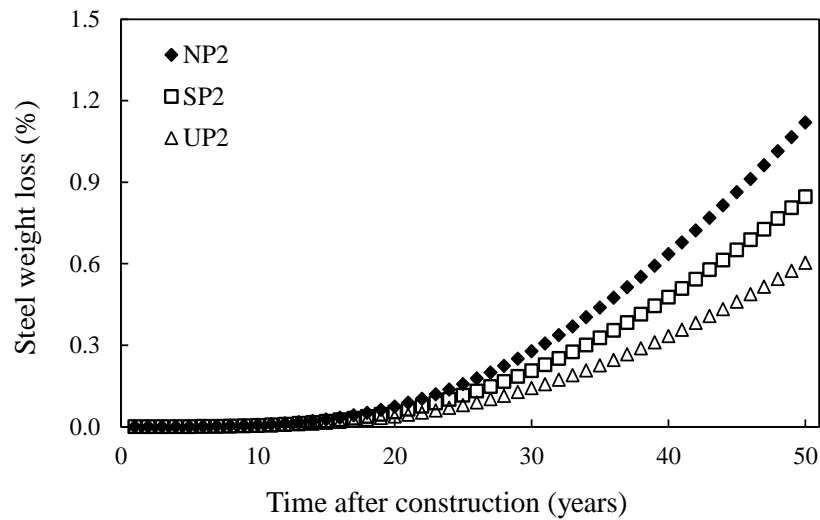
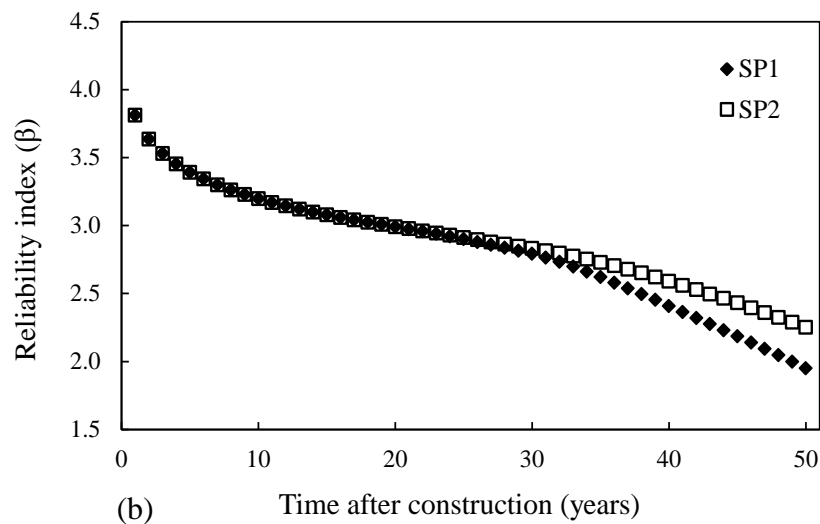
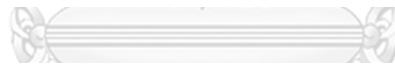
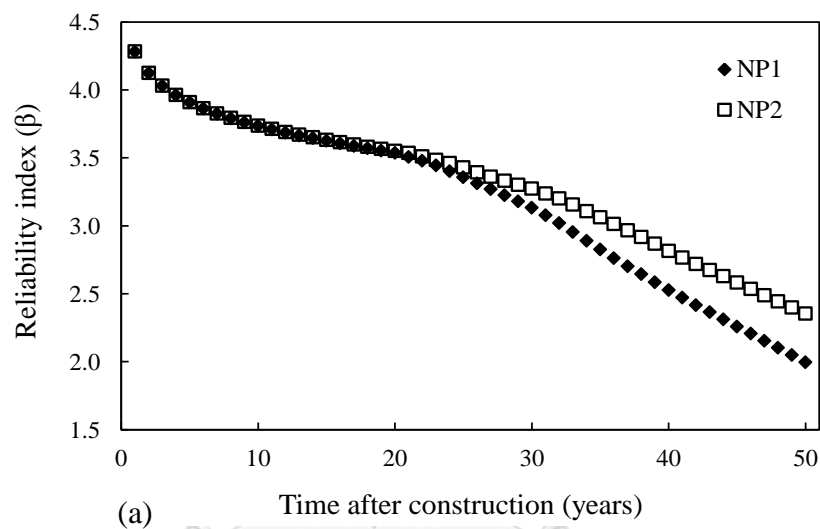


Figure 44 Relationship between the steel weight loss (%) and the time after construction (years) for RC pier at $d=0.5$ km

The relationship between the average steel weight losses (%) and the time after construction (years) of the RC pier are presented in Figures 43 and 44. The average steel weight loss depends on the hazard associated with airborne chloride. The average steel weight losses are calculated by the random variables. The amount of airborne chloride depends on the parameter listed in Table 4. The difference in wind speed, ratio of sea wind, and distance from coastal line results in having different airborne chlorides among three cities. The bridges in Niigata City have greater amounts of steel weight loss than those of Sendai City and Uwajima City. The effect of distance from coastal line can be clearly found between Figure 43 ($d = 0.1$ km) and Figure 44 ($d = 0.5$ km).



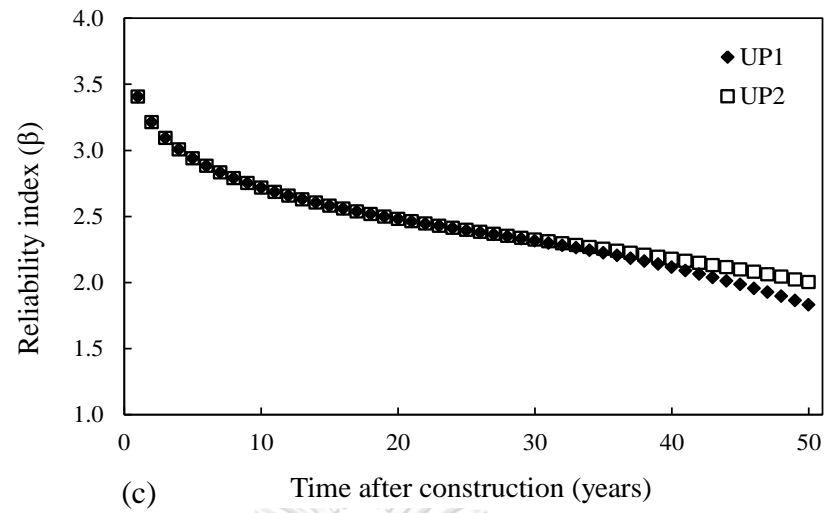


Figure 45 Effect of distance from the coastal line on seismic reliability of the RC pier



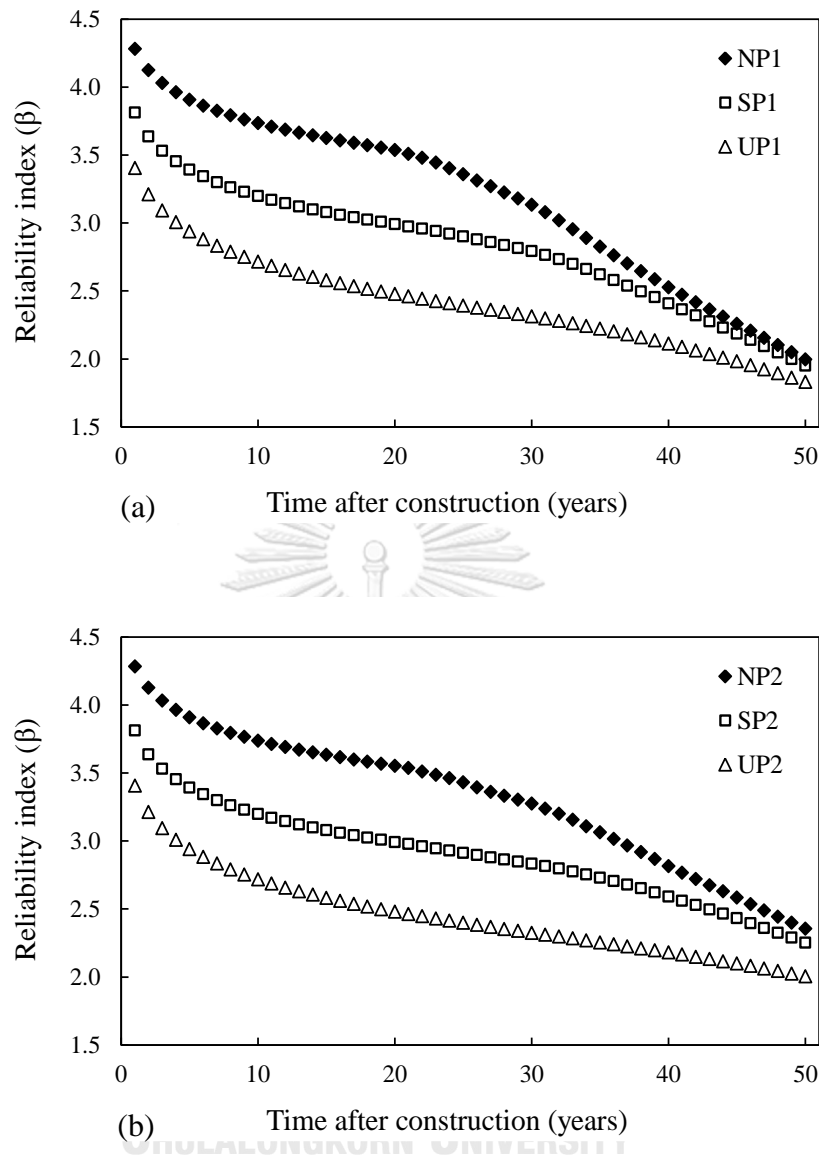


Figure 46 Comparison of seismic reliabilities of the RC piers among Niigata City, Sendai City, and Uwajima City

The seismic reliability of the RC pier is presented in Figures 45 and 46. Figure 45 shows the effect of distance from the coastal line on the seismic reliabilities. The seismic reliabilities at the beginning of the curve depend on the seismic hazard and gradually decrease with time due to material deterioration caused by the increasing of steel weight loss. Figure 46 show the comparison of seismic reliabilities among three cities both in cases of $d=0.1$ km and $d=0.5$ km. The seismic reliabilities of the RC pier in Niigata City are different with those of Sendai City and Uwajima City due to the most severe in seismic hazard among others. Once the effect of steel weight loss is concerned, the seismic reliabilities of Niigata City decrease with the steep slope than those of Sendai City and Uwajima City because Niigata City has a highest amount of steel weight loss as shown in Figures 43 and 44.

b) Results of Life-Cycle Reliability of the PC Girder

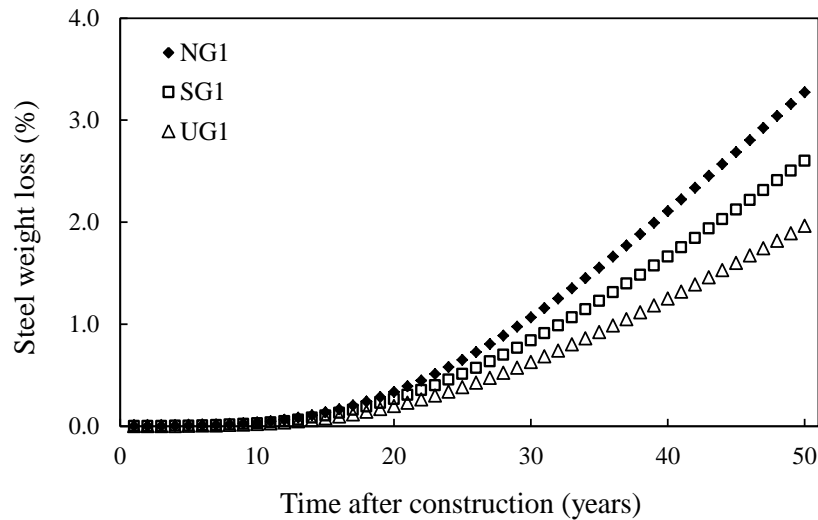


Figure 47 Relationship between the steel weight loss (%) and the time after construction (years) for the PC girder at $d=0.1$ km

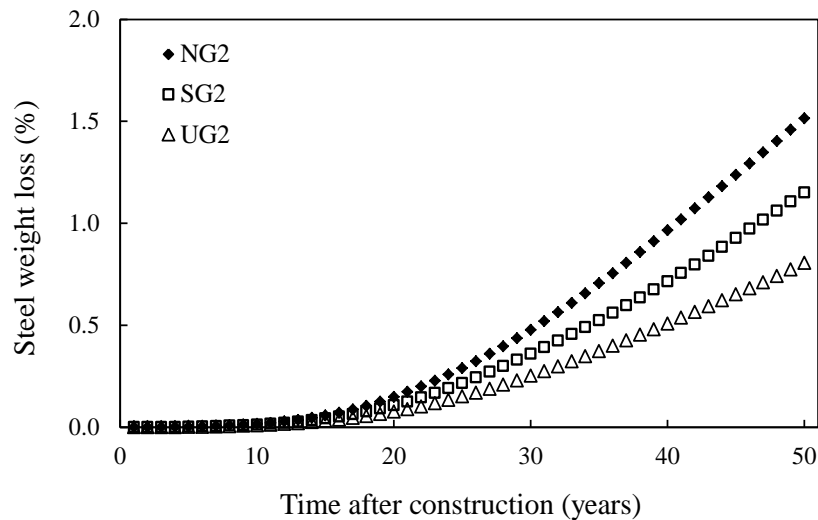


Figure 48 Relationship between the steel weight loss (%) and the time after construction (years) for the PC girder at $d=0.5$ km

The relationship between the average steel weight loss (%) and time after construction (years) of the PC girder are presented in Figure 47 and 48. The average steel weight loss depends on the hazard associated with airborne chloride. The average steel weight losses are calculated based on the parameters listed in Table 4, which present the severity of airborne chloride hazard. The difference in wind speed, ratio of sea wind, and distance from coastal line causes a difference in amount of airborne chlorides between three cities. Niigata City has highest average steel weight loss due to highest wind speed among three cities. The effect of distance from coastal line can be

clearly found between the steel weight losses of Figure 47 ($d = 0.1$ km) and Figure 48 ($d = 0.5$ km).

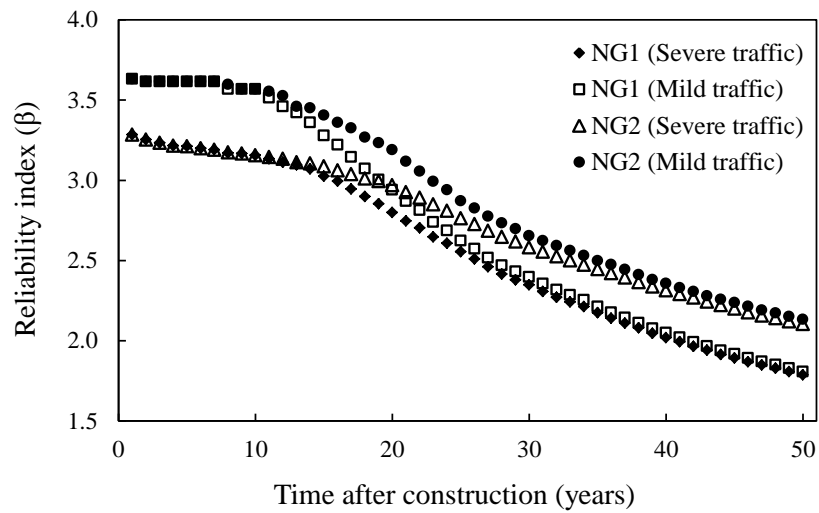


Figure 49 Relationship between life-cycle reliability and time after construction (years) for the PC girder in Niigata City

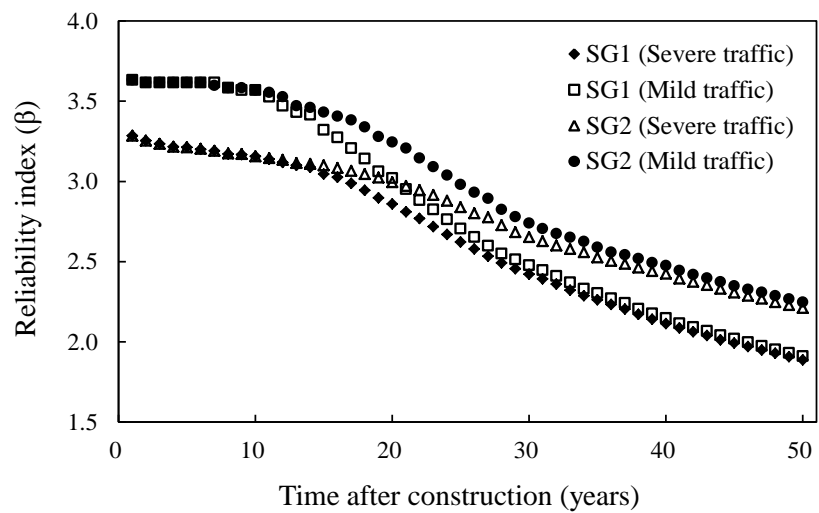


Figure 50 Relationship between life-cycle reliability and time after construction (years) for the PC girder in Sendai City

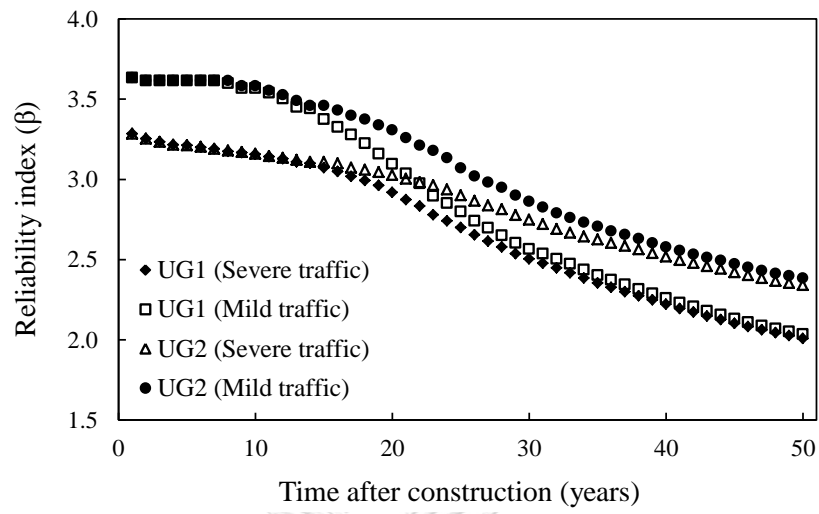


Figure 51 Relationship between life-cycle reliability and time after construction (years) for the PC girder in Uwajima City



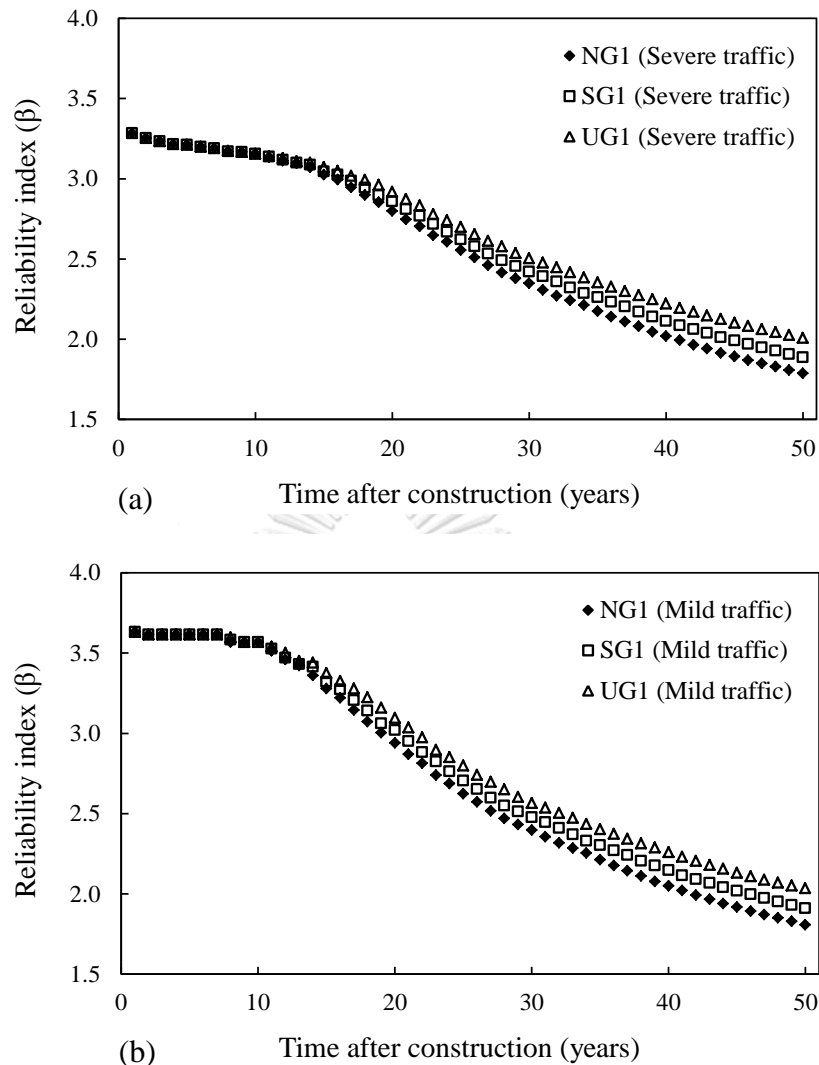


Figure 52 Comparison of life-cycle reliabilities for the PC bridge girder among Niigata City, Sendai City, and Uwajima City

The reliabilities of the PC girder are presented in Figures 49 to 51. The reliabilities at the beginning depend on the traffic hazard and gradually decrease with time due to material deterioration caused by an increasing of steel weight loss. The influences of severity of traffic hazard and the difference in the distance from coastal line are found. The difference in the reliabilities between severe and mild traffic condition are smaller with the time after construction because of the effect of converting value from a cumulative failure probability into a reliability index. As shown in Figure 13, the relationship between failure probability and reliability index is not a linear relationship.

Comparison of the reliabilities of the PC girders among three cities is shown in Figure 52. The reliabilities of the PC girder in Niigata City decrease with the time after construction with a higher slope than those of Sendai City and Uwajima City due to the higher amount of steel weight loss shown in Figures 47 and 48.

5.5.2 Life-Cycle Reliability Assessment with Inspection Results

a) Semi-Variogram Calculation and Kriging Interpolation

To estimate the parameters representing the spatial variability of steel weight loss, semi-variogram calculation are conducted. The example results of semi-variogram relation are shown in Figures 53 to 55. Semi-variogram parameters (Nugget, Sill and Range) for all cases study are listed in Table 11. The three parameters will be used for Kriging interpolation and statistical estimation.

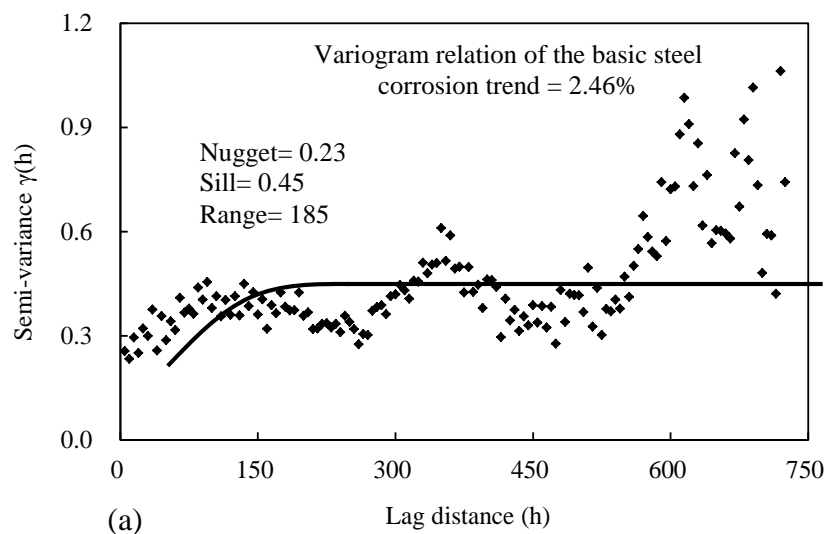


Figure 53 Semi-variogram relation for Case NG4

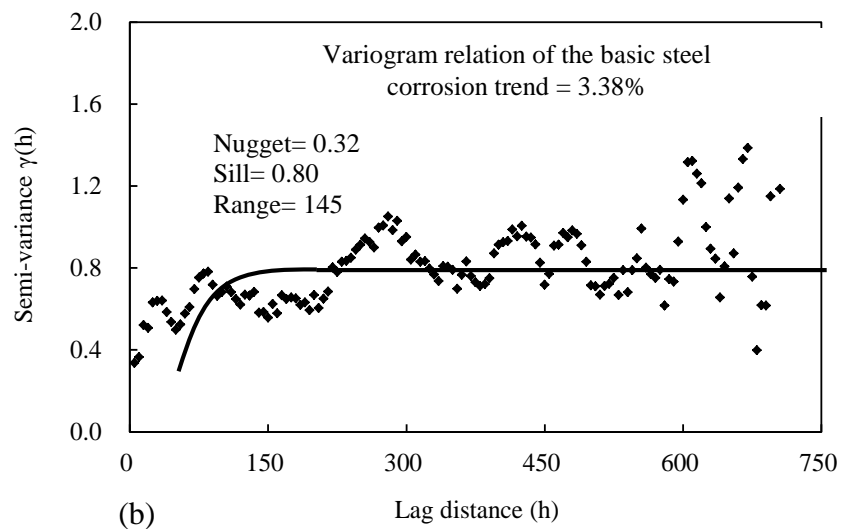


Figure 54 Semi-variogram relation for Case SP5b

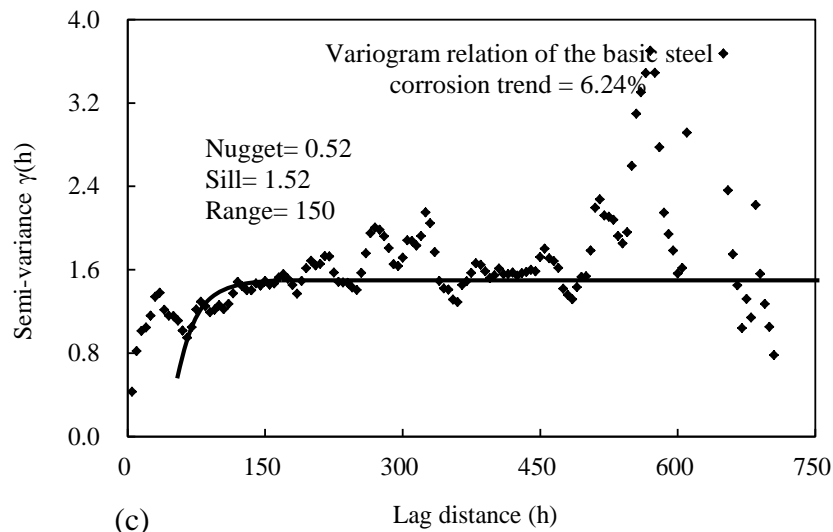
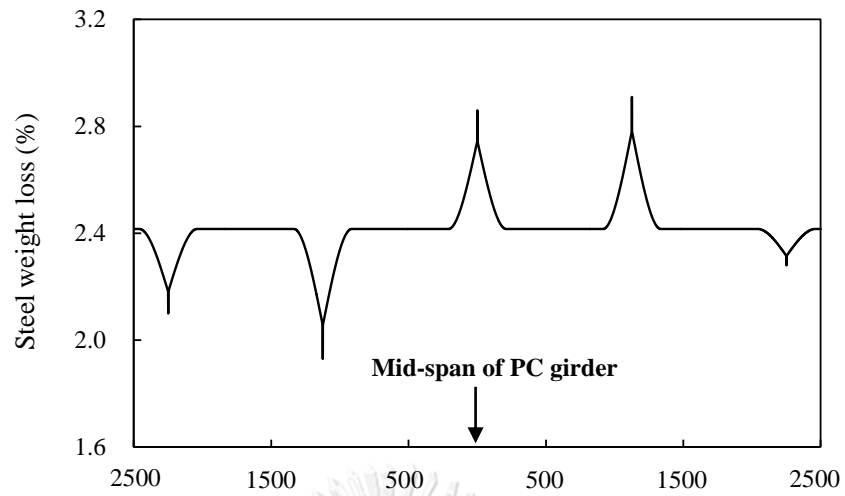


Figure 55 Semi-variogram relation for Case NG7b

Table 11 Semi-variogram parameters

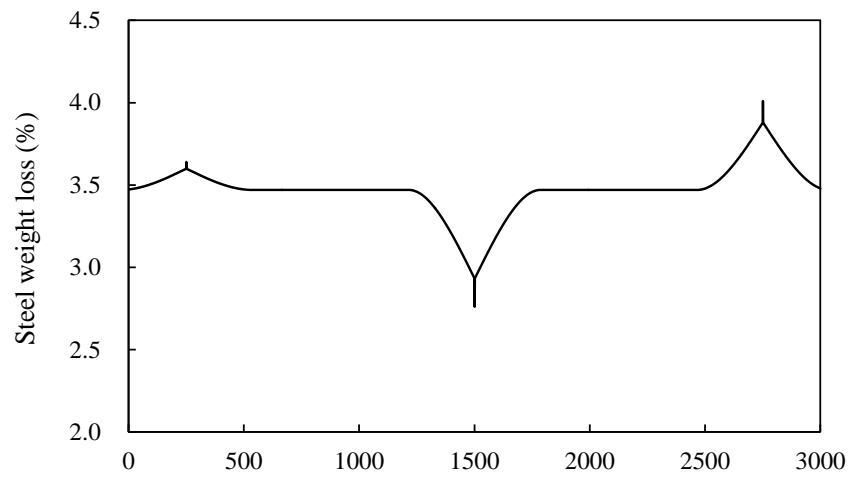
| Basic steel corrosion trend | Semi-variogram parameters | | |
|-----------------------------|---------------------------|-------|-------|
| | Nugget | Sill | Range |
| 0.27 % | 0.028 | 0.058 | 175 |
| 0.66 % | 0.075 | 0.12 | 220 |
| 1.01 % | 0.070 | 0.14 | 195 |
| 1.79 % | 0.19 | 0.27 | 180 |
| 2.29 % | 0.26 | 0.63 | 190 |
| 2.46 % | 0.23 | 0.45 | 185 |
| 3.38 % | 0.32 | 0.80 | 145 |
| 4.12 % | 0.45 | 0.85 | 190 |
| 6.24 % | 0.52 | 1.52 | 150 |

The examples of relationship between the steel weight loss (%) and the inspected length (i.e., plastic hinge length (L_p) of RC pier and region with maximum bending moment (L_B) of PC girder) are shown in Figures 56 to 58. Kriging steel corrosion trend are estimated based on the semi-variogram parameters and the amount of steel weight loss in each inspection location.



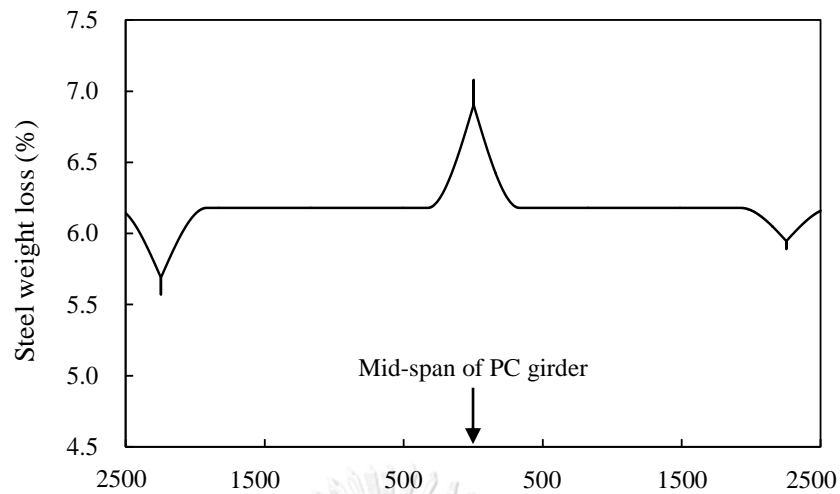
(a) Distance on the region with maximum bending moment

Figure 56 Kriging steel corrosion trend for Case NG4



(b) Distance on the plastic hinge length

Figure 57 Kriging steel corrosion trend for Case SP5b



(c) Distance on the region with maximum bending moment

Figure 58 Kriging steel corrosion trend for Case NG7b

b) Average and variance of steel weight loss

Tables 12 to 17 present the average and variance of steel weight loss based on inspection results in all cases study. Average steel corrosion (second column) is estimated by Kriging steel corrosion trend based on the inspection results and semi-variogram parameters. Statistical estimation error (third column) are calculated which depend on number of inspection location, interval of inspection location and variance of basic steel corrosion trend. Variance of basic steel corrosion trends (fourth column) are provided by experimental results. Variance (fifth column) is estimated by multiplying the variance of the basic corrosion trend with the statistical estimation error.

Table 12 Average and variance of steel weight loss for the RC pier in Niigata City

| Case | Average steel weight loss from kriging trend ($W_{updated}$) | Statistical estimation error | Variance of basic corrosion trend | Variance (v) |
|-------------|--|------------------------------|-----------------------------------|------------------|
| NP1 | No inspection result | | | |
| NP2 | | | | |
| NP3 | 1.54 % | 0.312 | 0.101 | 0.032 |
| NP4 | 1.58 % | 0.129 | 0.101 | 0.013 |
| NP5 | 1.36 % | 0.628 | 0.101 | 0.063 |
| NP6 | 0.69 % | 0.316 | 0.109 | 0.034 |
| NP7a | 1.54 % | 0.312 | 0.101 | 0.032 |
| NP7b | 4.43 % | 0.308 | 0.490 | 0.151 |

Table 13 Average and variance of steel weight loss for the PC girder in Niigata City

| Case | Average steel weight loss from kriging trend ($W_{updated}$) | Statistical estimation error | Variance of basic corrosion trend | Variance (v) |
|-------------|--|------------------------------|-----------------------------------|------------------|
| NG1 | No inspection result | | | |
| NG2 | | | | |
| NG3 | 2.43 % | 0.319 | 0.348 | 0.111 |
| NG4 | 2.46 % | 0.134 | 0.348 | 0.047 |
| NG5 | 2.22 % | 0.649 | 0.348 | 0.226 |
| NG6 | 1.72 % | 0.323 | 0.101 | 0.033 |
| NG7a | 2.23 % | 0.319 | 0.348 | 0.111 |
| NG7b | 6.22 % | 0.305 | 1.513 | 0.461 |

Table 14 Average and variance of steel weight loss for RC pier in Sendai City

| Case | Average steel weight loss from kriging trend ($W_{updated}$) | Statistical estimation error | Variance of basic corrosion trend | Variance (v) |
|-------------|--|------------------------------|-----------------------------------|------------------|
| SP1 | No inspection result | | | |
| SP2 | | | | |
| SP3 | 1.10 % | 0.320 | 0.126 | 0.040 |
| SP4 | 0.48 % | 0.329 | 0.109 | 0.036 |
| SP5a | 1.10 % | 0.320 | 0.126 | 0.040 |
| SP5b | 3.44 % | 0.308 | 0.743 | 0.229 |

Table 15 Average and variance of steel weight loss for PC girder in Sendai City

| Case | Average steel weight loss from kriging trend ($W_{updated}$) | Statistical estimation error | Variance of basic corrosion trend | Variance (v) |
|-------------|--|------------------------------|-----------------------------------|------------------|
| SG1 | No inspection result | | | |
| SG2 | | | | |
| SG3 | 1.85 % | 0.326 | 0.101 | 0.033 |
| SG4 | 1.02 % | 0.329 | 0.126 | 0.041 |
| SG5a | 1.85 % | 0.326 | 0.101 | 0.033 |
| SG5b | 4.10 % | 0.317 | 0.490 | 0.155 |

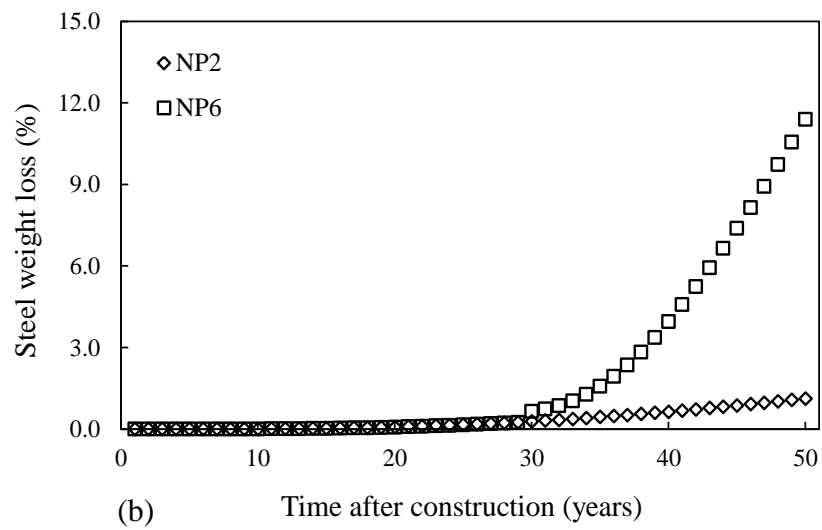
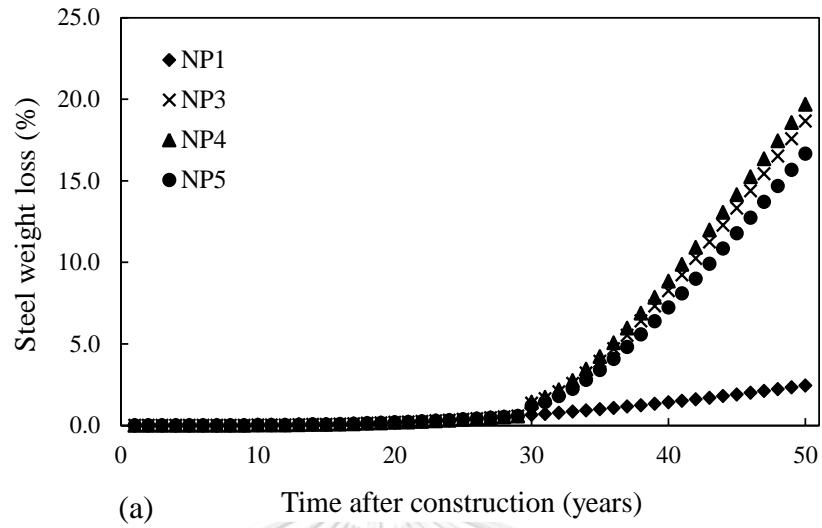
Table 16 Average and variance of steel weight loss for RC pier in Uwajima City

| Case | Average steel weight loss from kriging trend ($W_{updated}$) | Statistical estimation error | Variance of basic corrosion trend | Variance (v) |
|-------------|--|------------------------------|-----------------------------------|------------------|
| UP1 | No inspection result | | | |
| UP2 | | | | |
| UP3 | 0.68 % | 0.317 | 0.109 | 0.035 |
| UP4 | 0.29 % | 0.330 | 0.045 | 0.015 |
| UP5a | 0.68 % | 0.317 | 0.109 | 0.035 |
| UP5b | 1.80 % | 0.317 | 0.101 | 0.032 |

Table 17 Average and variance of steel weight loss for PC girder in Uwajima City

| Case | Average steel weight loss from kriging trend ($W_{updated}$) | Statistical estimation error | Variance of basic corrosion trend | Variance (v) |
|-------------|--|------------------------------|-----------------------------------|------------------|
| UG1 | No inspection result | | | |
| UG2 | | | | |
| UG3 | 1.00 % | 0.323 | 0.126 | 0.041 |
| UG4 | 0.61 % | 0.325 | 0.109 | 0.035 |
| UG5a | 1.00 % | 0.323 | 0.126 | 0.041 |
| UG5b | 2.25 % | 0.318 | 0.423 | 0.135 |

For illustrative example in this study, the effects of number of inspection locations on the structural reliability of the bridge are considered only in Niigata City. When comparing the variance v of Cases NP3 (three inspection locations) and NP5 (two inspection locations) with that of Case NP4 (five inspection locations), v in Case NP4 is reduced due to the increased number of inspection results. These differences affect the updating of random variables, reducing of uncertainties associated with prediction of steel weight loss.

c) Results of Updated Life-Cycle Seismic Reliability of the RC Pier

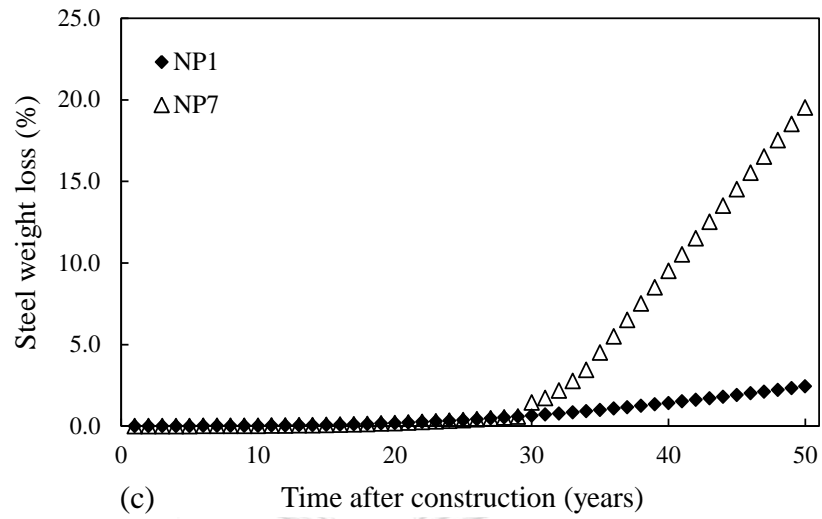
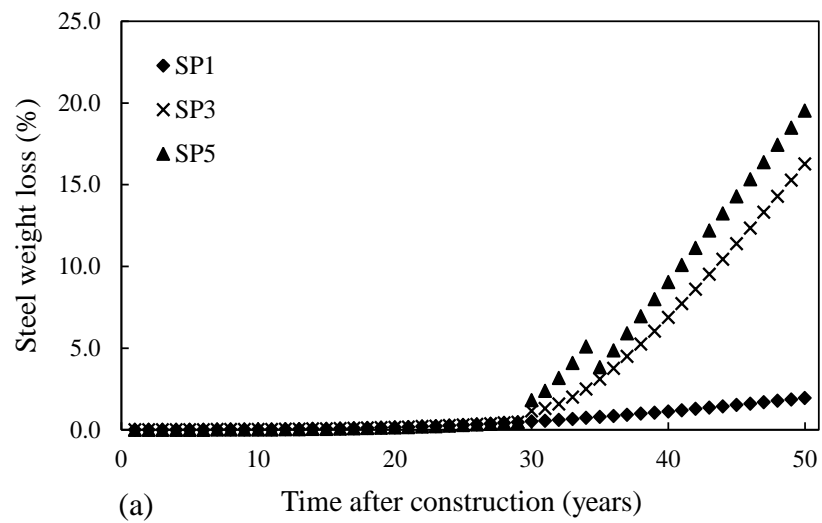


Figure 59 Relationship between updated steel weight loss (%) and time after construction (years) for the RC pier in Niigata City



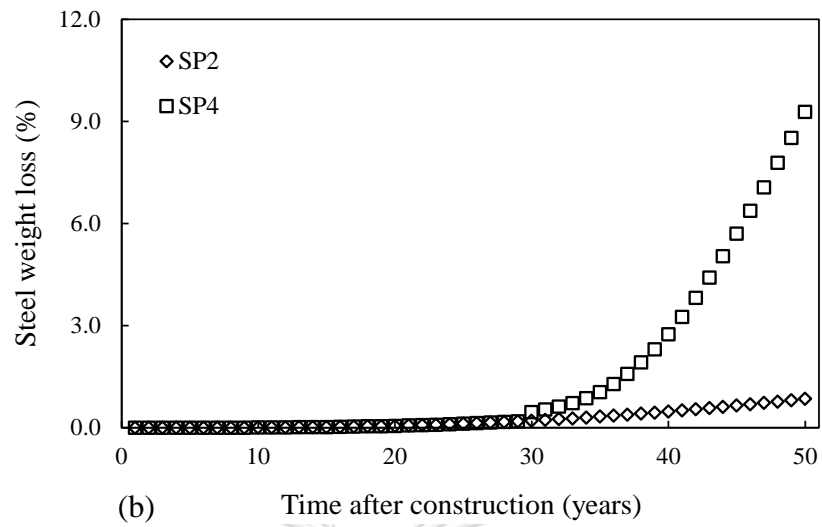
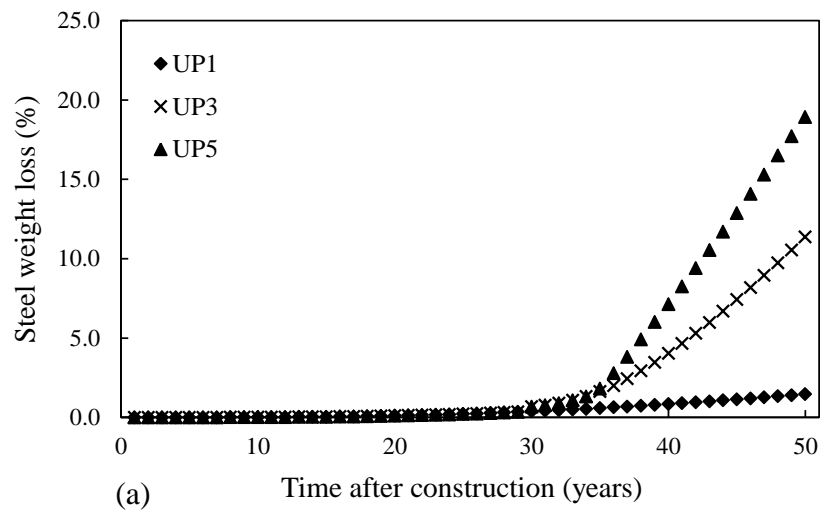


Figure 60 Relationship between updated steel weight loss (%) and time after construction (years) for the RC pier in Sendai City



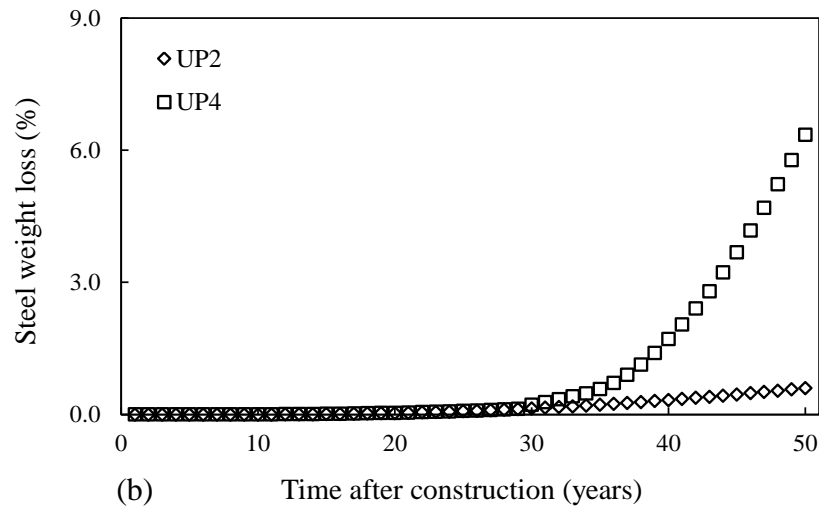
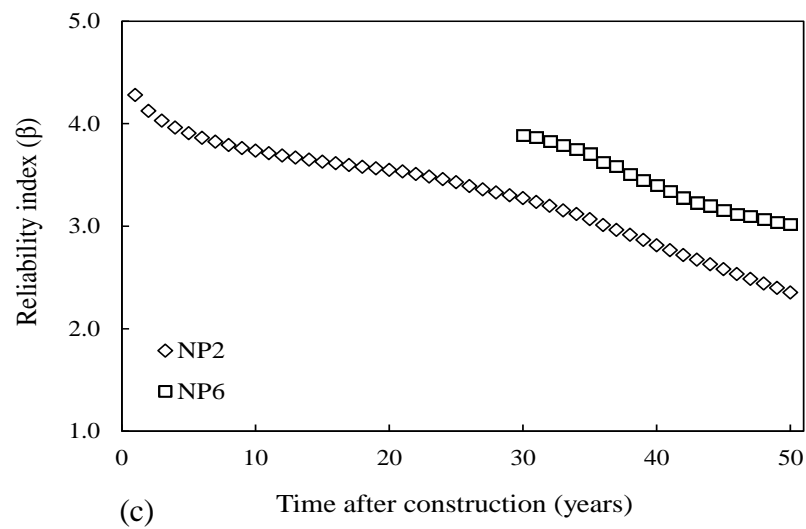
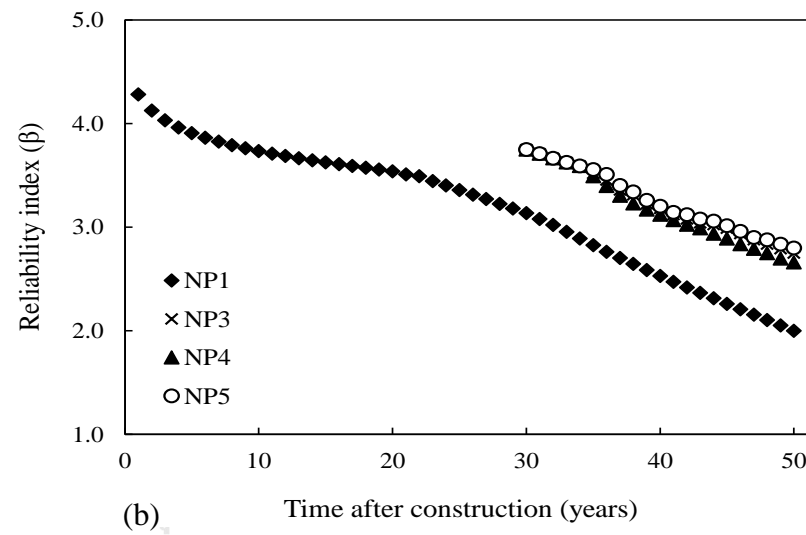
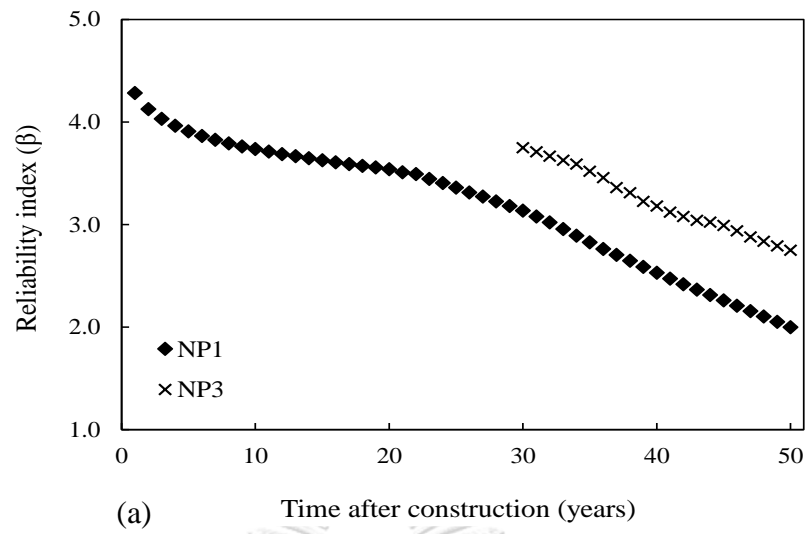


Figure 61 Relationship between updated steel weight loss (%) and time after construction (years) for the RC pier in Uwajima City

Figures 59 to 61 present the relationships between the average steel weight losses (%) and the time after construction (years) for the RC pier in Niigata City, Sendai City, and Uwajima City. When the existing RC pier is inspected to investigate the steel weight loss, the predicted steel weight loss at the time of inspection estimated by the random variable listed in Table 3 will be updated to be consistent with the given inspection results. For example, Case NP3 in Figure 59(a), the magnitude of the steel weight loss at 29 years (0.56%) is updated at 30 years (1.50%) based on given inspection result shown in Table 12. Average steel weight loss after updating is increased with the higher slope than that of before updating since all random variables related with the given inspection results are updated to be consistent with the level of inspection data which is higher than the prediction by using previous random variable.



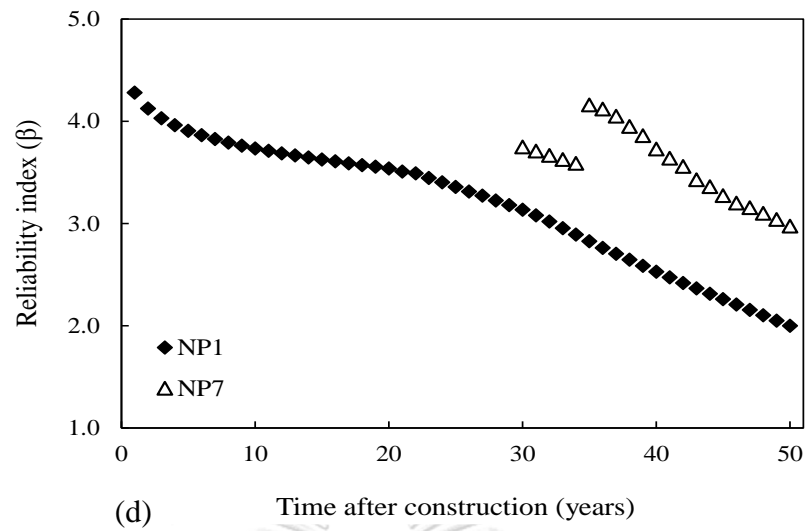


Figure 62 Relationship between updated seismic reliability and time after construction (years) for the RC pier in Niigata City



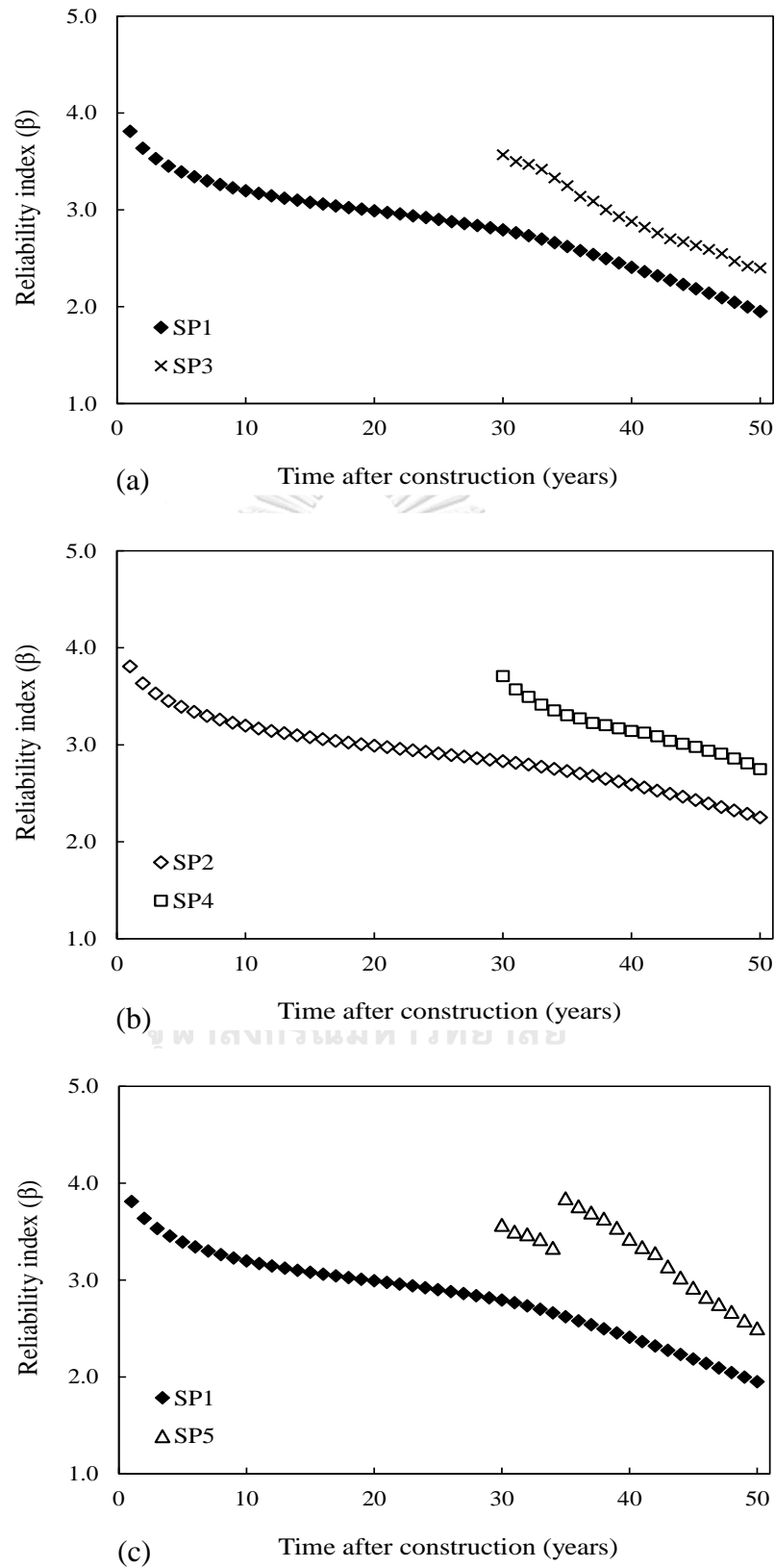


Figure 63 Relationship between updated seismic reliability and time after construction (years) for the RC pier in Sendai City

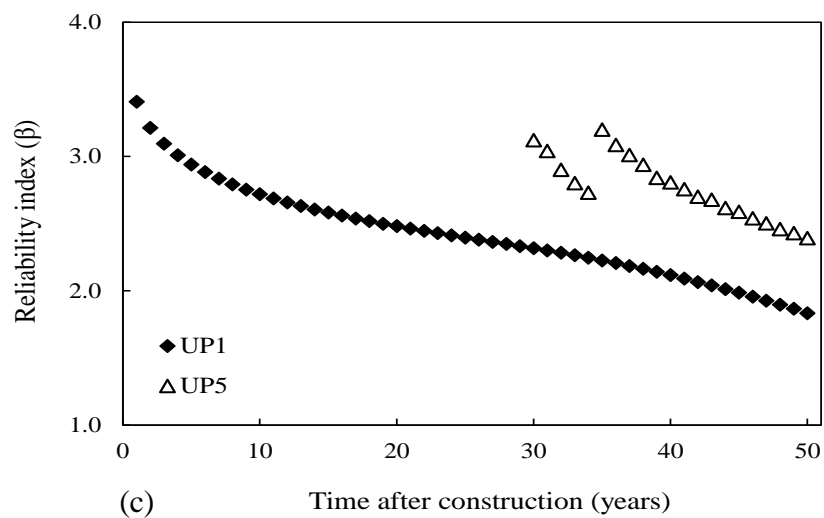
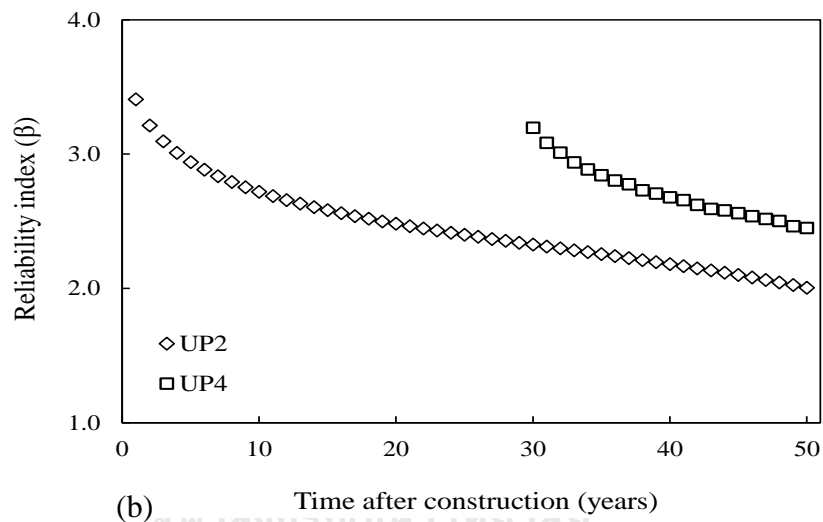
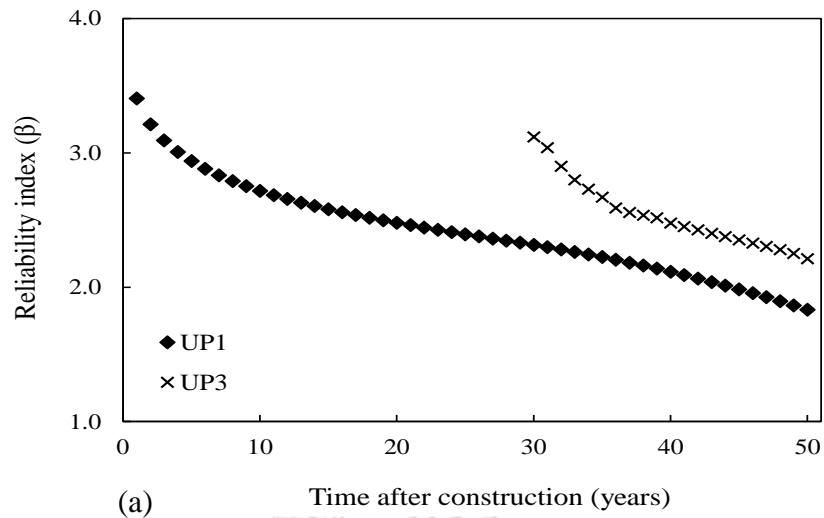
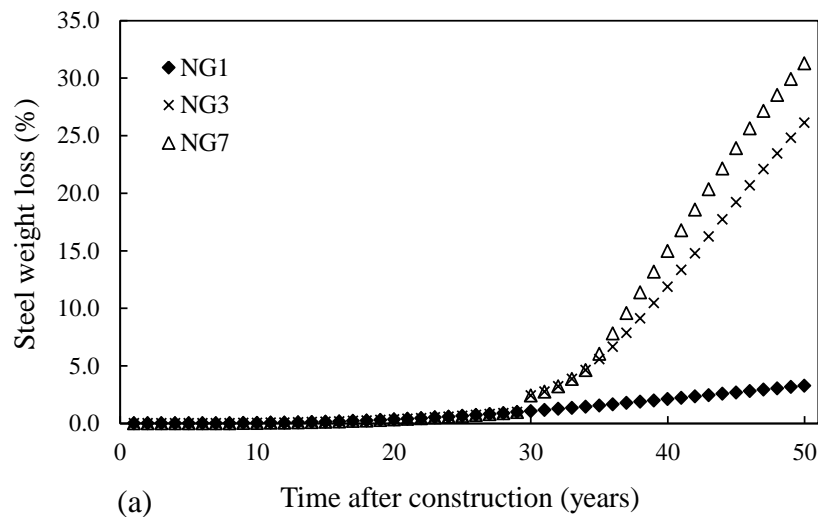


Figure 64 Relationship between updated seismic reliability and time after construction (years) for the RC pier in Uwajima City

Figures 62 to 64 show the updated seismic reliability of the RC piers for three cities. After updating using inspection data, the seismic reliabilities at 30 years are higher than those of before updating since uncertainties associated with prediction of steel weight loss listed in Table 3 are reduced based on updating process. For example, the seismic reliability of the RC pier of Case UP4 in Figure 64(b) is updated using average and variance of steel weight loss shown in Table 16. The seismic reliability with updating is higher than that of without updating (Case UP2). As illustrated in Figure 62(d), Figure 63(c), and Figure 64(c), the effects of frequency of inspection are presented. The seismic reliabilities at 35 years are increased again due to the latest inspection results.

The effect of the number of inspection locations are shown in Figure 62(b), although the seismic reliabilities of the RC pier are nearly identical among Case NP3 (three inspection locations), Case NP4 (five inspection locations), and Case NP5 (two inspection locations) because the magnitudes of steel weight loss from the inspection results are almost identical. However significant differences of using different number of inspection locations are explained using the correlation between random variables shown in Figure 71. These results illustrate that having more inspection locations will develop a more accurate life-cycle reliability assessment.

d) Results of Updated Life-Cycle Reliability of the PC Girder



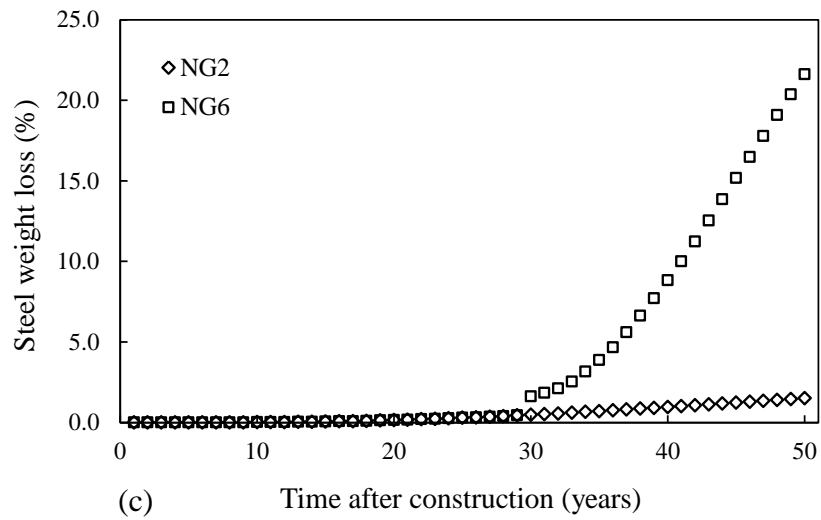
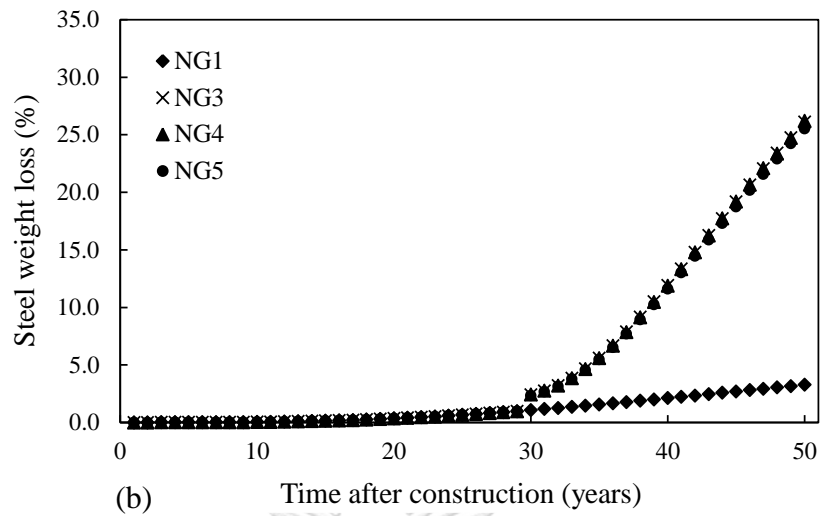


Figure 65 Relationship between updated steel weight loss (%) and time after construction (years) for PC girder in Niigata City

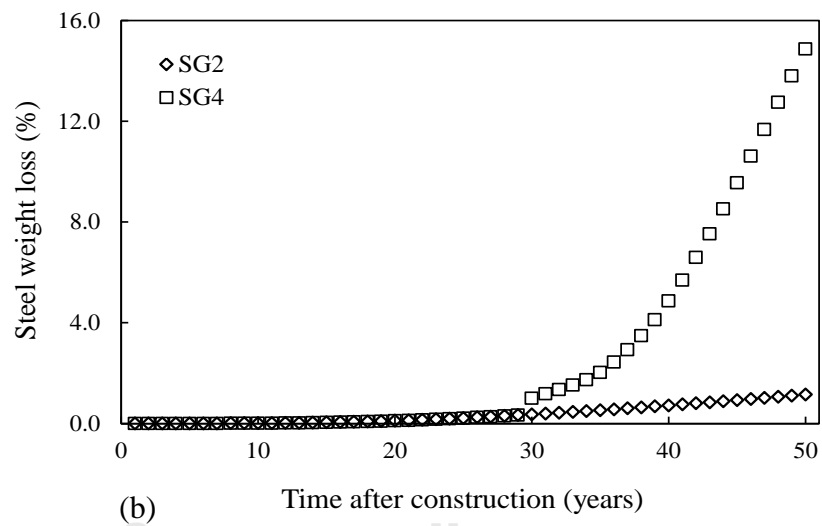
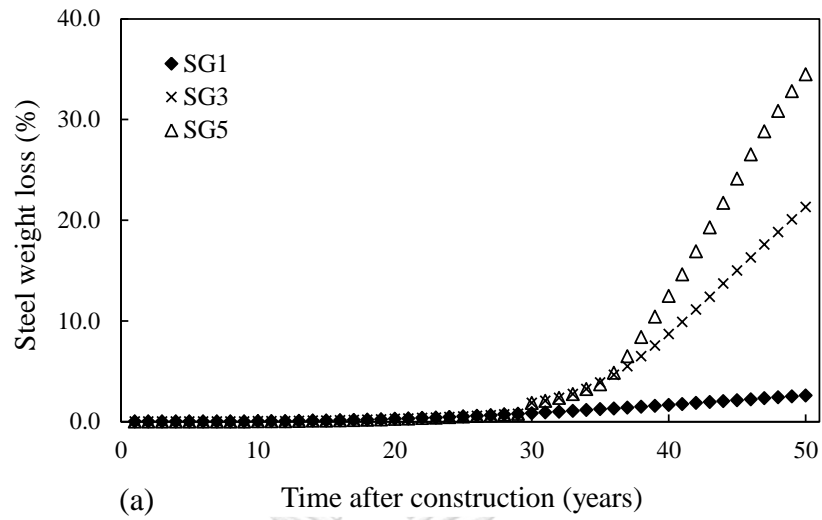


Figure 66 Relationship between updated steel weight loss (%) and time after construction (years) for PC girder in Sendai City

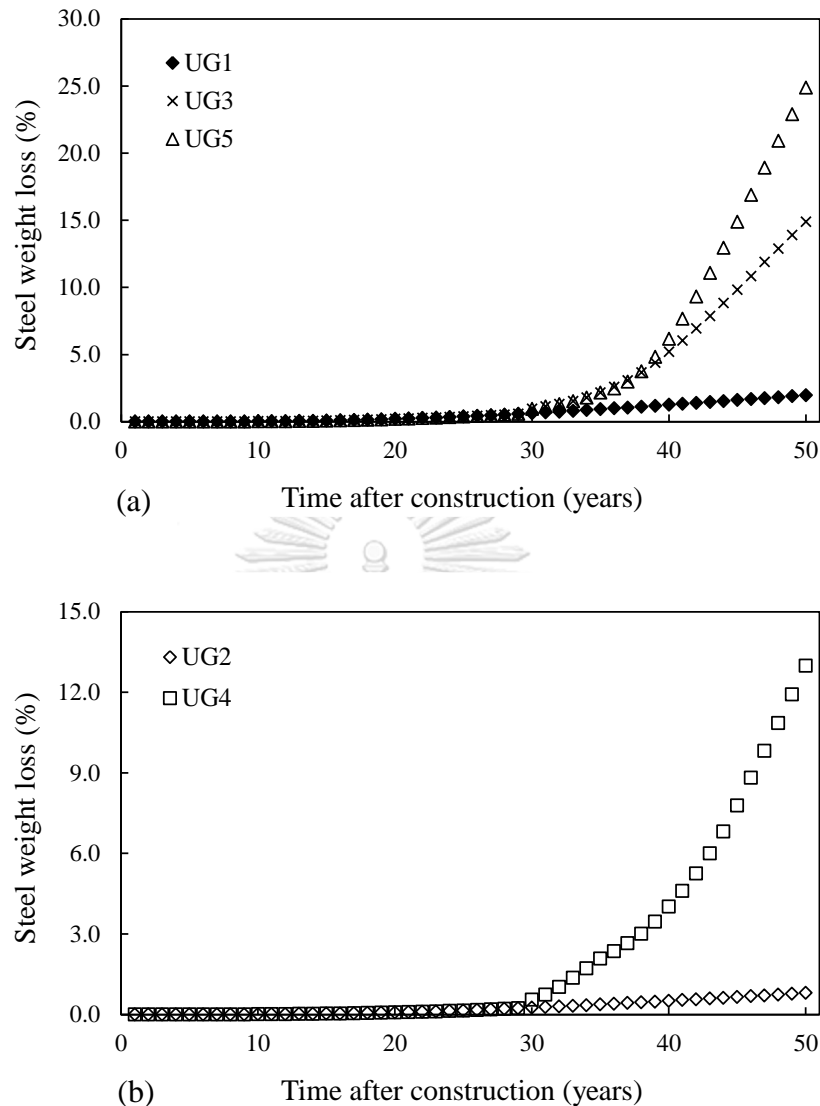
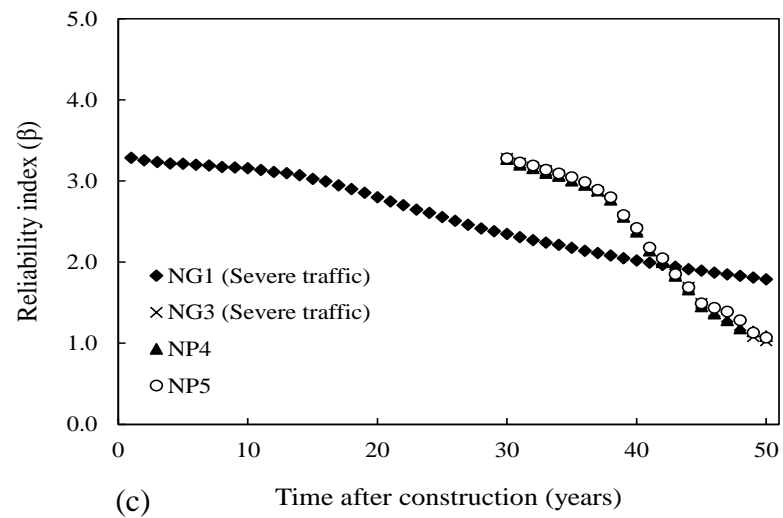
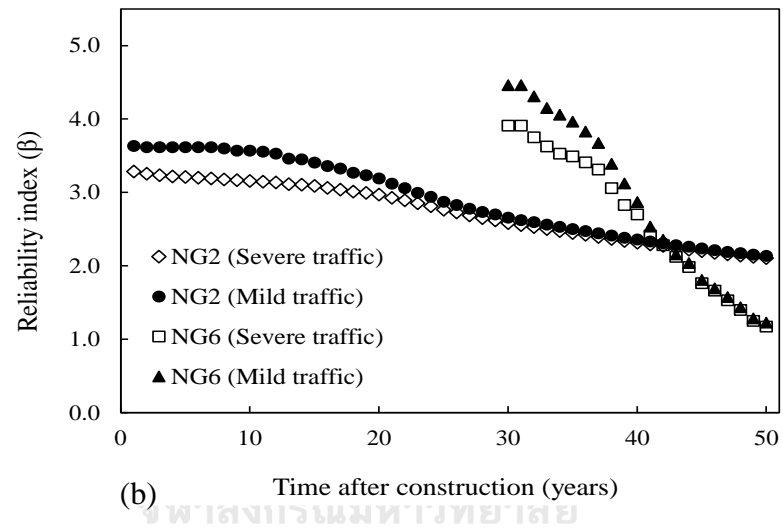
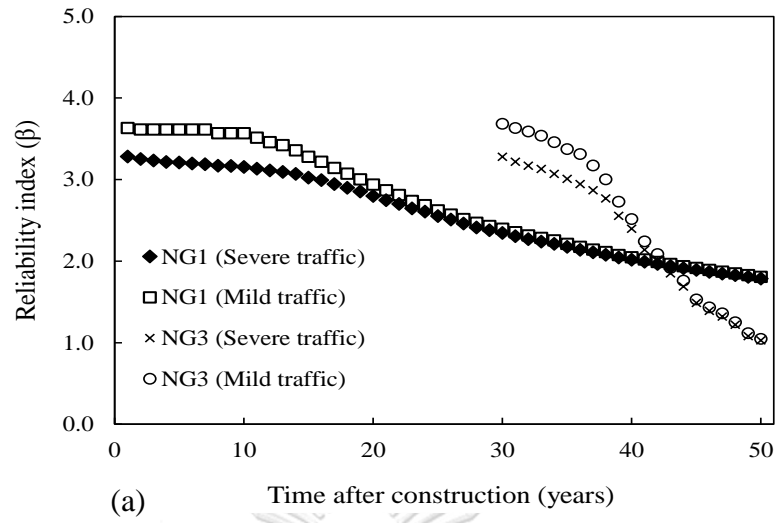


Figure 67 Relationship between updated steel weight loss (%) and the time after construction (years) for PC girder in Uwajima City

Figures 65 to 67 presents the relationship between the updated steel weight loss (%) and time after construction (years) for the PC bridge girder in Niigata, Sendai and Uwajima City. When the existing PC bridge girder is inspected to investigate the amount of steel weight loss, the predicted steel weight loss at the time of inspection estimated by the random variables listed in Table 3 must be consistent with the given inspection results. For example, Case SG4 in Figure 63(b), the magnitude of the steel weight at 29 years (0.33%) is updated at 30 years (1.02%) based on the inspection result shown in Table 15.



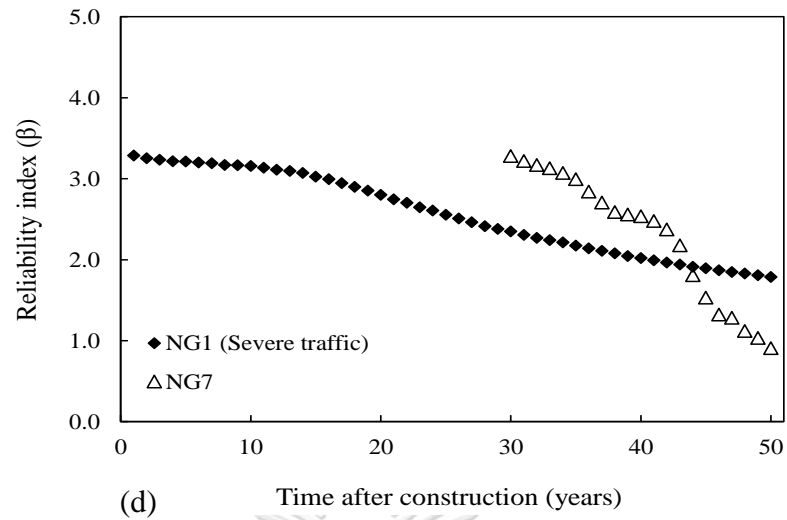
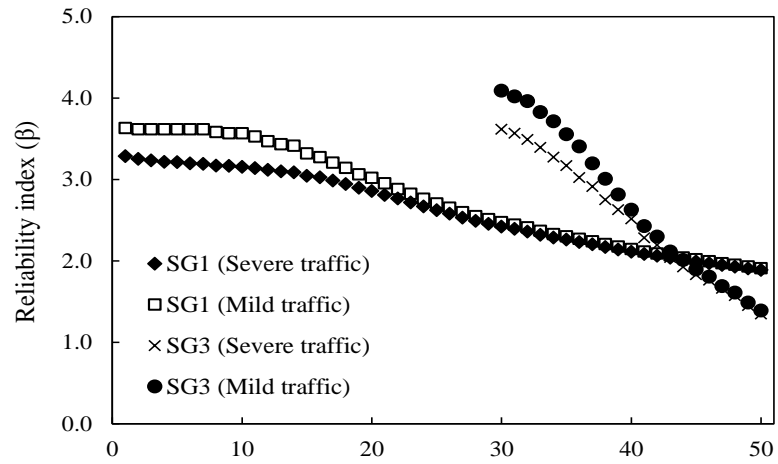
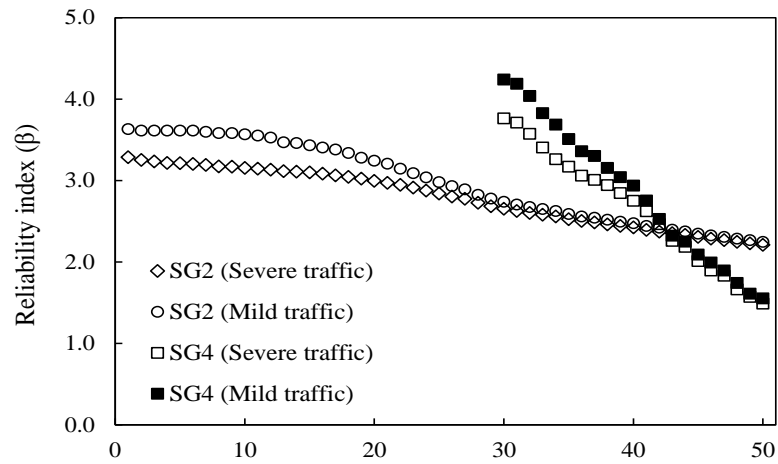


Figure 68 Relationship between updated life-cycle reliability and time after construction (years) for the PC girder in Niigata City

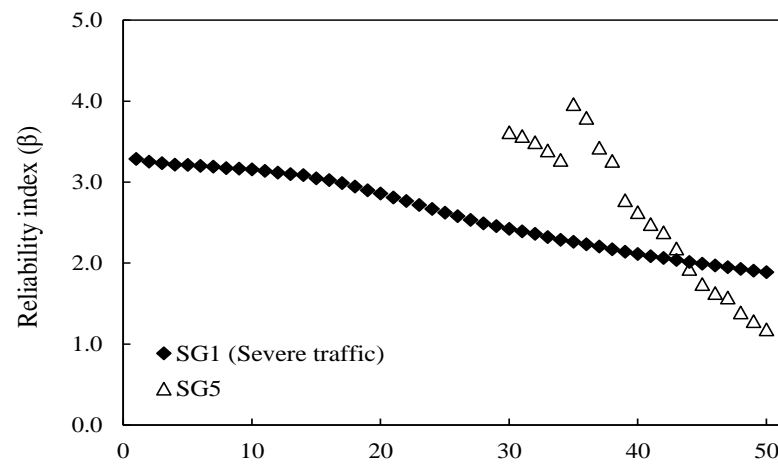




(a) Time after construction (years)



(b) Time after construction (years)



(c) Time after construction (years)

Figure 69 Relationship between updated life-cycle reliability and time after construction (years) for the PC girder in Sendai City

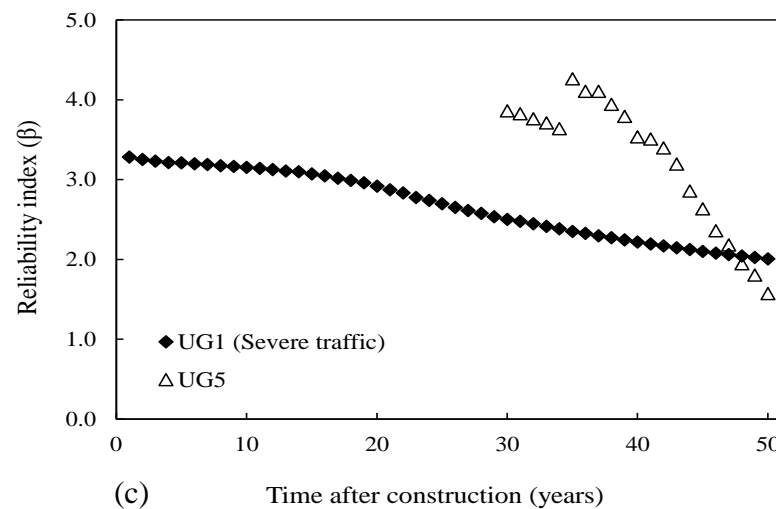
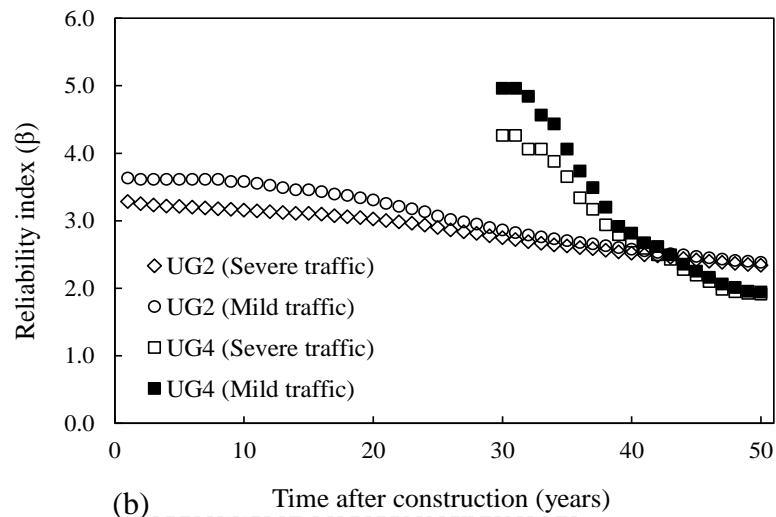
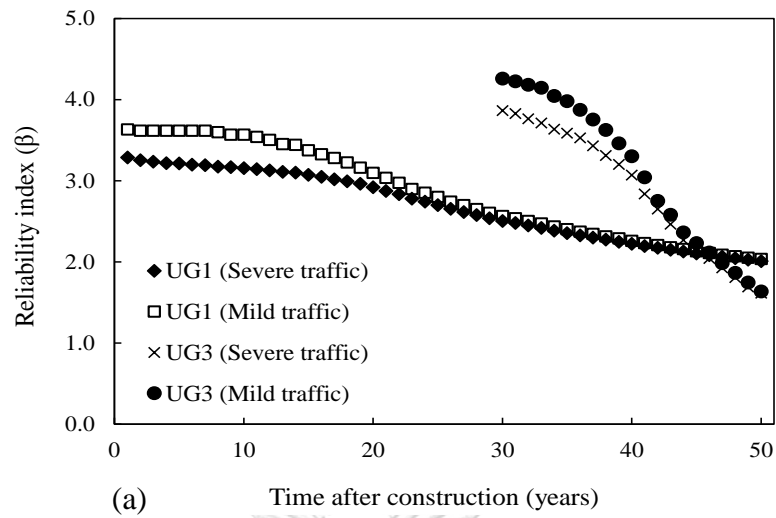


Figure 70 Relationship between updated life-cycle reliability and time after construction (years) for the PC girder in Uwajima City

Figures 68 to 70 show the updated reliabilities of the PC girder for three cities using inspection results. After updating, the reliabilities at 30 years are higher than those of before updating since uncertainties associated with prediction of steel weight loss are reduced based on updating process. For example, the reliability of the PC girder in Case SG3 shown in Figure 69(a) is updated using the average and variance of steel weight loss shown in Table 15. The reliability after updating at 30 years after construction is higher than that of without updating (Case SP1). After updating, the reliabilities decrease with higher slope than that of before updating since the average steel weight loss is considerably increased as shown in Figures 65 to 67. As illustrated in Figures 68(d), 69(c) and 70(c), the effects of the frequency of inspection are presented. The reliabilities at 35 years are increased again due to the latest inspection results except in Case NG7. The reliability of Case NG7 at 35 years is decreased since the amount of steel weight loss at the second inspection (6.22%), shown in Table 13, is significant higher than the prediction at 34 years (4.64%). The influences of severity of traffic hazard on the updated reliabilities can be observed in Figures 68 to 70. The effect of number of inspection locations for the PC girder is explained as the same with that of the RC pier as shown in Figure 71.

e) Effect of Reducing the Uncertainty due to Updating Process

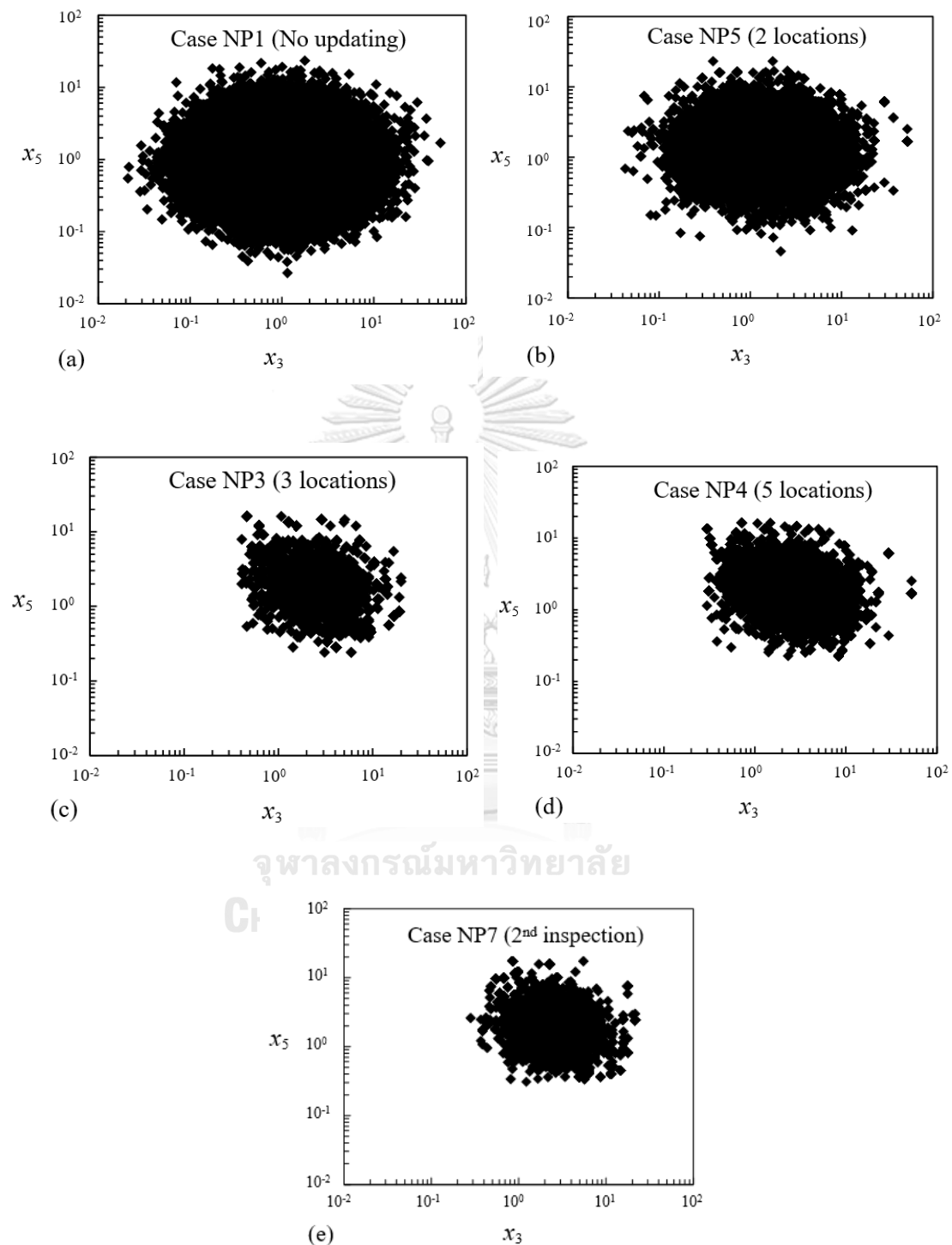


Figure 71 Correlation between random variables x_3 and x_5

Before updating, the random variables are assumed statistically independent. After updating, all random variables related with the prediction of the steel weight loss were updated simultaneously by SMCS using joint PDFs for the mean, COVs and correlations of the random variable. Figure 71 shows the correlations between the random variables x_3 and x_5 using 100,000 samples of SMCS. The computational results provided by the SMCS are approximately identical for all cases when the sample number exceeds 100,000. Therefore, the sample number is set to 100,000 for this analysis.

The effects of the number of inspection locations on the correlation level between the random variables are shown in Figure 71. As illustrated in Equation (50), the observational noise is determined as the variance calculated by the statistical error estimation theory. The effect of the magnitude of the observational noise on the correlation level between Cases NP1, NP3, NP4 and NP5, which have different numbers of inspection locations, is displayed in Figure 71. The correlation between x_3 and x_5 for Case NP4 after updating is increased compared with those of Cases NP3 and NP5 because Case NP4 has the highest number of inspection locations, thus contributing to the lowest observational noise (Table 13).

The existing RC bridges are located in a severe marine environment and have an increased possibility of larger steel weight losses. As shown in Figures 22 to 26, the spatial variability in the steel corrosion increased when the average steel corrosion increased. This increase will result in an increased tendency of errors in estimating the average steel weight loss from inspection data due to the fluctuation of the magnitude of the steel corrosion. The effect of the variation of steel corrosion must be compensated by using more inspection locations. In the computational analysis, using more inspection locations reduced the observational noise. This improvement can result in increased accuracy for estimating both the steel weight loss and structural reliability.

5.5.3 Comparison of Reliabilities between the RC Pier and the PC Girder and Determining the Time at which Maintenance action is Required

Life-cycle reliability assessment is used to help engineers and other decision makers determine when and where to spend bridge fund in order to enhance public safety, preserve existing infrastructures and serve commerce (Estes and Frangopol, 2003). Bridges are under deteriorations due to aging, mechanical stressors, and multiple aggressive environments. Under the combination of these factors, assessment of a safety of bridges associated with prediction of structural capacity, prediction of deterioration models, inspection process, repairs and/or maintenance action plans, and cost models must be effectively conducted using the life-cycle concepts (Ang 2005, Liu 2005). Determining of a threshold reliability level is one of main factor for probabilistic assessment of bridge structures used to determine the structural safety condition and define the needed maintenance time for the structures (Sykora 2014).

In order to prioritize maintenance actions among bridge components that have different failure modes and are exposed to different hazards, the recovery time must be considered when defining the limit state of each component. Based on previous seismic disasters in Japan, including the 1995 Kobe earthquake and 2011 Great East Japan earthquake, it would take a similar number of days to recover the RC components if the load effects were greater than the displacement at the longitudinal rebars yielding and less than the displacement at the onset of longitudinal rebars buckling (Kobayashi

2012). Therefore, in this paper, the limit state of the RC pier was defined based on the onset of local buckling of the longitudinal rebars and the limit state of the PC girder was defined by the yielding of the pre-stressing strand. Therefore, the reliabilities of RC piers and PC girders can be compared using the same reliability threshold to identify the component with the lowest reliability, even though their failure modes differ and they are exposed to different hazards. This study provides a novel reliability framework for comparing the life-cycle reliability of various bridge components exposed to multiple hazards. These results will help prioritize maintenance actions.

In this study, a reliability threshold of $\beta = 2.30$, which was provided by ISO/DIN 2394 (1998), was used to determine whether the reliability satisfies the required level. This threshold reliability was used when a moderate failure consequence was assumed. The time at which maintenance was required was defined as the time when the reliability reached the threshold. The time at which maintenance is required depends on the hazard levels and inspection results. Figures 72 to 86 compare the reliabilities of the RC piers and the PC girders with the threshold level for all cases study. Such comparisons can be used to evaluate maintenance options including repairing and/or strengthening. Tables 18 to 23 show the maintenance times for the RC pier and the PC girder for all cases study.

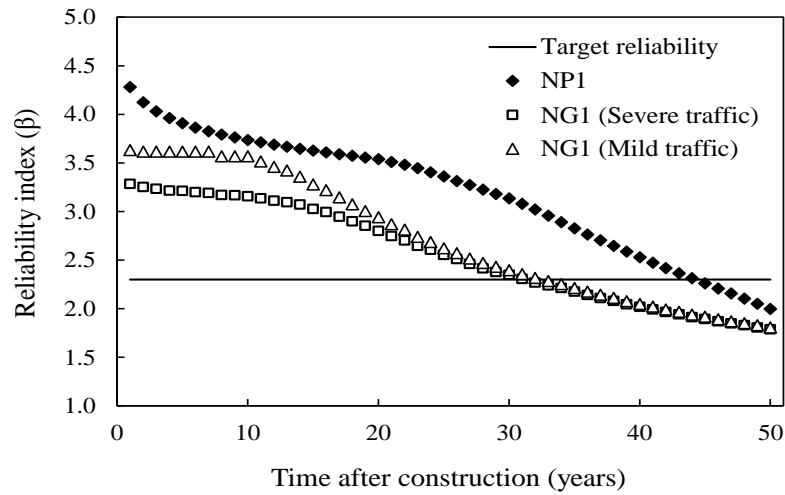


Figure 72 Comparison between reliabilities of the RC pier and the PC girder at Niigata City at $d=0.1$ km (without inspection results)

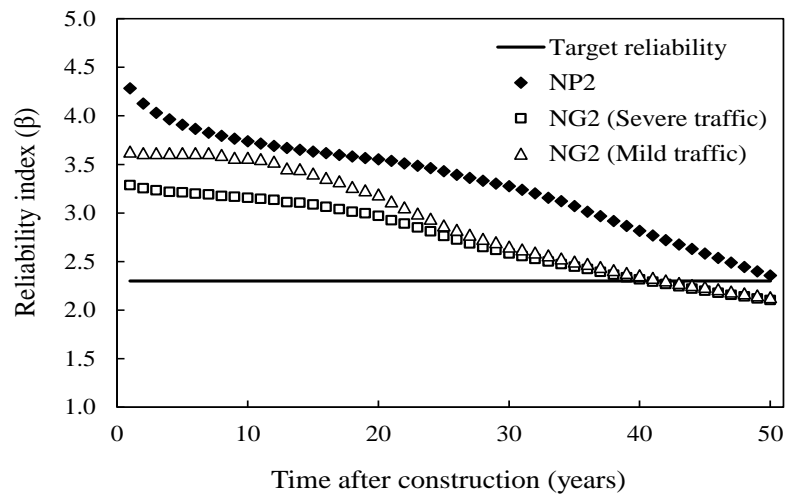


Figure 73 Comparison between reliabilities of the RC pier and the PC girder at Niigata City at $d=0.5$ km (without inspection results)

Table 18 Times at which maintenance action is required at Niigata City (without inspection results)

| Case | Years of maintenance |
|----------------------|----------------------|
| NP1 | 45 |
| NP2 | Larger than 50 |
| NG1 (Severe traffic) | 32 |
| NG1 (Mild traffic) | 33 |
| NG2 (Severe traffic) | 41 |
| NG2 (Mild traffic) | 43 |

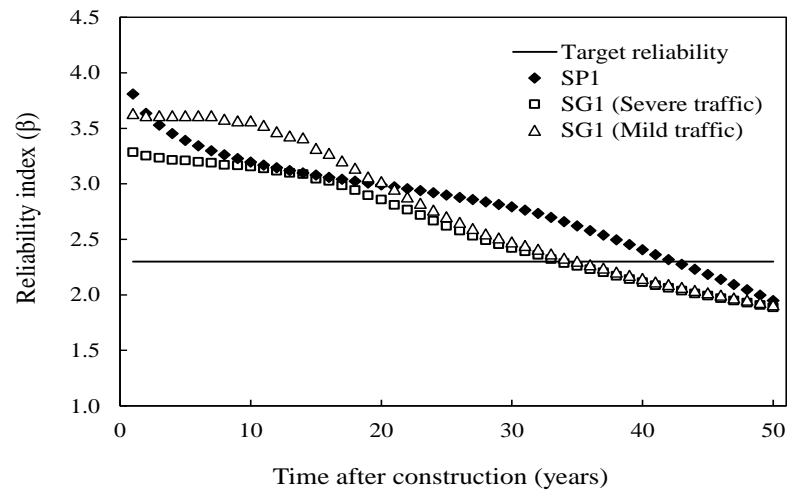


Figure 74 Comparison between reliabilities of the RC pier and the PC girder at Sendai City at $d=0.1$ km (without inspection results)

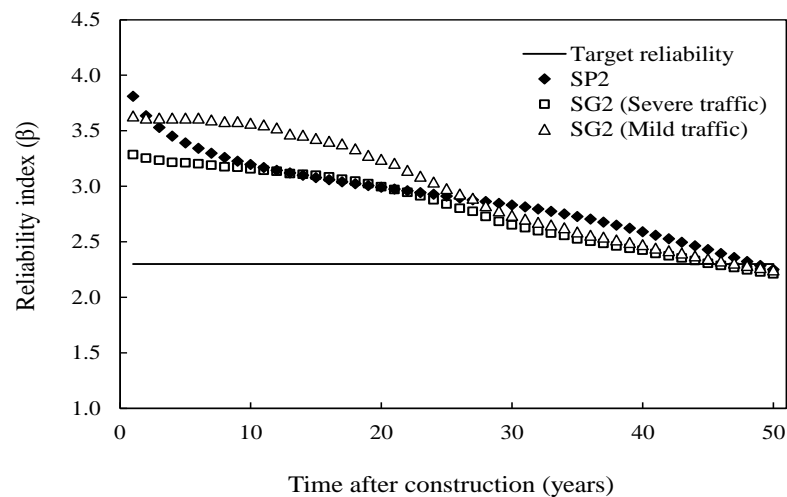


Figure 75 Comparison between reliabilities of the RC pier and the PC girder at Sendai City at $d=0.5$ km (without inspection results)

Table 19 Times at which maintenance action is required at Sendai City (without inspection results)

| Case | Years of maintenance |
|----------------------|----------------------|
| SP1 | 43 |
| SP2 | 49 |
| SG1 (Severe traffic) | 34 |
| SG1 (Mild traffic) | 35 |
| SG2 (Severe traffic) | 46 |
| SG2 (Mild traffic) | 48 |

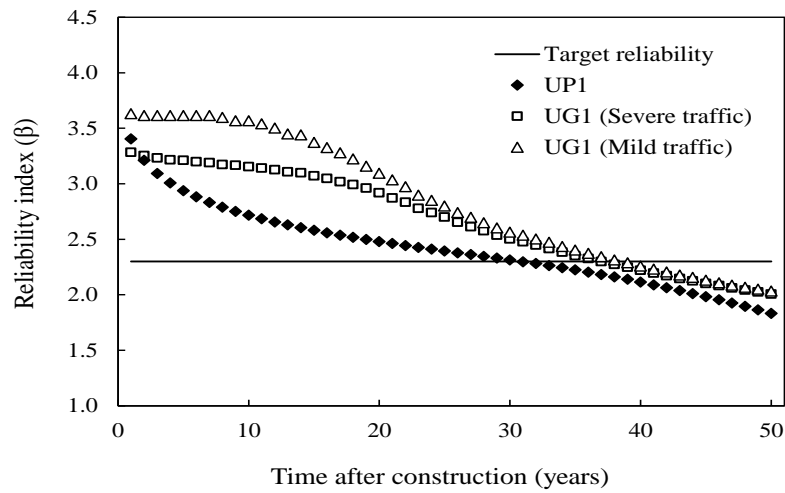


Figure 76 Comparison between life-cycle reliabilities of the RC pier and the PC girder at Uwajima City at d=0.1 km (without inspection results)

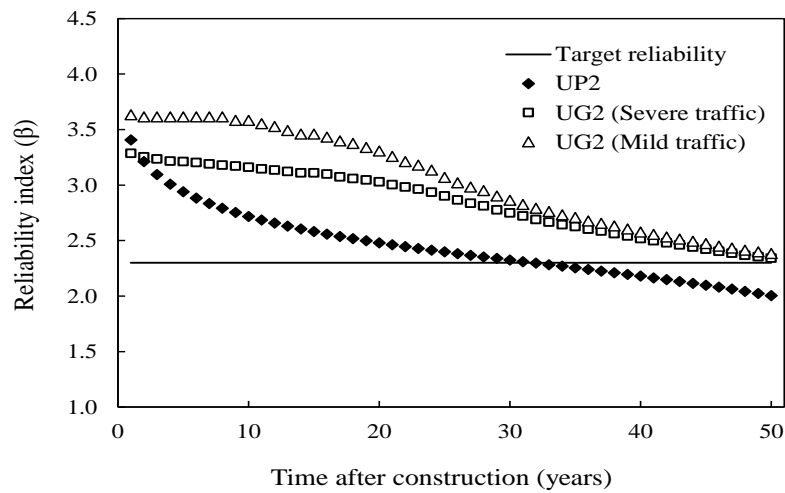


Figure 77 Comparison between life-cycle reliabilities of the RC pier and the PC girder at Uwajima City at d=0.5 km (without inspection results)

Table 20 Times at which maintenance action is required at Uwajima City (without inspection results)

| Case | Years of maintenance |
|----------------------|----------------------|
| UP1 | 32 |
| UP2 | 33 |
| UG1 (Severe traffic) | 38 |
| UG1 (Mild traffic) | 39 |
| UG2 (Severe traffic) | Larger than 50 |
| UG2 (Mild traffic) | Larger than 50 |

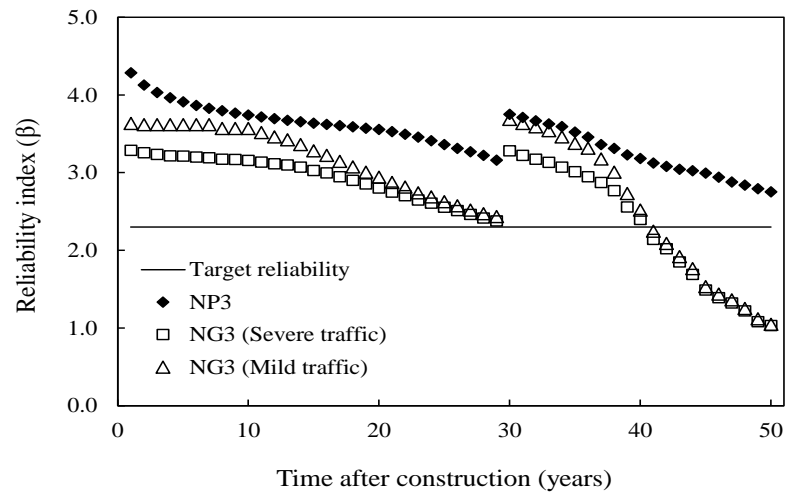


Figure 78 Comparison between updated reliabilities of the RC pier and the PC girder at Niigata City at $d=0.1$ km (with inspection results)

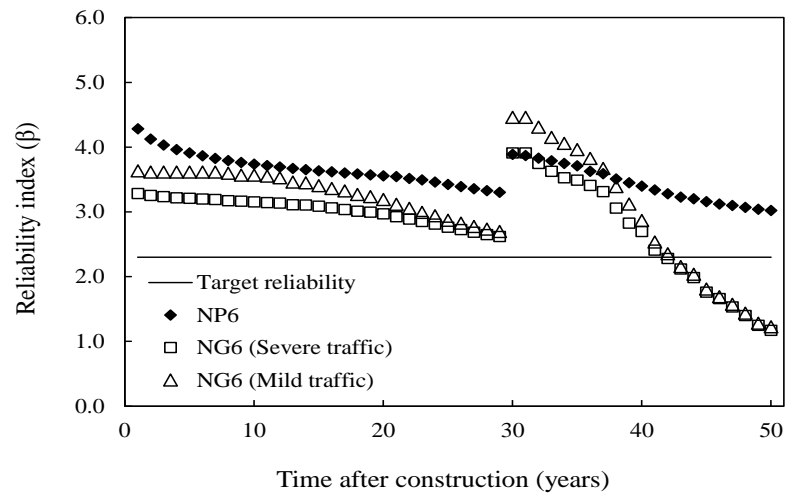


Figure 79 Comparison between updated reliabilities of the RC pier and the PC girder at Niigata City at $d=0.5$ km (with inspection results)

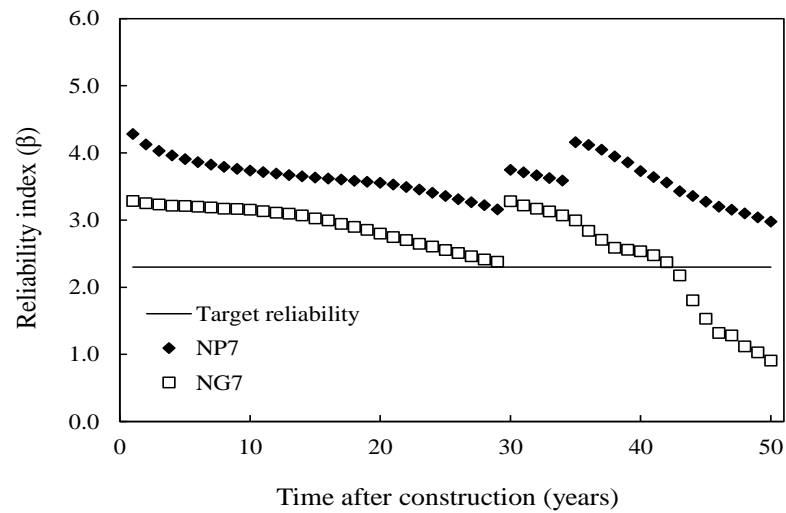


Figure 80 Comparison between updated reliabilities of the RC pier and the PC girder at Niigata City at $d=0.1$ km (2nd inspection)

Table 21 Times at which maintenance action is required at Niigata City (with inspection results)

| Case | Years of maintenance |
|----------------------|----------------------|
| NP3 | Larger than 50 |
| NP6 | Larger than 50 |
| NP7 | Larger than 50 |
| NG3 (Severe traffic) | 41 |
| NG3 (Mild traffic) | 42 |
| NG6 (Severe traffic) | 42 |
| NG6 (Mild traffic) | 43 |
| NG7 | 43 |

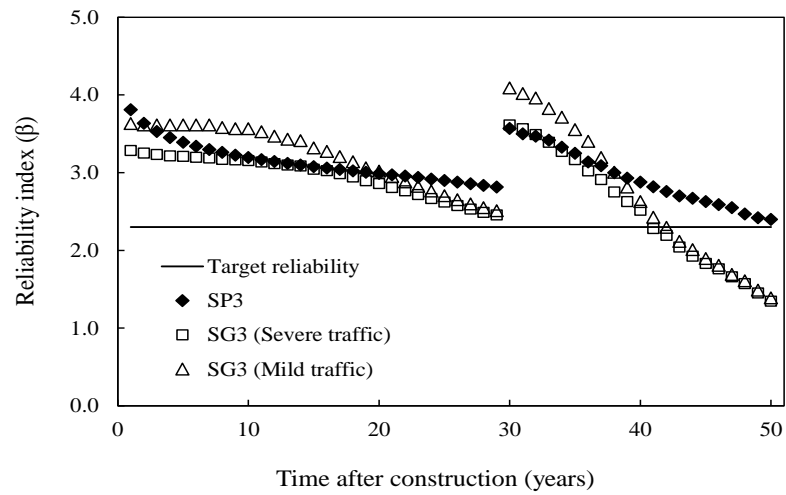


Figure 81 Comparison between updated reliabilities of the RC pier and the PC girder at Sendai City at $d=0.1$ km (with inspection results)

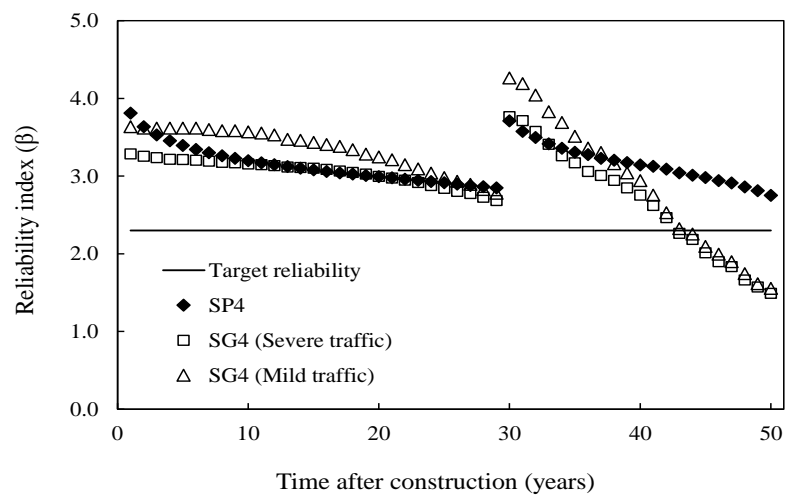


Figure 82 Comparison between updated reliabilities of the RC pier and the PC girder at Sendai City at $d=0.5$ km (with inspection results)

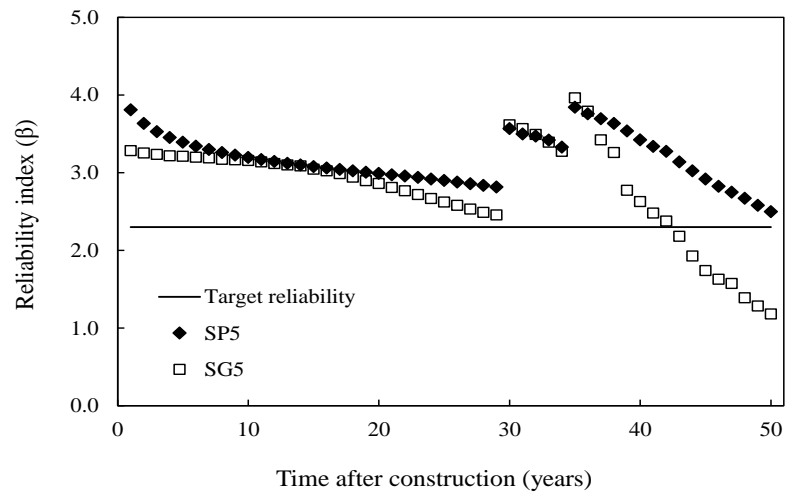


Figure 83 Comparison between updated reliabilities of the RC pier and the PC girder at Sendai City at $d=0.1$ km (2nd inspection)

Table 22 Times at which maintenance action is required at Sendai City (with inspection results)

| Case | Years of maintenance |
|----------------------|----------------------|
| SP3 | Larger than 50 |
| SP4 | Larger than 50 |
| SP5 | Larger than 50 |
| SG3 (Severe traffic) | 42 |
| SG3 (Mild traffic) | 43 |
| SG4 (Severe traffic) | 44 |
| SG4 (Mild traffic) | 45 |
| SG5 | 43 |

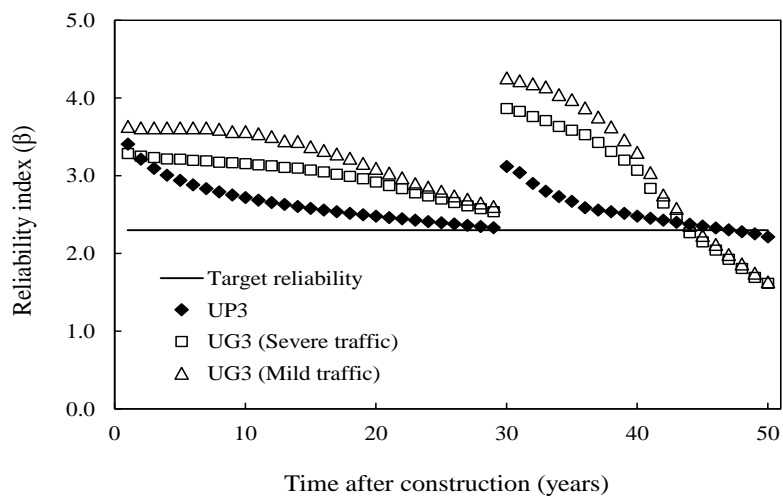


Figure 84 Comparison between updated reliabilities of the RC pier and the PC girder at Uwajima City at d=0.1 km (with inspection results)

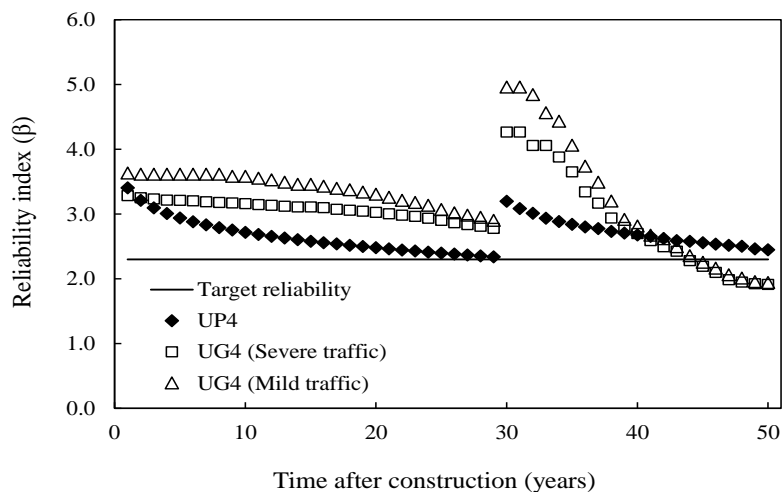


Figure 85 Comparison between updated reliabilities of the RC pier and the PC girder at Uwajima City at d=0.5 km (with inspection results)

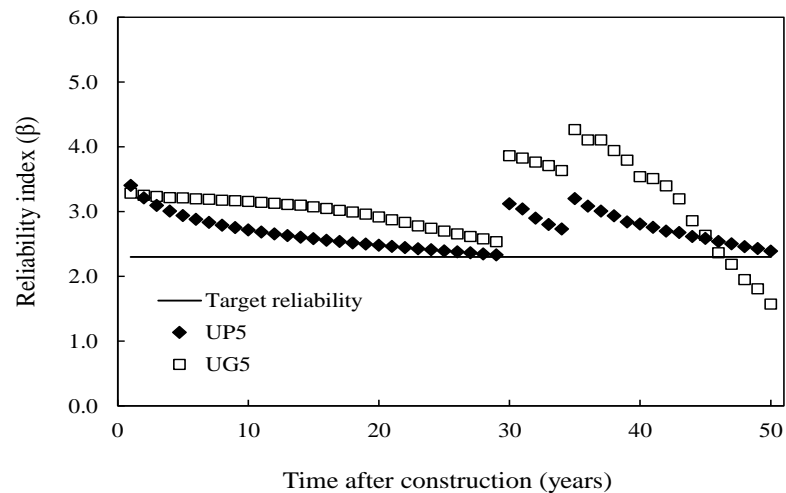


Figure 86 Comparison between updated reliabilities of the RC pier and the PC girder at Uwajima City at $d=0.1$ km (2nd inspection)

Table 23 Times at which maintenance action is required at Uwajima City (with inspection results)

| Case | Years of maintenance |
|----------------------|----------------------|
| UP3 | 48 |
| UP4 | Larger than 50 |
| UP5 | Larger than 50 |
| UG3 (Severe traffic) | 44 |
| UG3 (Mild traffic) | 45 |
| UG4 (Severe traffic) | 44 |
| UG4 (Mild traffic) | 45 |
| UG5 | 47 |

The bridge components with the lowest reliability are identified in Figures 72 to 86. The lowest reliability depends on the time of consideration, for example shown in Figure 85, the lowest reliability of the RC bridge in Uwajima City at $d=0.5$ km is controlled by RC pier due to the strong seismic hazard until about at 43 years, the lowest reliability is controlled by PC girder (severe traffic condition). In case of Niigata City, the lowest reliabilities in all cases are controlled by PC girder due to the effect of strong airborne chloride hazard.

Based on the results of comparison between reliabilities of the RC pier and that of the PC girder, deterioration rates of the PC girder, caused by the steel corrosion, is higher than that of the RC pier since 1) the PC girder was designed to have a smaller concrete cover (50 mm) than that of the RC pier (100 mm); 2) steel weight loss given by inspection results for the PC girders are assumed to be higher than those of the RC piers due to the effect of difference in concrete cover; 3) sensitivity of structural failure of the PC girder, caused by the amount of steel weight loss, is higher than that of the RC pier considered by fragility analysis.

In case of Uwajima City without inspection results shown in Figures 76 and 77, the lowest reliabilities are controlled by the RC pier due to the strong seismic hazard. After updating using inspection results, shown in Figures 84 to 86, and the uncertainties associated with prediction of steel weight loss are reduced, the lowest reliabilities are still controlled by the RC pier. However, due to the higher deterioration rate of the PC girder than that of the RC pier, until about 45 years after construction, the lowest reliabilities are changed to be controlled by the PC girder.

Times at which maintenance action is required for the bridge components without inspection results are shown in Tables 18 to 20. The times at which maintenance action is required of RC pier in Uwajima City are lowest due to the effect of strongest seismic hazard among three cities. Comparison of the times among Cases NP1, SP1 and UP1, the maintenance action were needed at 45, 43, and 32 years after construction, respectively. The times at which maintenance action is required for PC girder in Niigata City are lowest due to the strongest severity of airborne chloride hazard among three cities. Comparison of the times among Cases NG1, SG1 and UG1, the maintenance action were required at 32, 34, and 38 years after construction, respectively. Severity of traffic hazard also affect the time, Case SG1 need the maintenance action at 34 and 35 years after construction for severe and mild traffic condition, respectively.

Tables 21 to 23 present the time at which maintenance action is required for the bridge components in case of updating by inspection results. Based on updating process using inspection results, this updating affect a reducing of uncertainties associated with prediction of steel weight loss therefore the reliabilities for all cases after updating are higher than those of before updating. Due to the increasing of reliabilities level after updating, it affect the maintenance schedules. The times at which maintenance action is required after updating are different from those of without updating. For example in Case NG1, shown in Figure 72, the maintenance action was needed at 32 years after construction. Once the updating process is provided for Case NG3, shown in Figure 78, the time at which maintenance is required is at 41 years after construction. The frequency of inspection also affects the maintenance schedule, for example in Case UG3, shown in Figure 74, the maintenance action was needed at 44 years after construction. Once the second inspection at 35 years is provided for Case UG5, the time is postponed to be at 47 years after construction. However, updating process can affect to have a faster maintenance time, for example in Case SG2 (both severe and mild traffic conditions), the maintenance action was needed at 46 and 48 years after construction. Once the updating process is provided for Case SG4 (both severe and mild traffic condition), the times are changed to be at 44 and 45 years after construction, respectively.

The main factors affecting the faster or slower of time at which maintenance action is required after updating are 1) how much the uncertainties can be reduced after updating. This factor depend on the difference between the COVs of steel weight loss, provided by statistical estimation error, and the COVs of steel weight loss, calculated by random variables listed in Table 3. If the COVs of steel weight loss calculated by the random variables is much larger than the COVs provided by statistical estimation error, the uncertainties can be exceedingly reduced after updating. 2) structural deterioration rate after updating, this factor depends on the amount of average steel weight loss from the inspection process. If the steel weight loss given by inspection results is higher than the prediction calculated by random variables, all random

variables after updating have to be updated to be consistent with that inspection result. Therefore, the higher rate of deterioration after updating can be clearly seen by a higher slope of decreasing in reliability.

Updating the reliability estimates using inspection results can increase the precision of reliability assessment and also can reduce maintenance costs. In order to prioritize maintenance among bridge components with different failure modes and subject to different hazards, it is important to identify the member with the lowest reliability. This can be achieved using reliability analysis that has been updated with inspection results. The framework proposed in this study can help decision makers make informed decisions regarding prioritization of maintenance actions.

The research methodology presented in this study as shown in Figure x can be applied in Thailand if enough information is provided. Since the reliability flowchart present the general idea of estimating the structural reliability that consisting of several parts; structural capacity model, structural demand analysis, fragility analysis, and reliability estimation. All parts are based on general concept of statistical and mathematical estimation. However, the important thing which we have to concern to follow this flowchart is collection of reliable information. As can be seen, the reliability flowchart are related with a lot of information especially information of hazards. To estimate the amount of steel weight loss in existing RC bridge, information of severity of airborne chloride represented by wind speed and ratio of sea wind which blow from sea to land are needed to know. In Japan, there are 24 stations near the coastal line to collect this kind of information, this can make reliable and enough information for predicting a deterioration of RC structures. If this methodology will be used in Thailand, information about severity of airborne chloride must be collected. For other information such as traffic hazard, structural section can be easily investigated and these kinds of information do no take a long time to access. Presently, Chulalongkorn University has a research collaboration with University of Tokyo to study about the amount of airborne chloride and chloride diffusion coefficient in Phuket and Chonburi province which are located near coastal line in southern and western part in Thailand, respectively.

However, airborne chloride is not only one factor causing the steel weight loss in RC structures but carbonation. Especially in Bangkok, a lot of concrete structures (high-rise building, factory, bridge, and sky train (BTS) etc.) are deteriorated by effect of carbonation. To estimate the amount of steel weight loss induced by carbonation, the severity and effect of carbonation to RC structures must be collected and studied, respectively.

CHAPTER 6

CONCLUSIONS

- (1) A novel procedure to estimate the life-cycle seismic reliability of corroded existing RC structures based on inspection data by incorporating the spatial variability of steel corrosion is established.
- (2) Parameters that represented the one-dimensional stochastic field were determined based on previous experimental results that used X-rays to visualize the spatial distribution of steel corrosion are determined. The methodology to estimate the mean and variance of the steel weight loss in the plastic hinge of an existing RC bridge pier is presented based on the previous experimental results from corroded RC specimens acquired by X-ray technologies. The number of inspection locations on the analyzed RC bridge pier is considered in the statistical estimation error process.
- (3) The effect of the number of inspection locations and frequency of inspections on the updated seismic reliability was investigated in the illustrative example. Having more inspection locations and increasing the frequency of inspections resulted in the reduction of uncertainties associated with the prediction of steel weight loss.
- (4) The procedure for identifying the most important hazards with respect to the structural safety of existing RC bridges, as well as which bridge component has the lowest reliability is presented. Comparing the life-cycle reliabilities of various bridge components exposed to multiple hazards can help prioritize maintenance and/or repair actions for existing RC structures. Updating life-cycle reliability estimates using inspection results can increase precision and contribute to maintenance cost reductions.
- (5) Further research is needed to consider the methodology for the life-cycle management of RC structures, notably for the life-cycle cost analysis, safety and optimization (Frangopol 1997, Frangopol 2011). The effects of insufficient data and knowledge of the long-term structural performance analysis of an existing structure should also be determined. Even though, more inspection locations and frequency of inspections can help to conduct a seismic reliability assessment more precisely however the type of inspection, optimal time, spatial interval, and number of inspection locations must be established through a risk-cost benefit analysis to produce a reliability-based criterion of inspection processes for existing structures.

CHAPTER 7

FUTURE RESEARCH WORK

7.1 Improvement of Inspection Process for Life-Cycle Reliability Assessment

RC structures located in marine environment deteriorate with time due to chloride-induced corrosion. Steel corrosion process on RC structure is initiated by chloride penetration through a concrete cover if the concrete cover quality is poor (Akiyama 2010). Steel corrosion causes a decreasing of long-term structural performance due to cracking and spalling of concrete cover. It is essential to know that the properties of concrete material are random due to the spatial variability (Nguyen 2013). This randomness of concrete cover causes spatially steel corrosion damage on RC structures (O'Connor 2012). For RC structures, the concrete cover provides both chemical and physical barrier to protect the chloride-induced corrosion of steel reinforcement (Browne 1980). Spatial variability of concrete cover quality, related to steel corrosion, is an important characteristic which qualify and quantify the physical and chemical properties of concrete cover. The interaction between steel corrosion and concrete cover quality is of concern to the engineers involved with infrastructure maintenance, if an effective investigation and maintenance strategy is to be planned. The important questions are which properties of concrete associated with the concrete cover quality mainly affects the initiation of steel corrosion, how the investigations of concrete cover quality can be conducted, and how we can apply the spatial variability of concrete cover quality into the life cycle reliability assessment.

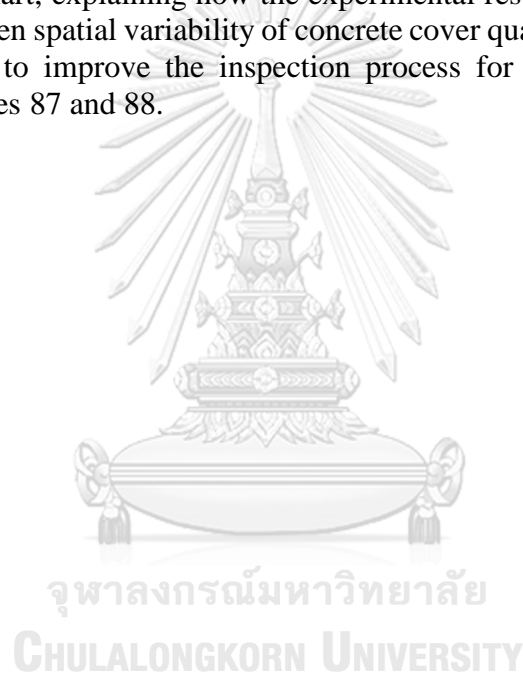
The spatial variability of concrete is an important characteristic, which qualifies the non-homogeneity of mechanical and physical properties on structural component. Assessing the spatial variability of concrete structures is of major interest for either locating potential damaged area in an existing structure, or reliability analysis (Nguyen 2013). In addition, recent reliability studies have shown that the spatial correlation may govern the reliability of structural component. Some studies have been carried out to analyze analyzing spatial variability. However, the study of the relationship between spatial variability of concrete cover quality and steel corrosion damage on RC structures is still lack in the literature.

It is important to regularly assess the condition of the RC structures to know when they must proceed to some maintenance or reparations (Val 2005). Visual inspection alone is not enough or might be inadequate to do so. Theoretically, it is possible to directly assess the spatial variability but this is very difficult in practice and impossible in many situations, since it requires a high number of cores. Taking cores throughout the concrete structure is not just expansive, but it also affects structural stability and safety (Cardenas 2015). That is a reason why NDT testing has been considered as an interesting tool for assessing the concrete condition.

Even though, NDT measurement can present current structural condition however, several NDT measurements with high inspection locations are also time consuming and expensive. Therefore, an optimize strategy for investigating the structural condition using NDT measurements need to be developed using the statistical tool (identified correlation length by variogram calculation), without decreasing the

estimation quality (Cardenas 2015). The variogram model and kriging method will be used to build the surface mapping of spatial variability of concrete in order to optimizing the location of cores. The range, correlation length at which the values can be considered as uncorrelated. This distance is important, since it provides an indication of how to conduct the investigation. The correlation length can be used to reduce drastically the number of measurements on the structure.

Steel corrosion problem in concrete structure is localized damage, the results provided by NDT test is also local information. Maintenance plan and repair zone can be determined based on a good inspection strategy while keeping the cost/benefit ratio within reasonable limits (Qasrawi 2000) (Cardenas 2015). If the correlation between spatial variability of concrete cover quality and deterioration of RC structure due to steel corrosion are presented and proper combination of NDT techniques are developed, the effective optimize strategy to inspect the structural condition can be designed (Nguyen 2013). The flowchart, explaining how the experimental result based on investigation a relationship between spatial variability of concrete cover quality and that of steel weight loss can be used to improve the inspection process for existing RC structure, are presented in Figures 87 and 88.



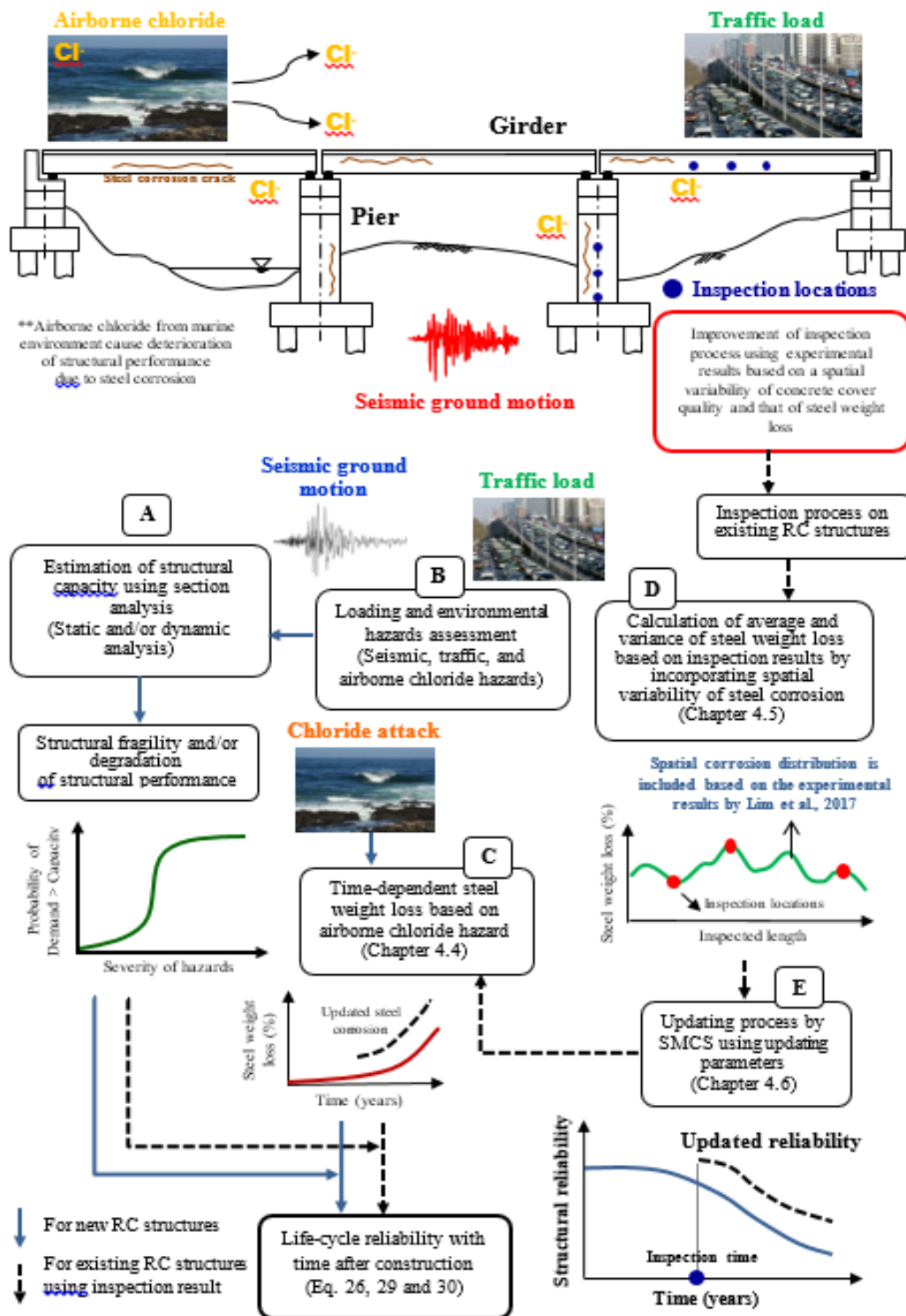


Figure 87 Flowchart for estimating life-cycle reliability of existing RC bridges structure including the improvement of inspection process

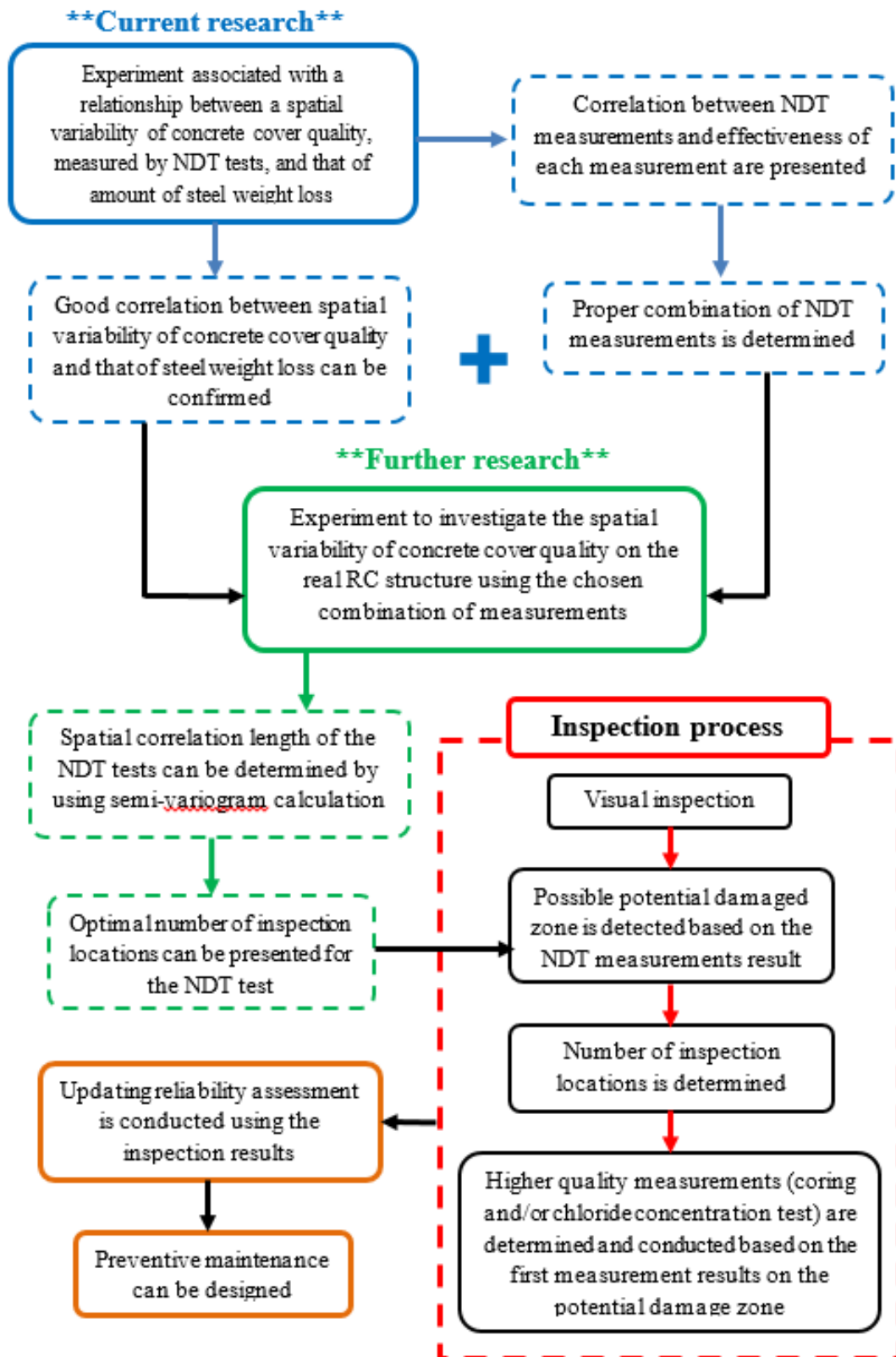


Figure 88 Flowchart explaining the experimental plan for improving the inspection process for existing RC structures

Figure 87 present the flowchart for estimating life-cycle reliability of RC structures which was adapted from Figure 12, the inspection process for existing RC structures is improved by the database of the experiments associated with a spatial variability of concrete cover quality and that of steel weight loss. The procedures to improve the inspection process are explained in Figure 85. The current research is an experiment associated with a relationship between a spatial variability of concrete cover quality, measured by several NDT tests, and that of amount of steel weight loss. Based on the experiment, correlations between NDT tests results will be determined and effectiveness of each NDT measurements was proposed. In addition, the correlation between NDT tests results and amount of steel weight loss is presented and the combination of the NDT test can be determined.

If a good correlation between the spatial variability of concrete cover quality, measured by the combination of NDT tests can be found, the further experiment will be conducted as presented in Figure 88. Investigation of spatial variability of concrete cover quality should be done on the real RC structures since an optimal number of inspection locations must be identified based on each NDT measurements. When considering the NDT tests result on real structures using a variogram calculation, spatial correlation length of each NDT measurements can be estimated. This distance is important, since it provides an indication of how to conduct the investigation. By using the correlation length, possible potential damaged zone can be detected. Then, next measurement (higher quality tests, such as coring and chloride concentration test), can be determined and conducted based on the result of first measurements.

When considering the results of all investigations including visual inspection, first measurements by NDT tests, and second measurements by higher quality of measurements, the updating structural reliability can be more accurately estimated based on the inspection results. Finally, if structural reliability reach to threshold level, an effective maintenance plan and repair zone can be determined based on a good inspection strategy while keeping the cost/benefit ratio within reasonable.

REFERENCES

- 224, A. C. (1994). "Control of Cracking in Concrete Structures." Manual of Concrete Practice Part 3.
- Akgul, F. (2002). Lifetime system reliability prediction for multiple structures type in a bridge network. USA, University of Colorado at Boulder. **Ph.D.**
- Akiyama, M., Frangopol, D. M (2014). "Long-term seismic performance of RC structures in an aggressive environment: emphasis on bridge piers." Structural Infrastructure Engineering **10**(7): 865-879.
- Akiyama, M., Frangopol, D. M., and Yoshida, I. (2010). "Time-dependent reliability analysis of existing RC structures in a marine environment using hazard associated with airborne chlorides." Engineering Structures **32**(11): 3768-3779.
- Akiyama, M., Frangopol, D. M., Matsuzaki, H. (2011). "Life-cycle reliability of RC bridge piers under seismic and airborne chloride hazard." Earthquake Engineering and Structural Dynamics **40**(15): 1671-1687.
- Akiyama, M., Frangopol, D. M., Suzuki, M. (2012). "Integration of the effects of airborne chlorides into reliability-based durability design of RC structures in a marine environment." Structure and Infrastructure Engineering **8**(2): 125-134.
- Akiyama, M., Matsuzaki, H., Dan, H. T., Suzuki, M. (2012). "Reliability-based capacity design for reinforced concrete bridge structures." Structure and Infrastructure Engineering **8**(12): 1096-1107.
- Al-Sulaimani, G. J., Kaleemullah, M., Basunbul, I. A., and Rasheeduzzafar (1990). "Influence of corrosion and cracking on bond behavior and strength of reinforced concrete members." ACI Structural Journal **87**(2): 220-231.
- Almusallam, A. A., Al-Gahtani, A. S., Aziz, A. R., Rasheeduzzafar (1996). "Effect of reinforcement corrosion on bond strength." Construction and Building Materials **10**(2): 123-129.
- Ang, A.-S., and De Leon, D (2005). "Modeling and analysis of uncertainties for risk-informed decisions in infrastructures engineering." Structure and Infrastructure Engineering **1**(1): 19-31.
- Anon (1982). "The Durability of Steel in Concrete." Building Research Establishment Digest **263**.
- Barone, G., and Frangopol, D. M (2013). "Hazard-based optimum lifetime inspection and repair planning for deteriorating structures." Journal of Structural Engineering **139**.

Barone, G., and Frangopol, D. M (2014). "Life-cycle maintenance of deteriorating structures by multi-objective optimization involving reliability, risk, availability, hazard and cost." Structural Safety **48**: 40-50.

Barone, G., Frangopol, D. M., and Soliman, M (2014). "Optimization of life-cycle maintenance of deteriorating bridges considering expected annual system failure rate and expected cumulative cost." Journal of Structural Engineering **140**.

Berke, N. S., Dallaire, M. P., Hicks, M. C., Hooper, R. J (1993). Corrosion of Steel in Cracked Concrete.

Berry M. P., E., M. O (2005). "Practical performance model for bar buckling." Journal of Structural Engineering **131**(7): 1060-1070.

Berto, L., Vitaliani, R., Saetta, A., Simioni, P (2009). "Seismic assessment of existing RC structures affected by degradation phenomena." Structural Safety **31**: 284-297.

Bhargava, K., Ghosh, A. K., Mori, Y., Ramanujam, S (2007). "Models for corrosion-induced bond strength degradation in reinforced concrete." ACI Structural Journal **104**(6): 594-603.

Browne, R. D. (1980). Mechanisms of Corrosion of Steel in Concrete in Relation to Design, Inspection, and Repair of Offshore and Coastal Structures. In Performance of Concrete in Marine Environment, ACI Publication SP-65.

Browne, R. D., Baker, A. F (1979). The Performance of Structural Concrete in a Marine Environment. In Development in Concrete Technology, ed. F. D. Lyden. London, Applied Science Publishers.

Cairns, J. (1995). Strength in shear of concrete beams with exposed reinforcement. Proceedings of the Institution of Civil Engineers, Structures and Buildings.

Cardenas, C. G., Sbartai, Z. M., Balayssac, J. P., Garnier, V., and Breysse, D (2015). "New optimization algorithm for optimal spatial sampling during non-destructive testing of concrete structures." Engineering Structures **88**: 92-99.

Casas, J. R., and Wisniewski, D (2013). "Safety requirement and probabilistic models of resistance in the assessment of existing railway bridges." Structure and Infrastructure Engineering **9**(6): 529-545.

Choe, D. E., Gardoni, P., Rosowsky, D., Haukaas, T (2009). "Seismic fragility estimates for reinforced concrete bridges subject to corrosion." Structural Safety **31**: 275-283.

Cornell, C. A., Jalayer, F., Hamburger, R. O., Foutch, D. A (2002). "Probabilistic basis for 2000 SAC federal emergency management agency steel moment frame guidelines." Journal of Structural Engineering **128**(4): 526-533.

Darmawan, M. S., Stewart, M. G (2007). "Spatial time-dependent reliability analysis of corroding pre-tensioned pre-stressed concrete bridge girders." Structural Safety **29**: 16-31.

Decò, A., Frangopol, D.M (2011). "Risk assessment of highway bridges under multiple hazards." Journal of Risk Research **14**(9): 1057-1089.

Diamond, S. (1986). Chloride Concentrations in Concrete Pore Solutions Resulting from Calcium and Sodium Chloride Admixtures, Cement, Concrete, and Aggregate.

Dong, Y., Frangopol, D. M., Saydam, D (2014). "Pre-earthquake probabilistic retrofit optimization of bridge networks based on sustainability." Journal of Bridge Engineering **19**(6): 1-10.

Ellingwood, B. R. (2005). "Risk-informed condition assessment of civil infrastructure: state of practice and research issues." Structure and Infrastructure Engineering **1**(1): 7-18.

Enright, M. P., Frangopol, D. M (1999). "Reliability-based condition assessment of deteriorating concrete bridges considering load redistribution." Structural Safety **21**(2): 159-195.

Estes, A. C., Frangopol, D. M (2003). "Updating bridge reliability based on bridge management system visual inspection results." Journal of Bridge Engineering **8**(6): 374-382.

Fang, C., Lundgren, K., Chen, L., Zhu, C (2004). "Corrosion influence on bond in reinforced concrete." Cement and Concrete Research **34**(11): 2159-2167.

Frangopol, D. M. (2011). "Life-cycle performance, management, and optimization of structural safety under uncertainty: accomplishments and challenges." Structure and Infrastructure Engineering **7**(6): 389-413.

Frangopol, D. M., Lin, K. Y., Estes, A. C (1997). "Reliability of reinforced concrete girders under corrosion attack." Journal of Structural Engineering **123**(3): 286-297.

Frangopol, D. M., Soliman, M (2016). "Life-cycle of structural systems: recent achievements and future directions." Structure and Infrastructure Engineering **12**(1): 1-20.

Frangopol, D. M., Strauss, A., Kim, S (2008). "Bridge reliability assessment based on monitoring." Journal of Bridge Engineering **13**(3): 258–270.

Ghosh, J., Caprani, C. C., Padgett, J. E (2014). "Influence of traffic loading on the seismic reliability assessment of highway bridge structures." Journal of Bridge Engineering **19**(3).

Ghosh, J., Sood, P (2016). "Consideration of time-evolving capacity distributions and improved degradation models for seismic fragility assessment of aging highway bridges." Reliability Engineering & System Safety **154**: 197-218.

Goovaerts, P. (1997). Geostatistics for natural resources evaluation. O. U. Press. New York: 483.

Hausman, D. A. (1967). Steel Corrosion in Concrete, Material Protection.

Honjo, Y., Otake, Y (2013). Statistical estimation error evaluation theory of local averages of a geotechnical parameter. Proceeding of Safety Reliability Risk and Life-cycle Performance of Structure and Infrastructure.

Jeppsson, J., Thelandersson, S (2003). "Behavior of reinforced concrete beams with loss of bond at longitudinal reinforcement." Journal of Structural Engineering **129**(10): 1376-1383.

John P, B. (2006). Corrosion of steel in concrete: Understanding, Investigation and Repair, CRC Press second edition.

Kashani, M. M., Crewe, A. J., Alexander, N. A (2013). "Nonlinear stress–strain behaviour of corrosion-damaged reinforcing bars including inelastic buckling." Engineering Structures **48**: 417-429.

Kashani, M. M., Crewe, A. J., Alexander, N. A (2013). "Use of a 3D optical measurement technique for stochastic corrosion pattern analysis of reinforcing bars subjected to accelerated corrosion." Corrosion Science **73**: 208-221.

Kawamura, C., Tanimura, Y., Sogabe, M., Sato, T., Hasegawa, M (2004). "Investigation of construction errors of the cover for railway RC rigid frame viaducts." Journal of Concrete Structure and Material Pavements, JSCE **64**: 254–266

Kobayashi, M., Mizuno, K. Ishibashi, T (2012). Damage caused to Shinkansen structures by the Great East Japan earthquake and early restoration. Proceedings of the International Symposium on Engineering Lessons Learned from the 2011 Great East Japan Earthquake, Tokyo, Japan.

Lawanwisut, W., Nowak, D., Teply, B (2001). Reliability Analysis of Reinforced Concrete Beams: Deterioration, Sensitivity and Spatial variability Aspects. Proceedings of ICOSSAR 2001, Eighth International Conference on Structural Safety and Reliability, Rotterdam.

Li, Y., Vrouwenvelder, T., Wijnants, GH., Walraven, J (2004). "Spatial variability of concrete deterioration and repair strategies." Journal of Structural Concrete **5**(3): 121–130.

- Lim, S., Akiyama, M., Frangopol, D. M (2016). "Assessment of the structural performance of corrosion-affected RC members based on experimental study and probabilistic modeling." Engineering Structures **127**: 189-205.
- Lim, S., Jiang, H., Akiyama, M., Frangopol, D. M., Jiang, H (2017). "Experimental investigation of the spatial variability of the steel weight loss and corrosion cracking of RC members: Novel X-ray and digital image processing techniques." Structure and Infrastructure Engineering **13**(1): 343-352.
- Liu, M., Frangopol, D. M (2005). "Bridge annual maintenance prioritization under uncertainty by multi-objective combinatorial optimization." Computer-Aided Civil and Infrastructure Engineering **20**(5): 343-352.
- Malioka, V., Faber, M. H (2004). Modeling of the spatial variability for concrete structures. Bridge maintenance, safety, management and cost, IABMAS 2004, Rotterdam.
- Maljaars, J., Steenbergen, R., Abspoel, L., Kolstein, H (2012). "Safety assessment of existing highway bridges and viaducts." Structural Engineering International **22**(1): 112-120.
- Mangat, P. S., Elgarf, M. S (1999). "Flexural strength of concrete beams with corroding reinforcement." ACI Structural Journal **96**(1): 149–158.
- Marsh, P. S., Frangopol, D. M (2007). "Lifetime multi-objective optimization of cost and spacing of corrosion rate sensors embedded in a deteriorating reinforced concrete bridge deck." Journal of Structural Engineering **133**(6): 777-787.
- Marsh, P. S., Frangopol, D. M (2008). "Reinforced concrete bridges deck reliability model incorporating temporal and spatial variations of probabilistic corrosion rate sensor data." Reliability Engineering and System Safety **93**(3): 394-409.
- Martin, H., Schiessel, P (1969). "The Influence of Cracks on the Corrosion of Steel in Concrete." In Int. Symp. Durability of Concrete, RILEM, Prague: 205-218.
- Matsuzaki, H., Akiyama, M., Ohki, F., Nakajima, K., Suzuki, M (2010). A method for structural reliability analysis of concrete beams under marine environment over lifetime and its application to pre-tensioned PC beams. Proceeding of JSCE conference 2010.
- Mattock, A. H. (1965). "Rotational capacity of hinging regions in reinforced concrete beams." American Concrete Institute **12**: 85–142.
- Mehta, P. K., and Monteiro, P. J. M (1993). Concrete: Structure, Properties, and Materials, Prentice-Hall.

Melchers, R., Li, CQ., Lawanwisut, W (2008). "Probabilistic modeling of structural deterioration of reinforced concrete beam under saline environment corrosion." Structural Safety **30**: 447-460.

Mindess, S., Young, J. F (1981). Concrete, Prentice-Hall.

Minh H, M. H., Taniguchi H, Niitani K (2003). Experiments on the behavior of post-tensioned concrete beams deteriorated by corrosion. Proceeding of Japan Concrete Institute.

Minh, H., Mutsuyoshi, H., Konno, Y., Niitani, K (2004). Experimental investigation on chloride-induced corrosion in post-tensioned concrete beams. Proceeding of Japan Concrete Institute.

Minh, H., Mutsuyoshi, H., Nakamura, N., Hai, N. D (2006). Influence of grouting condition on crack and load-carrying capacity of post-tensioned concrete beam due to chloride-induced corrosion. Proceeding of Japan Concrete Institute.

Minh, H., Mutsuyoshi, H., Niitani, K (2007). "Influence of grouting condition on crack and load-carrying capacity of post-tensioned concrete beam due to chloride-induced corrosion." Construction and Building Materials **21**(7): 1568-1575.

Moan, T., Song, R (2000). "Implications of inspection updating on system fatigue reliability of offshore structures." Journal of Offshore Mechanics and Arctic Engineering **122**(3): 173-180.

Mori, Y., Ellingwood, B. R (1993). "Reliability-based service-life assessment of aging concrete structures." Journal of Structural Engineering **119**(5): 1600-1621.

Mount, N., Aplin, P., Priestnall, G (2008). Representing, Modeling, and Visualizing the 743 Natural Environments. B. R. CRC Press, FL: 416.

Nakagawa, T., Seshimo, Y., Onitsuka, S., Tsutsumi, T (2004). Assessment of corrosion speed of RC structure under the chloride deterioration environment. Proceedings of JCI symposium on the analysis model supporting the verification of long-term performance of concrete structure in design, Japan Concrete Institute.

Nguyen, N. T., Sbartai, Z. M., Lataste, J. F., Breyse, D., Bos, F (2013). "Assessing the spatial variability of concrete structures using NDT techniques – Laboratory tests and case study." Construction and Building Materials **49**: 240-250.

Nielson, B. G., DesRoches, R (2007). "Seismic fragility methodology for highway bridges using a component level approach." Earthquake Engineering and Structural Dynamics **36**(6): 823-839.

O'Connor, A. J., Kenshel, O (2012). "Experimental evaluation of the scale of fluctuation for spatial variability modeling of chloride-induced reinforced concrete corrosion." Journal of Bridge Engineering **18**(1): 3-14.

Okasha, N. M., Frangpol, D. M (2012). "Integration of structural health monitoring in a system performance based life-cycle bridge management framework." Structure and Infrastructure Engineering **8**(11): 999-1016.

Olea, R. A. (1999). Geostatistics for Engineers and Earth Scientists. New York, Kluwer Academic Publisher,: 303.

Ouglova, A., Berthaud, Y., Foct, F., Francois, M., Ragueneau, F, Petre-Lazar, I (2008). "The influence of corrosion on bond properties between concrete and reinforcement in concrete structures." Materials and Structures **41**: 969-980.

Padgett, J. E., and DesRoches, R (2007). "Bridge functionality relationships for improved seismic risk assessment of transportation networks." Earthquake Spectra **23**: 115-130.

Perrin, F., Sudret, B., Pendola, M (2007). Bayesian updating of mechanical models-application in fracture mechanics. Proceedings of the 18 Ème Congrès Françes De Mècanique.

Powers, T. C. (1958). "The Physical Structure and Engineering Properties of Concrete." Res. and Dev. Bull. No. 90, Portland Cement Association, Skokie,IL.

Prezzi, M., Geyskens, P., Monterio, P. J. J (1996). "Reliability approach to service life prediction of concrete exposed to marine environment." ACI Material Journal **93**(6): 544-552.

Qasrawi, H. Y. (2000). "Concrete strength by combined non-destructive concrete methods simply and reliably predicted." Cement and Concrete Research **30**: 739-746.

Qi, L., Seki, H (2001). "Analytical study on crack generation situation and crack width due to steel reinforcing steel corrosion." Journal of Material, Concrete Structure Pavement, JSCE **50**: 161-171.

Raooof, M., Lin, Z (1997). Structural characteristics of RC beams with exposed main steel. Proceedings of the Institution of Civil Engineers, Structures and Buildings.

Rasheeduzzafar, S. S., Al-Saadoun (1992). "Corrosion cracking in relation to bar diameter, cover, and concrete quality." ACI 1992 **4**(4).

Rodriguez, J., Ortega, L. M., Casal, J (1997). "Load carrying capacity of concrete structures with corroded reinforcement." Construction and Building Materials **11**(4): 239-248.

Sasani, T., Torii, K., Sato, K., Kawamura, M (1997). "A study on the evaluation of chloride ion penetration into the concretes under marine environment." Journal of Material, Concrete Structure Pavement, JSCE **36**: 91-104.

Saveswaran, V., Roberts, M. B., Ward, J. A (2000). "Reliability assessment of deteriorating reinforced concrete beams." Proceedings of the Institution of Civil Engineering, Structures and Buildings **140**: 239-247.

Shafei, B., Alipour, A (2015). "Estimation of Corrosion Initiation Time in Reinforced Concrete Bridge Columns: How to Incorporate Spatial and Temporal Uncertainties." Journal of Engineering Mechanics **141**(10).

Simon, J., Bracci, J. M., Gardoni, P (2010). "Seismic response and fragility of deteriorated reinforced concrete bridges." Journal of Structural Engineering **136**(10): 1273-1281.

Soliman, M., Frangopol, D. M (2014). "Life-cycle management of fatigue sensitive structures integrating inspection information." Journal of Infrastructure Systems **20**(2): 1-13.

Stewart, M. G. (2004). "Spatial variability of pitting corrosion and its influence on the structural fragility and reliability of RC beams in flexure." Structural Safety **26**: 453-470.

Stewart, M. G., Rosowsky, D. V (1998). "Time-dependent reliability of deteriorating reinforced concrete bridge decks." Structural Safety **20**: 91-109.

Stewart, M. G., Suo, Q (2009). "Extent of spatially variable corrosion damage as an indicator of strength and time-dependent reliability of RC beams." Journal of Structural Engineering **31**(1): 198-207.

Sykora, M., Holicky, M., Lenner, R., Manas, P (2014). "Target reliability levels for existing bridges considering emergency and crisis situations." Advances in military technology **9**(1): 45-57.

Torres-Acosta AA, N.-G. S., Teran-Guillen J (2007). "Residual flexure capacity of corroded reinforced concrete beams." **29**: 1145-1152.

Tsutsumi, T., Shirai, S., and Yasuda, N., Matsushima, M (1996). "Evaluation on parameters of chloride induced damage based on actual data." Journal of Material, Concrete Structure Pavement, JSCE **32**: 33-41.

Val, D. V. (2005). Effect of pitting corrosion on strength and reliability of reinforced concrete beams. Proceedings of the ninth international conference on structural safety, ICOSSAR, Rotterdam.

- Val, D. V. (2007). "Deterioration of strength of RC beams due to corrosion and its influence on beam reliability." Journal of Structural Engineering **133**(9): 1297-1306.
- Val, D. V., Stewart, M. G (2003). "Life-cycle cost analysis of reinforced concrete structures in marine environments." Structural Safety **25**(4): 343–362.
- Vrouwenvelder, A. C. W. M. (2002). "Developments towards full probabilistic design codes." Structural Safety **24**(2): 417-432.
- Vrouwenvelder, A. C. W. M., Scholten, N (2010). "Assessment criteria for existing structures." Structural Engineering International **20**(1): 62-65.
- Vu, K. A. T., Stewart, M. G (2005). "Predicting the likelihood and extent of RC corrosion-induced cracking." Journal of Structural Engineering ASCE **131**(11): 1681–1689.
- Wang, X., and Liu, X (2003). "Bond strength modeling for corroded reinforcements." Construction and Building Materials **20**: 177-186.
- Weters, E., Liu Y, Richard (1998). "Modeling the time-to-corrosion cracking in chloride contaminated reinforced concrete structures." ACI Materials Journal **95**(6).
- Yanweerasak, T., Akiyama, M., Frangopol, D. M (2016). "Updating the seismic reliability of existing RC structures in a marine environment by incorporating the spatial steel corrosion distribution: application to bridge piers." Journal of Bridge Engineering **21**(7).
- Yoshida, I. (2009). Data assimilation and reliability estimation of existing RC structure. Second international conference on Computational Methods in Structural Dynamics and Earthquake Engineering. Rhodes, Greece.
- Yun, S. Y., Hamburger, R. O., Cornell, C. A., Foutch, D. A (2002). "Seismic performance evaluation for steel moment frames." Journal of Structural Engineering **128**(4): 534-545.
- Zheng, R., Ellingwood, B. R (1998). "Role of non-destructive evaluation in time-dependent reliability analysis." Structural Safety **20**(4): 325-339.
- Zhu, B., Frangopol, D. M (2013). "Risk-based approach for optimum maintenance of structures under traffic and earthquake loads." Journal of Structural Engineering **139**(3): 422-434.

APPENDIX



จุฬาลงกรณ์มหาวิทยาลัย
CHULALONGKORN UNIVERSITY

VITA

Name: Thanapol Yanweerasak

Date of Birth: 8 April, 1991

Education:

2009 – 2013, Bachelor's Degree in Civil Engineering, Department of Civil Engineering, Faculty of Engineering, Chulalongkorn University, Bangkok, Thailand

2013-2015, Master's Degree in Civil Engineering (Structural Engineering), Department of Civil and Environmental Engineering, Faculty of Science and Engineering, Waseda University, Tokyo, Japan

2015-2018, Doctoral's Degree in Civil Engineering (Structural Engineering), Department of Civil Engineering, Faculty of Engineering, Chulalongkorn University, Bangkok, Thailand

Job:

2017 – Present, Lecturer in Faculty of Engineering at Kasetsart University, Chonburi, Thailand



จุฬาลงกรณ์มหาวิทยาลัย
CHULALONGKORN UNIVERSITY